ISTANBUL TECHNICAL UNIVERSITY ★ GRADUATE SCHOOL

ELECTROSPUN POLYACRYLONITRILE BASED COMPOSITE NANOFIBERS CONTAINING POLYINDOLE AND GRAPHENE OXIDE

Ph.D. THESIS

İlknur BOZKAYA GERGİN

Department of Polymer Science and Technology

Polymer Science and Technology Programme

MARCH 2023

ISTANBUL TECHNICAL UNIVERSITY ★ GRADUATE SCHOOL

ELECTROSPUN POLYACRYLONITRILE BASED COMPOSITE NANOFIBERS CONTAINING POLYINDOLE AND GRAPHENE OXIDE

Ph.D. THESIS

İlknur BOZKAYA GERGİN
(515092003)

Department of Polymer Science and Technology

Polymer Science and Technology Programme

Thesis Advisor: Prof. Dr. A. Sezai SARAC

MARCH 2023

İSTANBUL TEKNİK ÜNİVERSİTESİ ★LİSANSÜSTÜ EĞİTİM ENSTİTÜSÜ

POLİİNDOL VE GRAFEN OKSİT İÇEREN POLİAKRİLONİTRİL TABANLI KOMPOZİT NANOFİBERLER

DOKTORA TEZİ

İlknur BOZKAYA GERGİN
(515092003)

Polimer Bilim ve Teknolojisi Anabilim Dalı

Polimer Bilim ve Teknolojisi Programı

Tez Danışmanı: Prof. Dr. A. Sezai SARAÇ

MART 2023

İlknur Bozkaya GERGİN, a Ph.D. student of ITU Graduate School student ID 515092003, successfully defended the thesis/dissertation entitled "ELECTROSPUN POLYACRYLONITRILE BASED COMPOSITE NANOFIBERS CONTAINING POLYINDOLE AND GRAPHENE OXIDE", which she prepared after fulfilling the requirements specified in the associated legislations, before the jury whose signatures are below.

Thesis Advisor :	**Prof. Dr. A. Sezai SARAÇ** Istanbul Technical University	.....
Jury Members :	**Prof. Dr. Hale KARAKAŞ** Istanbul Technical University	.....
	Prof. Dr. Mustafa ÖKSÜZ Yalova University	.....
	Prof. Dr. Nilgün KIZILCAN Istanbul Technical University	.....
	Assoc. Dr. Elif ALTÜRK Okan University	.....

Date of Submission : 06 January 2023
Date of Defense : 06 March 2023

"Çoğu insan zekaya inanır, ben inanmıyorum. Bizi birbirimizden ayıran emektir. Ben çalışmaya inanıyorum." Aziz SANCAR

To my lovely family,

FOREWORD

I would like to thank to my supervisor, Prof. Dr. A. Sezai SARAÇ, for his guidance and discussions during my Ph.D. studies.

I am grateful to my thesis committee members Prof. Dr. Hale KARAKAŞ, Prof. Dr. Mustafa ÖKSÜZ for their valuable time and supports.

I would like to thank to Prof. Dr. Esma SEZER, Prof. Dr. Belkıs USTAMEHMETOĞLU, Prof. Dr. Ayşen ÖNEN and Prof. Dr. Ersin SERHATLI for their advice, encouragement, and supports.

I would like to acknowledgement to Prof. Dr. Maria OMASTOVA and Dr. Matej MICUSI from Slovak Academy of Sciences for the XPS measurements and analysis.

I would like to thank to Assoc. Prof. Dr. Argun GÖKÇEÖREN for his collobration and support.

I would like to thank to Dr. Ezgi İŞMAR ŞİR for her collobration and support.

I would like to thank to Dr. Barbaros AKKURT for his support.

I would like to thank to all the past and present members of Electropol-Nanotech Research Group especially my special friends Dr. Timuçin BALKAN, Dr. Aslı GENÇTÜRK, Selin GÜMRÜKÇÜ and Dr. Nazif Uğur KAYA, for their supports and valuable friendship during my Ph.D.

My endless grateful thanks go to Prof. Dr. Necmettin PAMİR who change my life very deeply and made me discover the importance of the life.

I would like to express my special thanks to my dear husband Serkan GERGİN for his support, patience, continuous encouragement and endless love. He is the person to encourage me to follow my dreams when I feel unmotivated. Also, I would like to express my deepest thanks to my very sweety son Fatih Eren GERGİN to show understanding to my working hard by weekends, holidays and late nights. I am deeply blessed and thankful to have both of you in my life.

I would like to express my sincere gratitude to my whole family members especially my dear mother Naime BOZKAYA who inspires me the most in the world, my dear brothers Onur BOZKAYA, Önder BOZKAYA and İlker BOZKAYA for their support, conversational motivation and love. More importantly, without my lovely family, I would not the person who I am today.

This work was financially supported by the Scientific Research Projects Coordination Unit of Istanbul Technical University.

March 2023

İlknur BOZKAYA GERGİN
(Physicist, MSc)

TABLE OF CONTENTS

Page

ABBREVIATIONS

AFM : Atomic Force Microscope
ATR-FTIR : Attenuated Total Reflectance Fourier Transform Infrared
CNFs : Carbon Nanofibers
CPE : Constant Phase Element
CV : Cyclic Voltammetry
DL : Detection Limit
DMA : Dynamic Mechanical Analysis
DMF : N, N Dimethylformamide
DSC : Differential Scanning Calorimetry
EIS : Electrochemical Impedance Spectroscopy
GO : Graphene Oxide
ITOPET : Indium Tin Oxide Coated Polyethylene Terephthalate
PAN : Polyacrylonitrile
PIN : Polyindole
QL : Quantitation Limit
SEM : Scanning Electron Microscope
TEM : Transmission Electron Microscopy
TGA : Thermogravimetric Analysis
XPS : X-Ray Photoelectron Spectroscopy

SYMBOLS

C	**:** Capacitance
C_{dl}	**:** Double Layer Capacitance
C_{sp}	**:** Specific Capacitance
Q	**:** Constant Phase Element
R_{ct}	**:** Charge Transfer Resistance
R_s	**:** Solution Resistance
T_g	**:** Glass Transition Temperature
T_m	**:** Melting Temperature
Zim	**:** Imaginary Part of Impedance
Zre	**:** Real Part of Impedance
W	**:** Warburg Diffusion Element
γ	**:** Surface Tension

LIST OF TABLES

Page

LIST OF FIGURES

Page

ELECTROSPUN POLYACRYLONITRILE BASED COMPOSITE NANOFIBERS CONTAINING POLYINDOLE AND GRAPHENE OXIDE

SUMMARY

Studies on the conductive polymers has gained great interests when the Nobel Prize in Chemistry was awarded by discovery and development of the conductivity of polyacetylene in 2000. Conductive polymers are also called organic metals. They conduct electricity thanks to the conjugated chain structure consisting of consecutive single and double bonds in their structures. Conductive polymers, which are insulating in neutral state, gain conductivity by doping. Polyacetylene, polypyrrole, polythiophene, poly(3,4-ethylenedioxythiophene) (PEDOT) are some of the conductive polymers that have been studied extensively. These polymers can be used in solar cells, super capacitors, chemical and biosensor application areas. Polyindole (PIN) is one of the conductive polymers which can show electrochromic properties with high redox activity, good thermal stability, slow degradation rate and good air stability. Polyindole containing studies have been increasing in recent years and this polymer can be used in the pharmaceutical field, anticorrosion coatings, photovoltaic batteries, supercapacitor applications or anode material in batteries.

On the other hand, with the advancement of nanotechnology, it has been found that materials in nano scale show physical and chemical property differences compare to the bulk form. Nanoscale generally includes the range of 1-100 nm. When the size of the particle in the material becomes too small, the electronic structure of the material can change. For example; gold normally does not react, but can be active at the nano level. Nanofibers are fibers with a high length/volume ratio with average diameters in the order of nanometers. In addition to their chemical properties also depending on the surface properties such as morphology and topography, materials can improve and can be used various areas. Due to their low densities, large surface areas with porous structures, it has a wide range of research and application areas of nanofibers such as filtration, tissue engineering, drug release systems, biomedical, textile, energy storage and sensor.

Especially in recent years, electrospinning technique has attracted interests by scientists to generate nanofibers because of it is extremely simple, cheap and practical usage. On the other hand, scientists have great expectations since discovering a few atoms thick materials. Graphene oxide (GO) is a two dimensional material with high surface area. It can be semiconductor or insulating material which depends on the degree of oxidation, sheet size, microstructure and among many other factors. Moreover, graphene oxide contains some functional groups (epoxy, hydroxyl, carbonyl, etc.) on the structure which makes the dispersive ability in the solvent. These oxygen containing functional groups enable the development of GO-based composites, especially due to their ability to disperse in the solvent. Unfortunately, nanofiber production from conductive polymers and GO like materials can be limited or not possible by electrospinning method. For this reason, nanofibers of conductive

polymers and GO are produced by making blend or composite with a different polymer called as carrier polymer, whose nanofibers can be easily obtained by electrospinning.

Polyacrylonitrile (PAN) is one of the carrier polymer which is a very common usage area especially in the textile manufactory and carbon fiber production. Also, PAN fibers are the precursor of high quality of carbon fibers. PAN is choosen as a carrier polymer and PAN based composites are studied in this thesis.

In the first part of the study; the oxidative chemical reaction of polyindole has taken place in the presence of $FeCl_3$. Nanofibers were produced by mixing polyindole with polyacrylonitrile in N, N-Dimethylformamide (DMF) solvent at different weight / volume ratios. Polyacrylonitrile and polyindole blends were generated in different proportions of polyindole. Composite fibers were produced from the solutions by adjusting the optimum conditions using electrospinning method. Morphological, thermal properties, spectral analysis of these fibers were investigated by Atomic Force Microscopy (AFM), Scanning Electron Microscopy (SEM), Attenuated Total Reflectance Fourier Transform Infrared Spectroscopy (FTIR-ATR) and Differential Scanning Calorimetry (DSC). Electrochemical characterization of fibers has been studied by Electrochemical Impedance Spectroscopy (EIS). The experimantal data was used to fit the equivalent circuit with Zsimpwin Software. In addition, it was found that the electrochemical properties (such as double layer capacitance, solution resistance and charge transfer resistance) of composite fibers were effected by surface tension and conductivity of solution. Iron, is an important element in the industry, environment, medical applications areas, biological studies and human health. Different methods such as electron spin coulometry and ion selective electrodes are used in the determination of Fe(II). Differently, in this study, Electrochemical Impedance Spectroscopy is presented as an alternative technique to determine Fe(II) concentration. Electroactive behavior of the fiber electrode was investigated by Cyclic Voltammetry (CV). Electroactivity of the nanofiber selected depending on the impedance and morphological properties of the nanofibers was measured with the help of $K_3Fe(CN)_6/K_4Fe(CN)_6$ electrolyte. It was discussed that the presence of Polyindole (PIN) content showed an electrocatalytic activity against $K_3Fe(CN)_6/K_4Fe(CN)_6$. The lowest Fe(II) ion analyte concentration detection limit for the selected electrode was calculated as $1x10^{-4}$ $mol.l^{-1}$.

In the second part of the study which is different from the first part, graphene oxide (GO) is choosen as a material to improve the capacitive property of Polyacrylonitrile. Polyacrylonitrile / Graphene oxide (GO) nanofibers were produced by using a rotary collector instead of a fixed collector in the electrospinning device. Thus, thinner, more aligned nanofibers with higher young modulus were acquired. Oxidative stabilization and carbonization applied to composite nanofibers through the thermal process. In particular, the stretching applied to the nanofiber during oxidation determines the mechanical strength and structure of the final product carbon nanofiber to be formed. Therefore, understanding of the oxidation mechanism is an essential part of the production of carbon nanofibers (CNFs). The stress, temperature and application time utilized to the material in oxidation affect the structure of the carbon nanofiber. Oxidation step of electrospun polyacrylonitrile based composite nanofibers was studied and morphological, spectral and electrochemical properties of composite nanofibers were investigated. Morphological and spectral characterizations of composite nanofibers were performed by FTIR-ATR and Raman Spectroscopy, SEM, AFM and Transmission Electron Microscopy (TEM). Mechanical tests were performed with Dynamic Mechanical Analysis (DMA). Thermal behaviours of

composite nanofibers were investigated by Thermal Gravimetric Analysis (TGA). Capacitive behavior of nanofibers were performed by EIS and CV. When there is GO in the structure, the ions in the solution can penetrate into the pores which cause the double layer capacitance (C_{dl}) value increasement. Average pore diameters have been measured with the ImageJ program to be around 38.5 nm and it has been found that the double layer capacitance (C_{dl}) of PAN nanofibers containing GO is 0.600 μF which is the highest value. Also, it was observed that the capacitive behaviour of carbon nanofiber formed in the presence of graphene oxide improved. PAN/GO carbon nanofibers exhibit potential for capacitive applications in the light of these results.

In the third part of the study, X-ray Photoelectron Spectroscopy (XPS) and FTIR analysis methods were used to understand the oxidative stabilization deeply. The thermal oxidative stabilization of polyacrylonitrile has a complex mechanism with the cyclization and dehydrogenation steps. Polyacrylonitrile (PAN) composite nanofibers with GO were fabricated, and thermal oxidation were performed to these nanofibers. The oxidation process were applied at various temperatures (250 °C, 280 °C, and 300 °C) during 1h and 3h. Nanofibers were significantly effected by high temperature with during long duration time. The effect of GO addition into the nanofibers were analyzed by XPS, FTIR-ATR and, EIS. After heat treatment, change in C1s spectra and development of sp^2 carbon was detected by XPS. It was concluded that the presence of GO accelerated the oxidation mechanism and developed the final structure.

POLİİNDOL VE GRAFEN OKSİT İÇEREN POLİAKRİLONİTRİL TABANLI KOMPOZİT NANOFİBERLER

ÖZET

Nobel Kimya Ödülü'nün 2000 yılında iletken polimerler (poliasetielen) konusunda kazanılmasıyla bu polimerlerle yapılan çalışmalar hız kazanmıştır. İletken polimerler, elektriği ileten organik yapıdaki polimerlerdir. İletken polimerler, organik metal olarak da adlandırılırlar. Yapılarında bulunan ardışık tek ve çift bağlardan oluşan konjuge zincir yapısı sayesinde elektriği iletirler. Nötral halde yalıtkan olan bu polimerler, doplama (katkılama) yapılmak suretiyle iletkenlik özelliği kazanırlar. Poliasetilen, polipirol, politiyofen, poli (3,4-etilendioksitiyofen) (PEDOT) üzerinde çok çalışılan bazı iletken polimerlerdendir. Bu polimerler; güneş pilleri, süper kapasitörler, kimyasal ve biyosensör uygulama alanlarında kullanılabilmektedir.

Poliindol (PIN) iletken bir polimer olup polipirol ve polianiline göre daha zayıf elektriksel ve elektrokimyasal iletkenlik göstermektedir. Bu sebeple, enerji depolama uygulamalarında diğerlerine göre daha az çalışılmaktadır. PIN; termal stabilitesi oldukça iyi, redox özelliği yüksek, degradasyonu yavaş ve hava stabilitesi iyi olan elektrokromik özellik gösterebilen iletken bir polimerdir. Bu yüzden, poliindol içeren çalışmalar son yıllarda artmakta olup poliindolün; farmasotik alanda, antikorozyon kaplamalarda, fotovoltaik pillerde, süper kapasitör uygulamalarda ya da bataryalarda anod malzemesi olarak kullanımı mümkün olabilmektedir.

Öte yandan nanoteknolojinin ilerlemesiyle nano ölçekte malzemelerin külçe haline göre fiziksel ve kimyasal özelliklerinde farklılıklar gösterdiği bulunmuştur. Nano ölçek genellikle 1-100 nm aralığını kapsamaktadır. Malzeme içerisindeki parçacığın boyutu çok küçüldüğünde, malzemenin elektronik yapısı değişebilmektedir. Örneğin; altın normalde reaksiyona girmez ama nano seviyesinde aktiflik gösterebilmektedir. Nanofiberler ise ortalama çapları nanometreler mertebesinde olan yüksek uzunluk/hacim oranına sahip liflerdir. Nanofiberler; kimyasal özelliklerinin yanında morfoloji ve topografi gibi yüzey özelliklerine bağlı olarak da malzemelerin kullanım alanlarını iyileştirebilmekte ve genişletebilmektedirler. Nanofiberlerin; düşük yoğunlukları, geniş yüzey alanları ve gözenekli yapılarından dolayı filtrasyon, doku mühendisliği, ilaç salınım sistemleri, biyomedikal, tekstil, enerji depolama, sensör gibi çok geniş yelpazede araştırma ve uygulama alanı bulunmaktadır. Özellikle son yıllarda, elektroçekim yöntemi ile malzemelerden nanofiber elde edilmesi, bu yöntemin son derece basit, ucuz ve kullanışlı olmasından dolayı ilgi çekmektedir.

Bilim adamlarının birkaç atom kalınlığındaki malzemeleri keşiflerinden itibaren malzemelerle ilgili büyük beklentileri oluşmuştur. Grafen oksit (GO) yüksek yüzey alanına sahip iki boyutlu bir malzemedir. GO; oksidasyon derecesine, tabaka boyutuna, mikro yapıya ve diğer birçok faktöre bağlı olarak yarı iletkenlik veya yalıtkanlık özelliği gösterebilmektedir. Ayrıca, grafen oksit yapısında bulunan oksijen içeren fonksiyonel grupların (epoksi, hidroksil, karbonil vb.) varlığı nedeniyle çözücü içerisinde dağılma özelliğine sahiptir ve bu nedenle GO bazlı kompozitlerin geliştirilmesine olanak sağlanmaktadır.

Ne yazık ki, iletken polimerlerden ve grafen oksit gibi malzemelerden elektro çekim metodu ile nanofiber eldesi; düşük molekül ağırlıkları, çözücü içerisindeki çözünürlüklerinin zayıf olması ve sert zincir yapıları sebebiyle kısıtlı olabilmektedir ya da mümkün değildir. Bu sebeple iletken polimerlerin ve grafen oksit vb. yapıların elektro çekim yöntemi ile elde edilen nanofiberleri taşıyıcı (nanofiberi kolay elde edilen) görevi gören farklı bir polimerle blend ya da kompoziti yapılarak üretilmektedir.

Çalışmanın ilk bölümünde; poliindolün poliakrilonitril (PAN) taşıyıcı polimeri ile N,N-Dimetilformamid (DMF) çözücüsü içerisinde farklı ağırlık/hacim oranlarında karışımları yapılarak nanofiberleri üretilmiştir. PAN, özellikle tekstil endüstrisinde sıkça kullanılan uygulama alanı geniş bir polimerdir. Ayrıca, karbon nanofiber prekürsoru olarak da kullanılmaktadır. Poliindolün oksidatif kimyasal reaksiyonu $FeCl_3$ varlığında gerçekleştirilerek poliakrilonitril ile farklı oranlarda blendleri elde edilmiştir. Elde edilen çözeltilerden elektro çekim yöntemiyle fiberler üretilmiştir. Bu fiberlerin morfolojisi, termal özellikleri, spektral analizleri incelenmiştir. Fiberlerin elektrokimyasal karakterizasyonu, elektrokimyasal empedans spektroskopisi (EIS) ile çalışılmıştır. Ayrıca, çözeltilerin çözelti iletkenliği, yüzey gerilimi değerleri bulunarak PIN içeren fiberlerin yük transfer direnci, çözelti direnci ve çift tabaka kapasitansı gibi elektrokimyasal özelliklerine etkisi araştırılmıştır. Demir; endüstriyel, çevresel, medikal uygulamalarda, biyolojik çalışmalarda ve insan sağlığında önemli olan bir elementtir. Fe(II) tayininde elektron spin rezonansı, UV-vis spektrofotometri, florometrik analiz, kontrollü potansiyel kulometri ve iyon seçici elektrotlar gibi farklı yöntemler kullanılmaktadır. Farklı olarak bu çalışmada, Fe(II) konsantrasyonunu belirlemek için elektrokimyasal empedans spektroskopisi alternatif bir teknik olarak sunulmuştur. Döngülü voltametri (CV) ile fiber elektrodun elektroaktif davranışı incelenmiştir. Nanofiberlerin empedans ve morfolojik özelliklerine bağlı olarak seçilen nanofiberin elektroaktivitesi $K_3Fe(CN)_6/K_4Fe(CN)_6$ elektroliti yardımıyla ölçülmüştür. Seçilen elektrot için en düşük Fe(II) iyon analit konsantrasyonu algılama sınırı $1x10^{-4}$ mol.l^{-1} olarak hesaplanmıştır.

Çalışmanın ikinci bölümünde ise; poliakrilonitril/grafen oksit (GO) nanofiberleri birinci bölümden farklı olarak elektro çekim cihazında sabit kollektör yerine döner kollektör kullanılarak üretilmiştir. Böylelikle, Young modülü daha yüksek olan ince, yönlendirilmiş nanofiberler elde edilmiştir. Grafen, yoğunluğu çelikten düşük olmasına rağmen çeliğe göre çok daha güçlü, ısı ve elektriği çok iyi ileten, karbonun yüksek yüzey alanına sahip bir allotropudur. Grafenin; alan etkili transistörler, transparan elektrotlar, organik fotovoltaik cihazlar, nanokompozitler olmak üzere uygulama alanları bulunmaktadır. Bu çalışmada, grafenin üstün özellikleri yanında çözücü içerisindeki dispersiyonundaki zorluklar sebebiyle, grafene göre yalıtkan bir malzeme olan ama yapısındaki oksijen içeren fonksiyonel grupların (epoksi, hidroksil,karbonil vb.) varlığı sayesinde çözücü içerisinde dispersiyonu çok daha kolay olan grafen oksit (GO) tercih edilmiştir.

Karbon nanofiber üretiminde oksidasyon ve karbonizasyon olmak üzere çok önemli iki aşama vardır. Özellikle, oksidasyon sırasında nanofibere uygulanan germe, oluşacak son ürün karbon nanofiberin mekanik dayanımını ve yapısını belirler. Oksidasyonda malzemeye uygulanan stres, sıcaklık, uygulama süresi karbon nanofiberin yapısını etkiler. Dolayısıyla, oksidasyon prosesinin mekanizmasını da anlamak karbon nanofiber üretiminde büyük önem taşımaktadır. Oksidasyon, halkalaşma ve dehidrojenasyon aşamalarını içermektedir. Oksidasyon uygulanan nanofiberlerin morfolojik, spektral ve elektrokimyasal özellikleri incelenmiştir.

Yapıda GO varken bu nanofiberlerdeki gözeneklerin ortalama çapının yaklaşık 38,5 nm civarında olduğu ImageJ programı ile ölçülmüştür. Çözelti içindeki iyonlar gözeneklerin içine nüfuz edebildiğinden GO içeren PAN nanofiberlerinin çift tabaka kapasitans (C_{dl}) değerinin arttığı bulunmuştur. Grafen oksit varlığında oluşan karbon nanofiberin kapasitif özelliğinin arttığı gözlenmiştir. PAN/GO karbon nanofiberleri kapasitif uygulamalar için potansiyel teşkil etmektedir.

Çalışmanın üçüncü bölümünde ise oksidasyon sürecini anlamak için FTIR ve XPS analiz yöntemleri kullanılmıştır. Grafen oksit (GO) içeren poliakrilonitril (PAN) kompozit nanofiberler üretilmiştir. Ayrıca, PAN/GO nanoliflerinin oksidasyon sürecini araştırmak için PAN/GO kompozit nanofiberlerinin termal oksidasyonu farklı sıcaklıklarda (250 °C, 280 °C ve 300 °C) ve farklı zaman aralıklarında (1 ve 3 saat) gerçekleştirilmiştir. Nanolifler, uzun süre boyunca yüksek sıcaklıktan önemli ölçüde etkilenmiştir. Poliakrilonitrilin termal oksidasyon süreci, halkalanma ve dehidrojenasyon aşamaları yoluyla karmaşık bir mekanizmaya sahiptir. Tüm oksitlenmiş numuneler için, GO ilavesinin nanofiberler üzerindeki etkisini araştırmak için X-ışını fotoelektron spektroskopisi (XPS), Elektrokimyasal empedans spektroskopisi (EIS) ve Fourier dönüşümlü kızılötesi-Azaltılmış toplam yansıma (FTIR-ATR) spektroskopik sonuçları, karşılaştırmalı olarak değerlendirilmiştir. Isıl işlemden sonra, saf poliakrilonitrilden oksitlenmiş forma C1s spektrumlarındaki değişim ve sp^2 karbon gelişimi tespit edilmiştir. Grafen oksitin varlığı, nihai yapının oksidasyonunu ve gelişimini hızlandırmıştır.

1. INTRODUCTION

Electrospinning is a versatile and one of the favorable technique to produce fibers with micro or nano scales (Ding et al., 2019). Electrospinning is called electrostatic fiber spinning method to fabricate continuous nanofibers form both natural and synthetic polymers. Electrical potantial is applied to polymer solutions or melts to obtain fibers. Formhals patented electospinning of polymer solutions in 1934. Thus, investigation on electrically loaded liquid jets were started in 19th century (Anton Formhals, 1934). Studies show that fibers of at least 75 different kinds of natural, synthetic organic polymers have been produced by electrospinning. These fibers have various morphologies with a very high surface-to-volume ratio with porous structure (Ding et al., 2019). Electrospun nanofibers can be used in various applied areas because of these extraordinary morphologic and topologic structure. These electrospun nanofibers are generally used in biomedical area such as tissue engineering scaffolds, in wound healing, filtration, drug delivery, in immobilization of enzymes, as affinity membrane and biotechnology, biosensors, environmental engineering, healthcare, small diameter vascular graft implants, defense - security, energy storage, energy generation which is seen in (Figure 1.1) (Bhardwaj & Kundu, 2010).

The structure and the morphology of electrospun nanofibers are determined by electrospinning process and polymer solution (Deitzel, Kleinmeyer, Harris, & Beck Tan, 2001). Morphology of the fibers can be adjusted by electrospinning parameters classified as solution parameters (polymer concentration, molecular weight of polymer, viscosity, surface tension and conductivity), processing parameters (potential, distance between tip to collector, flow rate and type of collector) and ambient parameters (temperature and humidity) (Ding et al., 2019).

One of the most important feature of electrospun fiber which is related to the process is fiber diameter (Huang, Zhang, Kotaki, & Ramakrishna, 2003). Mechanical, electrical and optical characteristics of fiber is determined by the fiber diameter change. It was studied that both the electrical and mechanical properties such as conductivity and the strength of electrospun fibers are sensitive to fiber diameter

(Yördem, Papila, & Menceloğlu, 2008). Also, the control of fiber diameter to adjust electrospinning parameters is very important to produce desired nanofibers.

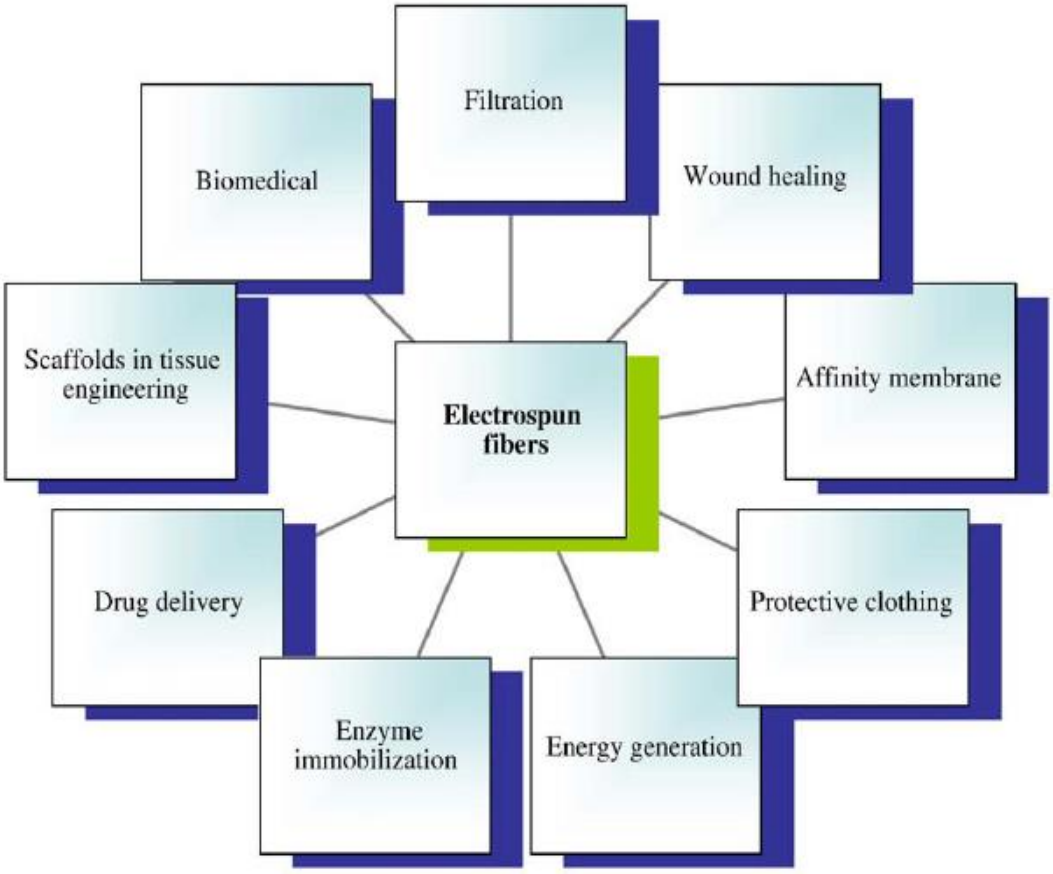

Figure 1.1: Applications of electrospun fibers in different sectors.

An electrical potential applied to a polymer solution held by its surface tension at the end of a syringe in the electrospinning technique. This electric potantial induce the charge on the liquid surface. A force opposite to surface tension occurs as a result of mutual charge repulsions. The Taylor cone occurs when the intensity of the electric field increases (Doshi & Reneker, 1995) which is seen in (Figure 1.2) (Khishigbayar, Joo, & Cho, 2017).

As the voltage exceeds a threshold value, a fine charged jet is ejected which means the electrostatic forces overcome the surface tension. Due to the entanglements of polymer chain and viscosity of the polymer solution, the jet doesn't transform into spherical droplets, it remains stable. After the jet is formed, the solvent begins to evaporate immediately. The jet moves towards a ground plate which acts as a counter electrode. The result is the deposition of a thin polymer fiber formed on a metal collector (Bognitzki et al., 2001).

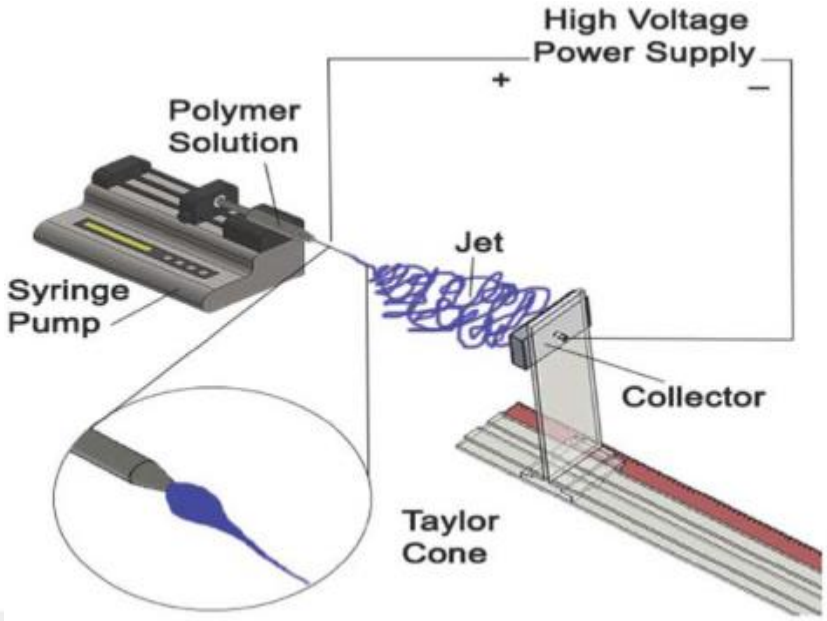

Figure 1.2 : Electrospinning apparatus and its working principle.

Randomly oriented nanofiber mats are collected on static collector whereas parallel aligned oriented nanofiber mats are collected on rotating collector such as drum or disk (Beachley & Wen, 2009). Aligned oriented nanofibers have some advantages compared than non-aligned nanofibers. Studies show that mechanical strength and the young modulus getting higher according to the fiber alignment with high aspect ratio (l/d) (Fennessey & Farris, 2004). Furthermore, this advantage can be extended to biological studies. Orientation of fibers improves cell adhesion and cell growth to develop biomaterial studies (Nitti et al., 2018).

Electrospinning is a simpler and cheaper process compared to the traditional preparation methods to produce composite nanofibers and carbon nanofibers such as catalyst, spraying, vapor grown methods etc. Purification process is not necessary during the electrospinning process therefore, electrospinning is gradually regarded as the most suitable technique for the preparation of uniform and continuous carbon nanofibers (C. K. Liu et al., 2015). Polyacrylonitrile (PAN) (Agend, Naderi, & Fareghi-Alamdari, 2007; Chakrabarti et al., 2006; Dissertations & Fennessey, 2014; Kim et al., 2007, 2006; Lee, Kim, Ku, Kim, & Joh, 2012; C. K. Liu, Lai, Liu, Yao, & Sun, 2009; Oh, Ju, Jung, & Lee, 2008; S. J. Park & Im, 2008; Prilutsky, Zussman, & Cohen, 2008; Shao, Wei, Zhang, Cai, & Jiang, 2008; Sutasinpromprae, Jitjaicham, Nithitanakul, Meechaisue, & Supaphol, 2006), pitch (Mochida et al., 1996), polybenzimidazole (Kim, Kim, & Kim, 2004), and polyimide (Chung, Jo, & Kim,

2005) types precursor of carbon nanofibers have been researched in the literature. Generally, electrospun PAN is used to produce carbon nanofibers for being simple carbonization process and high carbonization rate (C. K. Liu et al., 2015).

Genarally, there are two approaches to produce carbon fibers: spinning and vapor growth. Vapor growth method was discovered in 1970s and 1980s (N. M. Rodriguez, 1993; Tibbetts, Lake, Strong, & Rice, 2007; L. Zhang, Aboagye, Kelkar, Lai, & Fong, 2014). Carbon fibers were synthesized by catalytically separating appropriate hydrocarbons in the presence of metal catalysts, but unfortunately, it was confronted considerable problems in the mass-production. Spinning method which involves spinning of polymeric precursor generally such as polyacrilonitrile , cellulose, pitch after that follows thermal treatment. PAN precursor has received great attention with high carbon yield and best mechanical property of the produced carbon fibers among the other precursors. PAN is used for the precursor of carbon fibers about 90 % of manufactured lately (L. Zhang et al., 2014). Polyacrylonitrile based composite materials are prefered precursors of carbon fibers to develope of carbon fibers melting point, high strength, and the rate of pyrolysis as well as carbon yield obtainable (Sayyar, Moskowitz, Fox, Wiggins, & Wallace, 2019). Electrical, mechanical and thermal properties of carbon fibers can be improved by incorporation of carbonaceous high surface area nanofillers into the precursor matrix which leads to order graphitic structure (Sayyar et al., 2019).

Carbon nanofibers resembling the chemical structure of carbon fibers are widely used in nanotechnology area such as biomedical applications, electronics or materials and devices usages for energy (Y. Zhang et al., 2021). Carbon nanofibers have beeen produced similiar to conventional carbon fibers followed by stabilization and carbonization process. Stabilization process was carried out between 200 °C and 300 °C in air atmosphere as carbonization is up to 2800 °C in an inert atmosphere (L. Zhang et al., 2014).

Polyindole is an electroactive polymer, which can be synthesized by electrochemical oxidation of indole in several electrolytes or chemical polymerization in the presence of oxidants like $FeCl_3$, $CuCl_2$ (D Billaud, Maarouf, & Hannecart, 1994; Z. Cai & Yang, 2010). Polyindole has the properties of both polypyrrole and poly(para-phenylene) together, as high redox activity, stability and fairly good thermal stability (D Billaud, Maarouf, & Hannecart, 1995), (Maarouf, Billaud, & Hannecart, 1994). On the other

hand, its air stable electrical conductivity is around 0.1 S cm^{-1} in the doped state (Lazzaroni et al., 1987) however its degradation rate is slow in comparison with polyaniline and polypyrrole (Syed Abthagir, Dhanalakshmi, & Saraswathi, 1998). Polyindole is being developed as a possible candidate for batteries, supercapacitors, sensors, diodes, electrochromic devices, anticorrosion, electrocatalysis, photocatalysis, and biological applications (Thadathil, Pradeep, Joshy, Ismail, & Periyat, 2022). It acts as a model for some biopolymers e.g. melanin (Goel, Mazumdar, & Gupta, 2010; Palumbo, d'Ischia, Misuraca, Prota, & Schultz, 1988).

Graphene is also known conductive material having a great attention recently. Graphene is a single atomic layer of sp^2 carbon atoms. These very thin graphene nanosheets were first explored by mechanical exfoliation ("Scotch-tape" method) of bulk graphite (Novoselov et al., 2004). Also, they were obtained by epitaxial chemical vapor deposition (Berger et al., 2006). Those methods are very suitable for precise device assembly, otherwise they are not much suitable for large scale fabrication. Chemical methods are more appropriate to obtain bulk scale graphene materials (Marcano et al., 2018; Ruoff, 2008). Although graphene is conductive, its dispersion in the solvent is very difficult. Also, this is the one of the reason to study on Graphene Oxide (GO) by scientists.

Graphene oxide (GO) is a hydrophilic nonconductive two dimensional carbon material have some abilities by used in electronics, electrode materials, conductive films, and composites (Dimiev & Tour, 2014; Marcano et al., 2018). It has great interests because of its large numbers of oxygen containing functional groups and high specific surface area (Jia et al., 2017). Moreover, GO is a semiconductor or insulating material which depends on the degree of oxidation, sheet size, microstructure and among many other factors (Guerrero-Bermea et al., 2017). Mostly, GO is chemically sythesized by exfoliation of graphite with strong acids . Although, GO have some similar structure with graphene by aromatic lattice, its differ from the graphene by alcohols, epoxides, carboxylic groups and ketone carbonyls (Shahriary & Athawale, 2014). These chemical groups improve graphene oxide dispersibility compared to graphene in the solvent (Y. Zhang et al., 2021). Graphene Oxide has been used as an additive to produce PAN-based carbon nanofibers to improve mechanical properties of carbon nanofibers and optimize crystal structure, however agglomeration can be occured by usage large amounts of Graphene Oxide (Y. Zhang et al., 2021).

1.1 Purpose of Thesis

The main purpose of this thesis is to develop polyacrylonitrile based composite nanofibers with polyindole and graphene oxide and investigate the novel materials by electrochemical, spectral and morphological properties. Also one of the aim of this thesis is to improve the electrochemical behaviour of PAN based composites and to represent the importance of stabilization process by during oxidation. It has been very attractive to study on PAN by scientists because of its some excellent properties such as good-spinnability which is very important to produce nanofibers and also being precursor of carbon fibers. Carbon nanofibers produced by oxidation and carbonization steps of electrospun PAN have been used as electrodes in electrochemical cells (S. Chen et al., 2011). The final properties of carbon nanofibers are mostly determined by the precursor material and the steps of conditions of oxidation and carbonization processes (Zussman et al., 2005). In terms of the quality of the carbon nanofiber formed, it is very important to understand the chemical events in the oxidation stage. In this doctoral dissertation, the effects of the oxidation stage, which is the pre-carbonization stage, on nanofiber structure and morphology has been studied with detailed analysis methods in terms of applying different temperature and time.

Conjugated conductive polymers have great interests since their conductivity properties comparable with metals. Conductive polymers have been used many areas such as antistatic coatings, electromagnetic shieldings, corrosion inhibitors, solar cells, biosensors, batteries etc. Their lately invention of improvement the conductivity led the scientists to think about the new composite materials with conductive polymers. However, their unique electrical properties of conductive polymers, nanofibers of these polymers can not be produced easily by electrospinning technique because of their low molecular weight and dielectric properties. Thus, nanofibers of conductive polymers can be obtained by mixing with good-spinnability polymers. To meet this requirements, PAN has choosen as carrier polymer to produce nanofibers with conductive material in this thesis. On the other hand, Polyindole (PIN) is less studied conductive polymer because of its mechanical properties, weakness and low polymerization efficency than polyaniline and polypyrrole. Also, it has some advantages compare to them such as high-redox activity, good thermal stability, and slow degradation rate (Singh, Ohlan, Kotnala, Bakhshi, & Dhawan, 2008; Wan, Li,

Wan, & Xue, 2002; Zhijiang, Xingjuan, & Ruihan, 2013). PIN containing PAN based fibers were produced by electrospinning method which is stated in Chapter 2. Thus, these fibers deposited on ITOPET surface to analyze electrochemical activity against Fe II ions to develope new sensor electrode. It was discussed in Chapter 2 that the presence of Polyindole content showed an electrocatalytic activity against $K_3Fe(CN)_6/K_4Fe(CN)_6$ depending on structure of the organic matrix and preparation process.

On the other hand, graphene is known in the literature with its conductivity and high surface area. Although the conductivity of graphene oxide (GO) is lower than graphene, graphene oxide has much important properties due to its structure. GO has much easier dispersion compared to graphene in the solvent because the presence of some functional groups (hydroxyl, epoxy, carbonyl, etc) on the surface which makes the solution nearly homogenous and prevent the agglomeration of the particules. This thesis includes GO containing PAN based nanofibers (PAN/GO) in which discussed in Chapter 3 and Chapter 4. The effects of graphene oxide (GO) on the nanofiber structure were investigated by producing nanofibers of graphene oxide containing polyacrylonitrile based composites. Oxidative stabilization was performed to these nanofibers which was necessary and critical process to produce carbon nanofibers. Thermal oxidative stabilization of samples was applied under an oxygen atmosphere during 1 h and 3 h, and by changing temperatures (250 °C, 280 °C and 300 °C). Heat was applied to the material during 1h and 3h to investigate the effect of oxidation process on the nanofiber.

2. SYNTHESIS AND ELECTROCHEMICAL INVESTIGATION OF POLYINDOLE BASED FIBER AS SENSOR ELECTRODE BY EIS METHOD[1]

Conjugated conducting polymers have gained much importance in material science in the past 20 years because of the combination of physical and chemical properties oforganic polymers and the electrical characteristics of metals. During the last decade, different methods have been used to prepare one dimensional nanostructures by a number of processing techniques such as drawing (Ondarçuhu & Joachim, 1998), template synthesis (Feng et al., 2002), phase separation (P. X. Ma & Zhang, 1999), self-assembly (G. Liu et al., 1999) and electrospinning (Deitzel, Kleinmeyer, Hirvonen, & Beck Tan, 2001) to improve the sensitivity of the material by increasing the surface area. The electrospinning method known for almost thirty years on industrial use in textile was one of them. These electrospun fibers have been suggested on applications ranging from optical and chemosensor materials (Hohnholz, MacDiarmid, Sarno, & Jones, 2001), nanocomposite materials to scaffolds to tissue engineering, wound dressings, drug delivery systems (Jiang, Fang, Hsiao, Chu, & Chen, 2004), active coatings (Ying Zhu et al., 2007), sensors and actuators (Gu et al., 2009).

Electrospinning is a very simple and cheap method to obtain fibers in the nanoscales. In this method, an electricfield is applied to a polymer solution to obtain polymeric fibers onto a target collector (Baqeri et al., 2015). The electrospinning process can be summarized in five operational categories such as charging of the fluid, formation of the cone-jet, thinning of the jet in the presence of an electrical force, instability of the jet and collection of the jet on to the target (Rutledge & Fridrikh, 2007). Unfortunately, pure conducting polymers can not be directly electrospun related to the highly charged solution. This solution leads to electrical instability and prevents the formation of the

[1] This chapter is based on"**Gergin, İ., Gökçeören, A. T., and Sarac, A. S.** (2015). Synthesis and electrochemical investigation of polyindole based fiber as sensor electrode by EIS method. *Fibers and Polymers*, *16*(7), 1468-1477."

well-known Taylor cone during the process. Besides of in appropriate electrical behavior for electrospinning,pure conducting polymers are inherently brittle which causes mechanical instability. Therefore, conducting polymers are blended with nonconducting host polymers to improve mechanical behavior and the processability of electrospinning. Furthermore, the chemical structure of the host polymer in the composite affects the electron or proton transfers during charge conduction, providing an opportunity to tune the electrical properties of the composite (Low et al., 2015).

Polyindole (PIN) is a conducting polymer, which possesses a good thermal stability, high-redox activity and slow degradation rate properties collected (He, 2004; Zhijiang, Xingjuan, & Ruihan, 2013), in comparison to their antagonist polyaniline and polypyrrole. PIN is one of the many electroactive polymers, which can be obtained by anodic oxidation of indole in various electrolytes (Unal, Sahan, & Erol, 2012). Because of the structural resemblances of indole to pyrrole most of the structure and polymerization mechanism for PIN have been taken from polypyrrole studies (Arjomandi, Nematollahi, & Amani, 2014; Denis Billaud, Humbert, Thevenot, Thomas, & Talbi, 2003; Eraldemir, Sari, Gök, & Ünal, 2008; Pandey & Prakash, 1998; Ryu et al., 2003; Saraji & Bagheri, 1998). Although, PIN films have mainly been synthesized through electrochemical oxidation (Sazou, 2002), chemical oxidation of indole monomer by the direct chemical oxidation in the presence of $FeCl_3$, $CuCl_2$ or $(NH_4)_2S_2O_8$ (Joshi & Prakash, 2012; Taylan, Sari, & Unal, 2010) has also been reported. PIN has found usage in various areas; such as electronics, microwave absorbing materials, anode material in batteries, anticorrosion coatings, photovoltaics and supercapacitor applications (J.-J. Cai, Zuo, Cheng, Xu, & Yin, 2010; Rajasudha et al., 2011; Saleh, Chandra, Christian Kemp, & Kim, 2013; Sanchez, Julián, Belleville, & Popall, 2005). In spite of the described advantages, PIN has comparatively been less studied in accordance to analogue conductive polymers, as indole monomer has low polymerization efficiency with chemical oxidants and poor mechanical properties due to its tendency on forming a powdery product (Singh et al., 2008; Wan et al., 2002). But, a recent application has found usage of PIN as a fiber polymer electrode for lithium ion secondary battery (Zhijiang, Xingjuan, & Yanan, 2013).

On the other hand, Polyacrylonitrile (PAN) is a well-known polymer widely used for commercial studies with good-stability and mechanical properties. PAN and its copolymers are intensely used in textile industry in the form of fiber. Besides its good

spinning capability, its environmental nature and commercial practicality were also very importantto produce their fibers (Cetiner, Kalaoglu, Karakas, & Sarac, 2010). The obtained smart textile products are mainly used for industrial applications, such as microwave absorbing, electrostatic discharge, electromagnetic interference (EMI) shielding, and sensor applications (Devaux et al., 2007; Mičušík et al., 2007; Molina, del Río, Bonastre, & Cases, 2008).

Iron is a key element in industrial, environmental, medical applications and in biological studies (Lieu, Heiskala, Peterson, & Yang, 2001) also crucial for the human health. Generally, 1-1.5 mg of iron is ingested by the nutriments taken through a day. Although, ferrous iron in food and pharmaceuticals could be directly assimilated, ferric iron must be used after being reduced to ferrous (Q. Chen, 1989) structure. The presence of iron has even or odd impacts on different biological systems varying from cellular levels to mammal beings. It plays a crucial role for the transportation and storage of oxygen to the tissues with hemoglobin and electron transport with myoglobin and also in enzyme activities (Mahmoud, 2001). The absence of iron in the organism causes anemia, resulting by a decrease in red blood cell number. Iron deficiency anemia is one of the world' s most common nutritional diseases (Musser, R.D., O'Neil, 1969), while the excess of iron during treatment with iron salts may produce severe poisoning such as gastric irritation, vomiting, paleness and vascular failure.

Conducting polymers are good candidates for battery applications because of their high electronic conductivity and reversible redox-active chemistry. In particular p-doped polymers frequently reported as electroactive organic electrode materials for rechargeable batteries and for supercapacitors.

Due to chemical affinity of iron ion and electronegative N atom of polyindole, doping of polyindole matrix with redox active ions, i.e. ferrocene (in addition to use of iron chloride and inclusion in the polymer matrix during the synthesis) where the doped ions can act as counter ion dopant to enhance the electronic conductivity of polymer chain and function as redox active site to add their capacity to the doped polyindole. This will help for the redox mechanism of polymer for p-doping -dedoping during the cycling.

In this investigation, we report the synthesis and characterization of electrospun solution mixture of PIN with PAN acting as carrier in order to improve PIN processability to obtain fibers. PAN was used as carrier because of its known good mechanical properties, high-impact strength and good thermal and oxidative stabilities.

Electrochemical impedance spectroscopy (EIS) has proved to be a valuable technique for determining the properties of the obtained fiber electrodes by a single experiment giving information on charge transfer resistance, double layer and specific capacitances. The importance of Fe(II) in food and pharmaceuticals has obliged different methods for the determination of Fe(II) such as electron spin resonance, UV-vis spectrophotometry, fluorometric analysis, controlled-potential coulometry and ion selective electrodes (Aglan, Rizk, Mohamed, El-Wahy, & Mohamed, 2014; Fung & Fung, 1977; Kozlov, Yegorov, Vladimirov, & Azizova, 1992; Sil, Ijeri, & Srivastava, 2005; Teixeira, Aniceto, & Fatibello-Filho, 1998; Tesfaldet, Van Staden, & Stefan, 2004; Waite & Morel, 1984; G. Zhu, Zhu, &G. Zhu, Zhu, & Qiu, 2002).

On beyond the use of Fe(II) ions to verify the electrocatalytic activity of the electrode, the possibility of EIS to be an alternative technique to determine accurate Fe(II) concentration was also investigated as a part of the present work.

2.1 Experimental

2.1.1 Materials

The monomer, indole (IN; Aldrich), and Polyacrylonitrile (PAN; Sigma-Aldrich) were used without further purification. Anhydrous Iron Chloride ($FeCl_3$; BDH Chemicals Ltd.) was chosen as an initiator. Dimethylformamide (DMF; Sigma- Aldrich), Acetonitrile (ACN; Sigma), Chloroform ($CHCl_3$; Sigma-Aldrich) were chosen as solvents.

2.1.2 Analysis and characterization techniques

PAN and PAN/PIN fibers were analyzed and characterized by using Attenuated total reflection-Fourier transform infrared spectroscopy (ATR-FTIR), differential scanning calorimetry (DSC), cyclic voltammetry (CV) and electrochemical impedance spectroscopy (EIS) conductivity measurements. FTIR spectra of the samples were

recorded on Perkin Elmer Spectrum One (FTIR-reflectance, Universal ATR with diamond and ZnSe) spectrophotometer using the samples in powdered form. DSC was performed on a TA DSC-Q10 under a continuous flow of nitrogen in a flowing nitrogen atmosphere, by heating from 30 °C to 340 °C and the thermograms were recorded at a heating rate of 20 °C/min. The glass transition (T_g) and melting (T_m) temperatures of the samples were determined by this method. The AFM images were obtained with Nanosurf Easy Scan 2™. In all AFM analyses, the non-contact mode was employed by using ACLA-20 model, Al-coated high resonance frequency silicon tips (145 kHz) with 7 μm thicknesses, 43 μm mean width, 225 μm length and 48 N/m force constant. High resolution images (1024×1024 pixels) and the raw data were collected by the Easy Scan 2™ (version 1.5.0.0.) software.

Cyclic voltammograms (CVs) were obtained between -0.5 V to 0.5 V at the scan rate 50 mV/s by using a Parstat 2263 potentiostat. Fibers were chosen as the working electrode which were deposited on Indium-tin-oxide coated Poly(ethylene terephthalate) (ITO-PET) semi-transparent and flexible surface, platinum (Pt) wire was used as the counter electrode, and a silver (Ag) wire as the pseudo-reference electrode were used for all electrochemical characterizations in aqueous solution with 0.1 mol/l $NaClO_4$ supporting electrode system. All fibers were doped before analysis at 1.0 V for 10 minutes. The electrochemical activity of the fibers was evaluated from the current-voltage curves obtained by cyclic voltammetry. The conductivities of the materials were also calculated from the data obtained by EIS in the frequency of 10 mHz to 10 kHz. The experimental data was used to fit the equivalent circuit with ZSimpwin 3.10 software.

2.1.3 Preparation of Polyindole (PIN) homopolymer

Polyindole was synthesized chemically using $FeCl_3$ as an oxidant (Eraldemir et al., 2008). The molar ratio of oxidant to monomer was taken as equal. The oxidant was dissolved in $CHCl_3$. The monomer dissolved in $CHCl_3$ was added dropwise into the oxidant solution. The reaction was pursued under nitrogen atmosphere for 12 hours. The obtained polymer was collected by filtration and then washed with distilled hot water (90 °C) to remove any unreacted indole monomer. The black colored precipitate was dried in vacuum oven at 70 °C for 24 hours.

2.1.4 Preparation and electrospinning of Polyacrylonitrile (PAN)/PIN fibers

The PIN fibers were prepared by electrospinning method using a mixture of PAN (10 wt/v %) and PIN (at different wt/v %) blend in DMF solution. The solution was mixed using a magnetic stirrer for 24 hours at room temperature and was notated as PAN/PIN. Blend solutions were poured into a 2 ml syringe and delivered at a constant flow rate of 0.5-2.0 ml/h (New era, NE-300) to a needle with a blunt tip connected to a high voltage power supply (Gamma high voltage research) producing a voltage of 15 kV. The solvent evaporates and charged polymers were deposited on the aluminum foil collector at a distance of 19 cm, in the form of fibers. The obtained fibers were scraped off from the aluminum surface and vacuum-dried until additional solvent residue evaporated for morphological analysis. The fibers were obtained on ITO-PET electrode surface for electrochemical analysis and notated as S0-S5 (0.0, 0.2, 0.5, 1.0, 1.5 and 2.0 wt/v%). Samples S1f, S2f and S3f were prepared at similar condition and contents with spin-coating method on ITO-PET electrode surface.

2.2 Results and Discussion

2.2.1 Morphological analysis

The AFM and SEM micrographs of samples S0-S5 are shown in (Figure 2.1). All fiber samples were obtained at 30 sec. electrospinning condition on ITO-PET surface. As it can be seen from the AFM micrograph, S0 (Figure 1(a)) had a more dense structure, while the S4 blend fiber shown in (Figure 1(b)) had a more uniform structure.

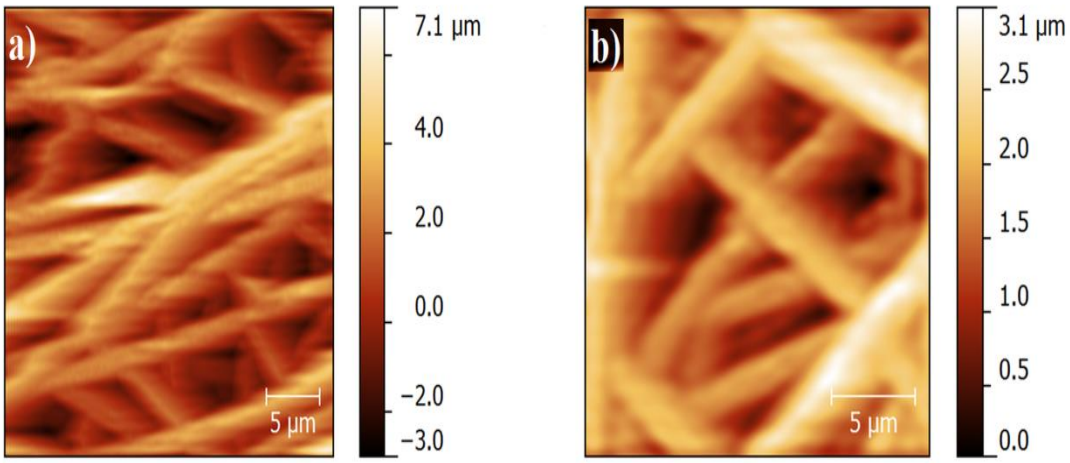

Figure 2.1 : AFM micrographs of (a) S0 and (b) S4 fibers.

The SEM micrograph seen in (Figure 2.2 (b)-(f)) for PAN/PIN shows a fibrin formation with wider diameter dispersion at high PIN content. The S2, S4 and S5 showed a similar structure, while the S3 sample showed a decrease in fiber diameter.

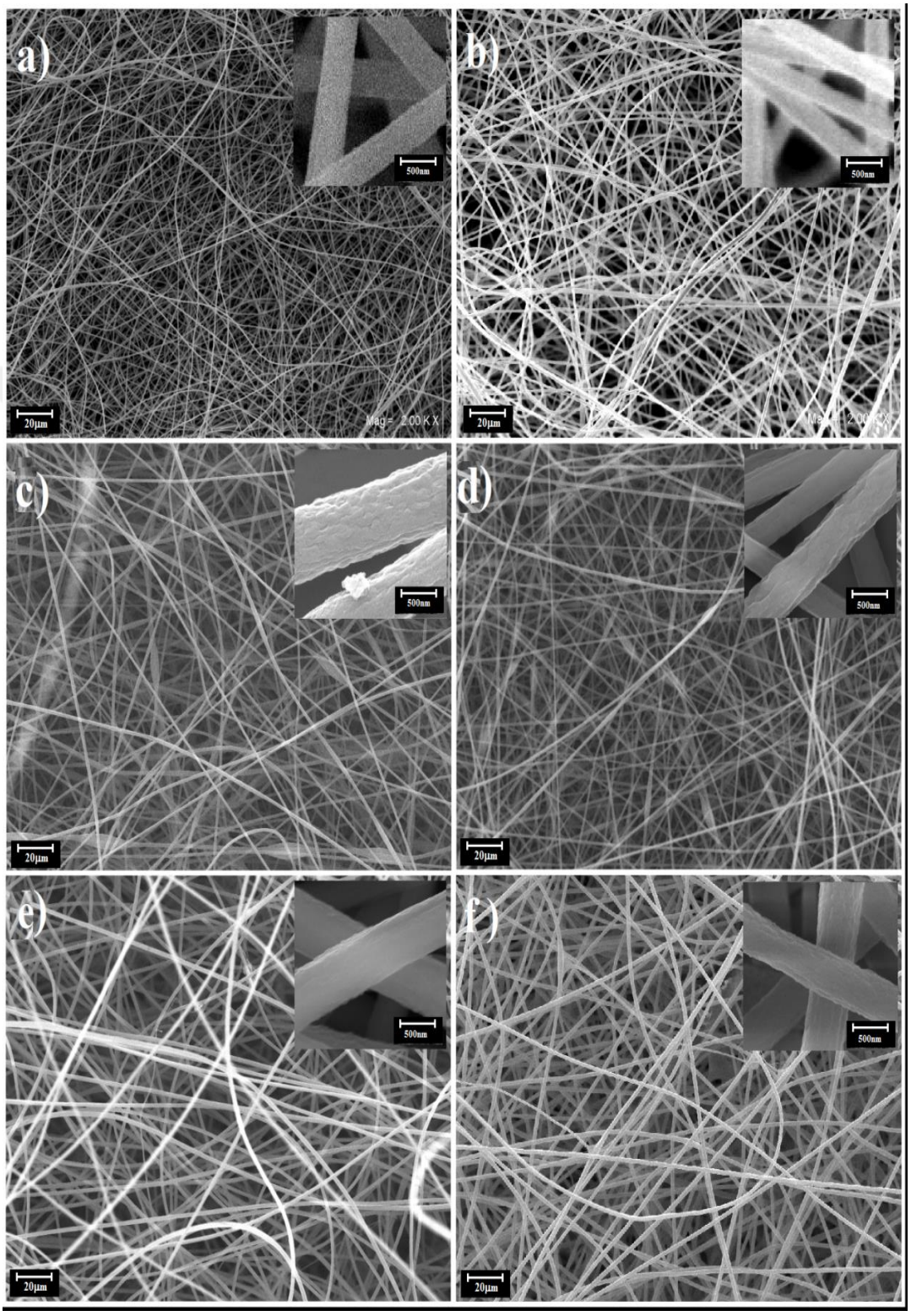

Figure 2.2 : SEM micrographs of (a) S0, (b) S1, (c) S2, (d) S3, (e) S4, and (f) S5 fibers. Insets: at higher resolution.

Fiber diameters were measured within electron micrographs from a population of fifty fibers taken from each sample and then the average values were calculated. SEM micrographs of different samples containing different PAN/PIN ratios (S0-S5) can be seen in (Figure 2.2). As seen from (Figure 2(a)), the PAN fibers have a smooth surface with a diameter range of 371.61±36 nm (Figure 2.3) and increased systematically with the PIN content (S1: ø 529 nm, S4: ø 694 nm). On the other hand it showed a deviation from this linearity by a decrease in thickness with a diameter range of 505.61± 55 nm at 1.0 wt/v % PIN content sample (S3) leading to a higher surface area.

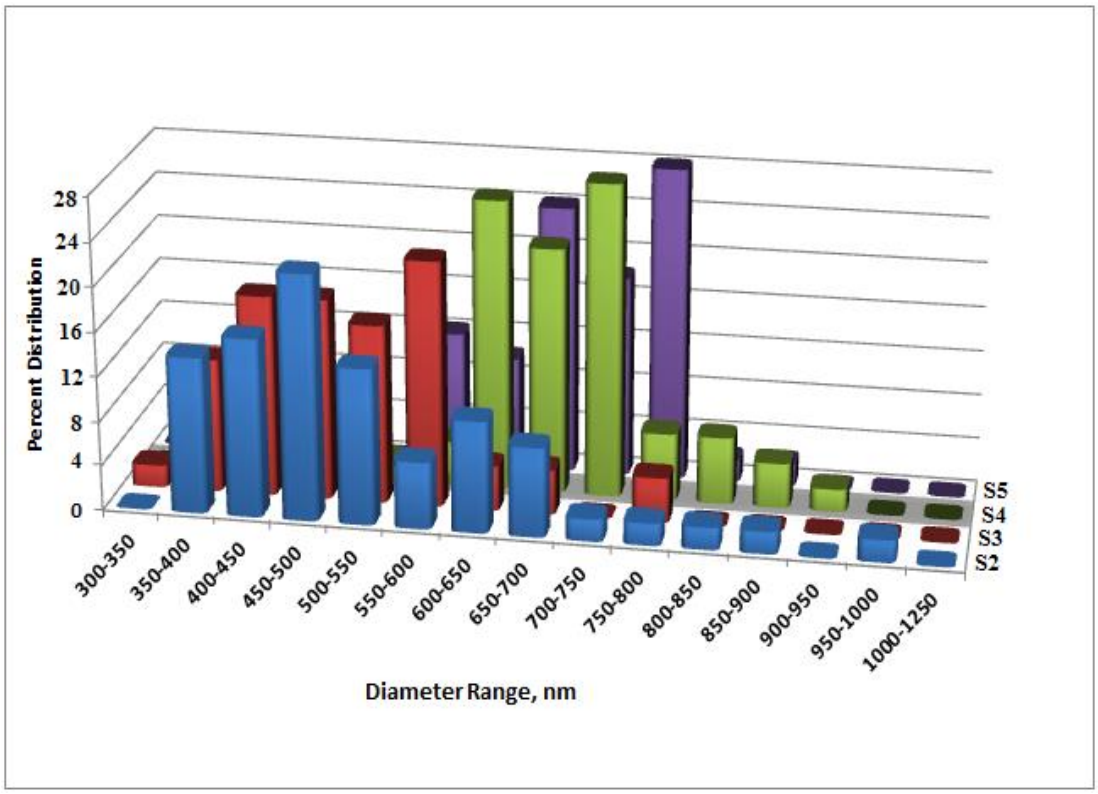

Figure 2.3 : Fiber diameter distribution for the S2, S3, S4, and S5 samples.

2.2.2 Thermal and FTIR analysis

According to (Figure 2.4), a double endothermic transition at about 67.6 °C (T_{g1}) followed by a baseline shift at about 122.7 °C (T_{g2}) is observed for PAN homopolymer, which is in accordance with the literature (Bajaj, Sreekumar, & Sen, 2001). While, a sharp single exothermic peak (T_m=314 °C) is observed between 255 °C and 326 °C revealing the well-known free radical cyclization reaction mechanism. A new glass transition peak at 45 °C and a melting peak at 105 °C related with the presence of indole content for S2 and S4 fiber samples are observed. The PAN showed a close interaction with indole moieties. The T_m shifted to higher temperature (324 °C) due to

a stronger nitrile polar interaction for PAN while T_{g2} shifted to a lower value (104 °C) and the T_{g1} peak vanished. The T_g peak related to indole moieties showed a non-apparent difference with the content ratio. On the other hand, S3 showed a deviation from this behavior by an increase in T_{g1} (69 °C) and T_{g2} (128 °C), while T_m remains almost stable (~318 °C).

On the other hand, the FTIR absorbance spectra shown in (Figure 2.5) provide evidence to the presence of PIN and PAN contents on the obtained fibers. The bands with peak locations at 1458 cm^{-1} and 1364 cm^{-1} are attributed to the C=C bond (stretching) and to the C-N bonds for both PIN and PAN moieties.

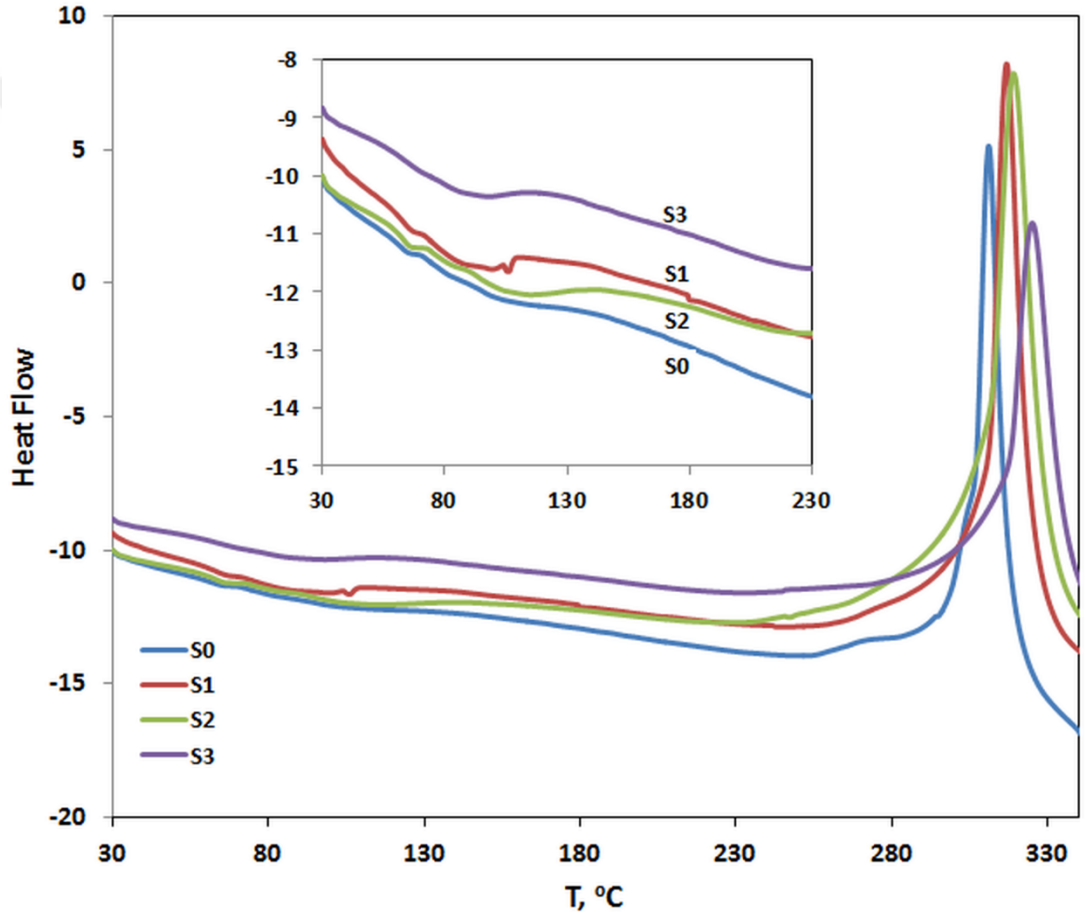

Figure 2.4 : DSC thermographs of S0, S1, S2, and S3 fiber samples by heating from 30 °C to 340 °C at a heating rate of 20 °C/min.

The band with peak position at 2941 cm^{-1} and 775 cm^{-1} corresponding to the C-H stretching vibration of the CH_2 and CH groups on the main chain are characteristic for PAN (Figure 2.5(f)). While, a series of bands at 3619, 1666, 1256 and 1069 cm^{-1} are related to the amid N-H and C-N stretching bond. The nitrile (C≡N stretch) bonding peak observed at 2246 cm^{-1} is distinctive for PAN. The peak at 1256 cm^{-1} related to

PAN decrease with increasing PIN content. On the other hand, the peaks related to the N-H stretching vibration observed at 1604 cm^{-1} and to the C-H out-of-plane deformation of the vinylidene group at 775 cm^{-1} shift to 1666 cm^{-1} and 739 cm^{-1} with increasing PIN content (Figure 2.5(a)). Unfortunately, the FTIR spectra show no apparent peak shift as evidence on the interaction between PAN, PIN and DMF, as spotted from the DSC measurements.

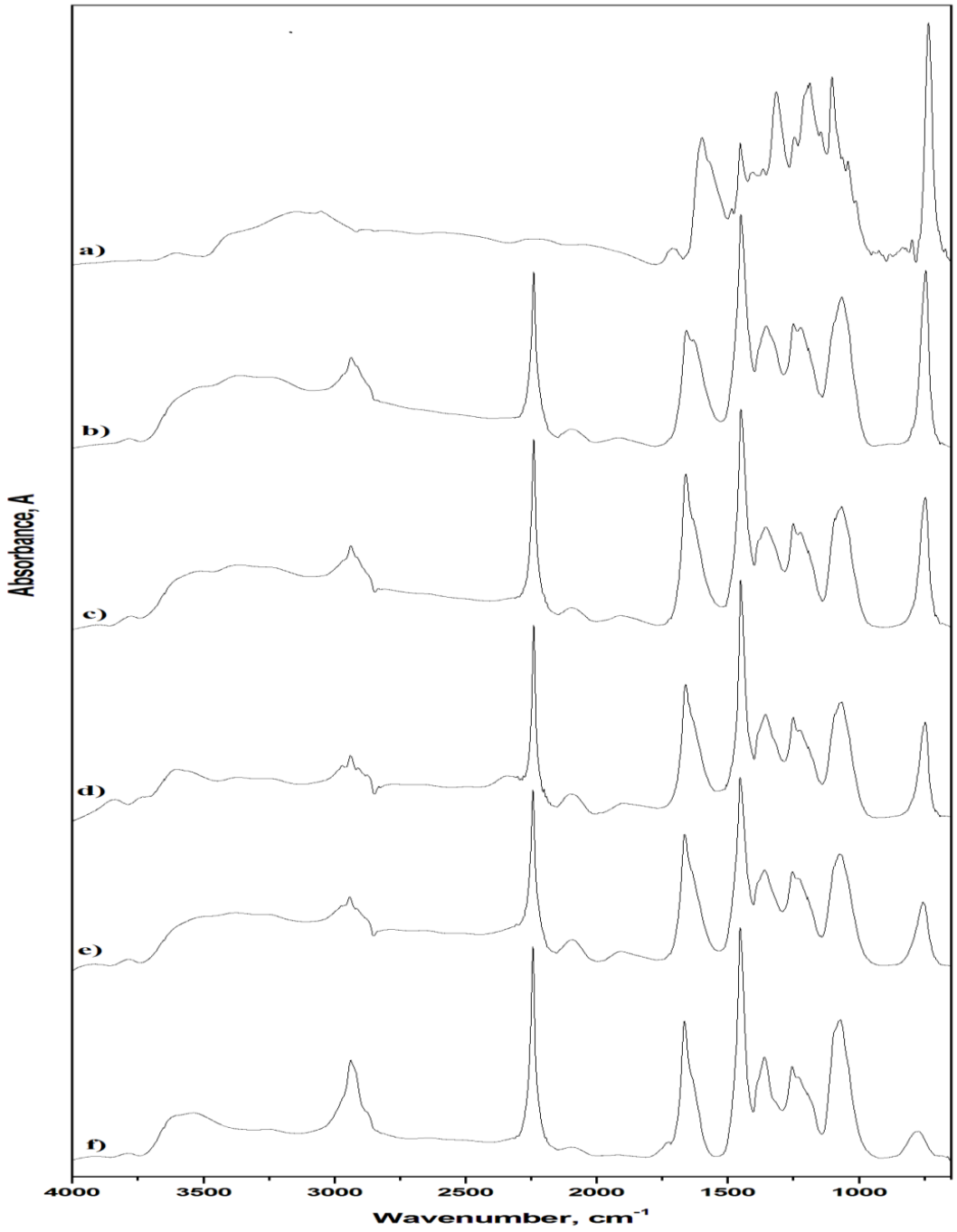

Figure 2.5 : FTIR spectra of PIN homopolymer (a), PAN/PIN (b-e) blends and PAN (f) fibers.

2.2.3 Electrochemical analysis of fiber and thin film PAN/PIN blends

The S0 and S2-5 blend fiber electrodes electroactive behaviors were determined in 0.1 M $NaClO_4$ supporting electrolyte containing aqueous solution. The EIS measurements showed the effect of the PIN content in the fiber electrode (Figure 2.6) and (Figure 2.7). The Nyquist diagram in (Figure 2.6) shows the fiber working electrode interaction with the solvent, which involves a two-step semi-circular structure. The first semicircle is related to the double layer capacitance (C_{dl}) and the charge transfer resistance (R_{ct}). The second semicircle was related to the electrode behavior, depending on the PIN content and preparative conditions of the fiber. The double layer capacitance is calculated from the Zim and the frequency (f) at the maximum point value of the first semi-circle given by the relationship $C_{dl} = 1/(2\pi f Z_{im})$.

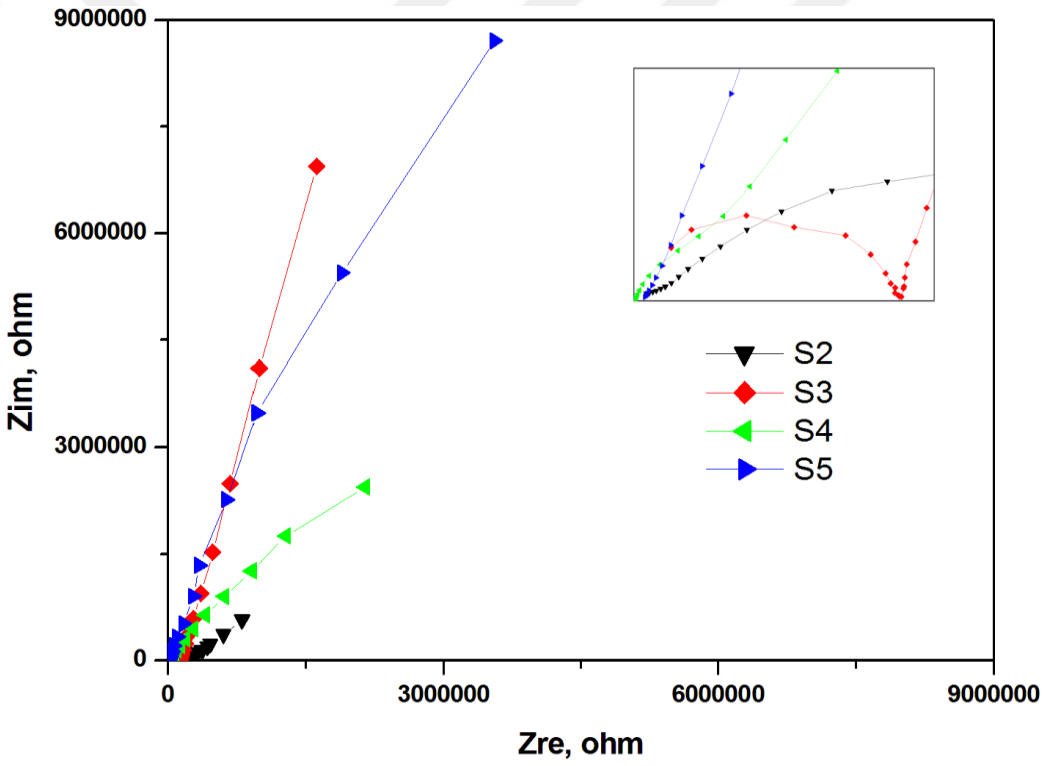

Figure 2.6 : Nyquist plots of S2, S3, S4 and S5 fibers. The enlarged data in high frequency are shown in inset. Symbols Zre and Zim refer to the real and imaginary components.

The simulated equivalent circuit models (with ZsimpWin software) were compared with the experimental results obtained from the Nyquist and Bode phase plots (R_{sol}, C_{dl} and R_{ct}) are given in (Table 2.1). The results showed two different circuit modelling. A R_{sol} ($Q_{dl}R_{ct}$) ($Q_{el}(R_{el}W_{el})$) equivalent circuit model was suited for samples S2, S4 and S5, while a R_{sol} ($Q_{dl}R_{ct}$ ($Q_{el}(R_{el}W_{el})$)) equivalent circuit model was defined

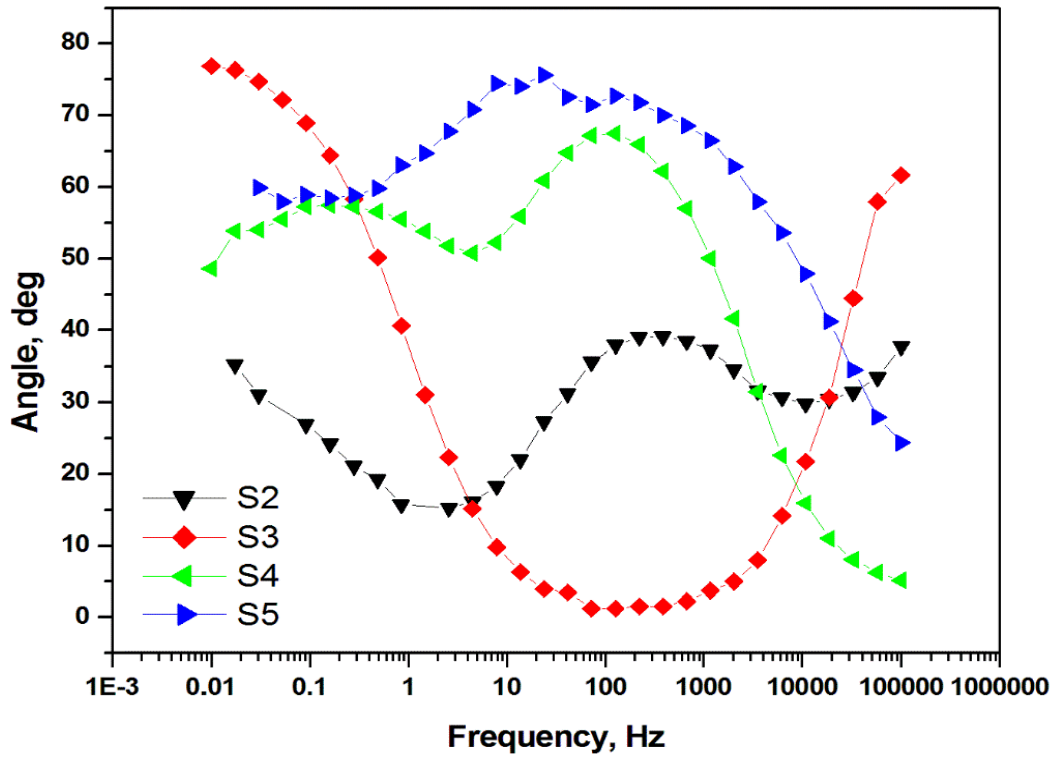

Figure 2.7 : Bode phase plots showing change in phase angle for S2, S3, S4 and S5 fibers.

for the S1f, S2f, S3f and S3 electrodes, with χ^2 defined as the sum of the squares of the residuals minimized to ~10^{-4} error are given in (Table 2.2). R_{sol} corresponded to the solution resistance, Q_{dl} and R_{ct} corresponded to the double layer phase element and charge transfer resistance with the electrode surface and the solution interface. While Q_{el} and R_{el} corresponded to the fiber and ITO-PET electrode capacitance and resistance combined.

The Q_{dl} double layer capacitance values were found to have a minima with increasing PIN content Q_{dl}=0.14 µF for S2, Q_{dl}=4.84×10^{-5} µF for S3, Q_{dl}=0.47 µF for S4 and Q_{dl}=0.02 µF for S5 in (Table 2.1). According to the Bode phase plot (Figure 2.7) the samples S2, S4 and S5 indicated a similar pattern, while S3 showed a totally different behavior. For samples S2, S4 and S5 the phase angle had two visible plateau regions.

The first region observed at 100 Hz-10 kHz frequencies increased with PIN content with a phase angle of 68°, while sample S3 had almost 0° angle in the same region. The second region observed at 100 mHz-1 Hz increased with a shift at higher frequency with the PIN content.

Table 2.1: EIS data simulations for S2, S4 and S5 fibers in aqueous solution.

Sample	R_{sol} ($\Omega.cm^{-2}$)	Q_{dl} (*C_{dl}) ($\mu S.s^{-n}.cm^{-2}$)	n	R_{ct} ($\Omega.cm^{-2}$)	Q_{el} (*C_{el}) ($\mu F.cm^{-2}$)	n	R_{el} ($\Omega.cm^{-2}$)	W_{el} ($\mu S.s^{-0.5}.cm^{-2}$)	χ^2 ($x10^{-3}$)
S2	4135	0.14	0.6325	$24.1x10^{3}$	$*5.89x10^{-4}$	-	$6.5x10^{3}$	4.03	1.483
S4	577.8	*0.47	-	$25.3x10^{3}$	1.78	0.7213	$5.31x10^{3}$	0.91	1.041
S5	5272	*0.02	-	$9.9x10^{3}$	$1.88x10^{-2}$	0.7723	$8.22x10^{8}$	$8.29x10^{-3}$	3.630

Table 2.2 : EIS data simulations for S1f, S2f, S3f and S3 fibers in aqueous solution.

Sample	R_{sol} ($\Omega.cm^{-2}$)	Q_{dl} (*C_{ITO}) ($\mu S.s^{-n}.cm^{-2}$)	n	R_{ct} ($\Omega.cm^{-2}$)	Q_{fib} (*C_{ITO}) ($\mu F.cm^{-2}$)	n	R_{fib} ($\Omega.cm^{-2}$)	W_{fib} ($\mu S.s^{-0.5}.cm^{-2}$)	χ^2 ($x10^{-4}$)
S1f	4669.5	$6.819x10^{-3}$	0.6911	$62.8x10^{3}$	11.18	0.9076	$803.7x10^{3}$	0.11	8.244
S2f	2446	$3.845x10^{-3}$	0.7369	$37.2x10^{3}$	6.77	0.823	$170.9x10^{3}$	7.64	16.71
S3f	1962.5	$4.38x10^{-3}$	0.7168	$27.6x10^{3}$	0.88	0.8103	$112.6x10^{3}$	8.58	8.790
S3	8884	$4.84x10^{-5}$	-	$121.5x10^{3}$	1.57	0.8507	$7.23x10^{14}$	–	25.95

Specific capacitance calculated from $C_{sp}=1/2\pi fZ_{im}$ at 10 mHz frequency, showed higher capacitive value for S2 due to the high porous surface (Figure 2.2(c) inset) with 30.7 $\mu F \cdot cm^{-2}$, while the capacitances were calculated for S3 with 2.3 $\mu F \cdot cm^{-2}$, S4 with 6.5 $\mu F \cdot cm^{-2}$, S5 with 1.8 $\mu F \cdot cm^{-2}$, S0 with 12.4 $\mu F \cdot cm^{-2}$ and for S1 with 11.3 $\mu F \cdot cm^{-2}$. The specific capacitance of S2 showed the highest value, while S5 had the lowest capacitance. On the other hand, sample S4 and S5 had a value lower than PAN fiber (S0) itself. This could be explained by the amorphous and porous structure of the fiber at low PIN content giving a higher surface and increasing the specific capacitance, but this behavior had an optimum point, since the sample S3 with the lowest diameter should have the highest capacitive behavior, but when the pore size is decreased, there is less and less space available for double layer charging since ions can not get into the smallest pores; as a consequence the capacitance is decreased (Largeot et al., 2008). This behavior was also found to be consistent with the different equivalent circuit modelling element (i.e. R_{sol}, R_{ct} and Q_{dl}) values as shown in (Figure 2.8).

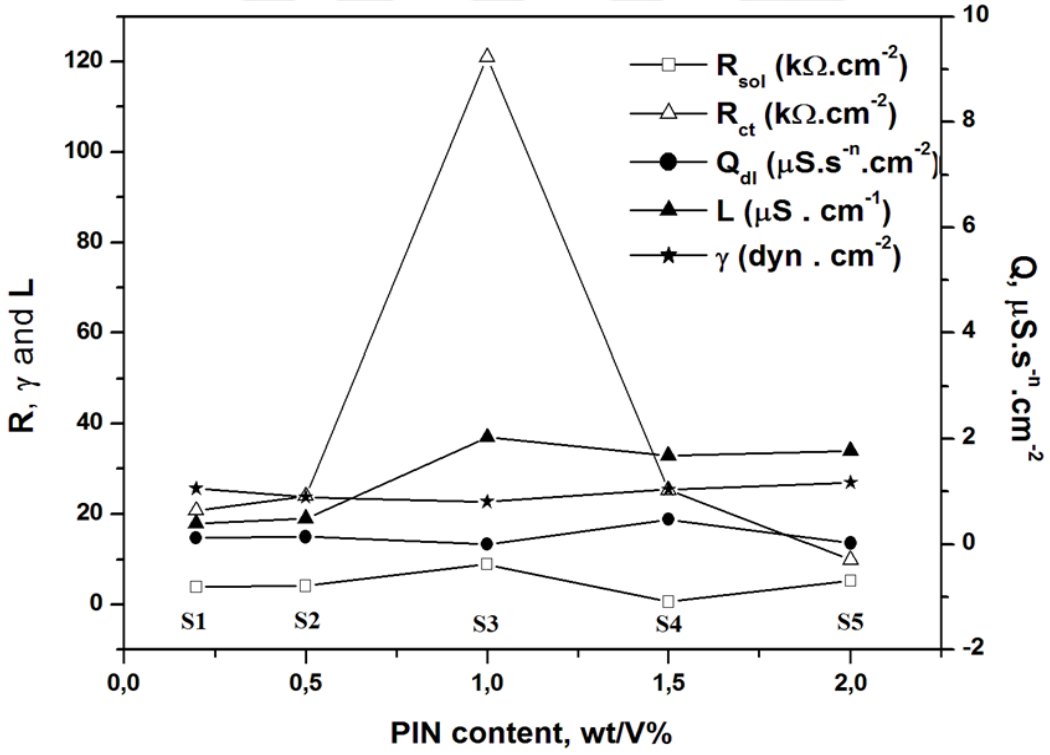

Figure 2.8 : Effect of PIN content on solution surface tension (γ), solution conductivity (L), double layer capacitance (Q_{dl}) and fiber charge transfer (R_{ct}) and solution (R_{sol}) resistances.

The R_{ct} value for PAN (1.4×10^{6} $\Omega \cdot cm^{-2}$) is higher than the PIN incorporated PAN fibers, which was consistent with the insulating character of polyacrylonitrile giving a

more resistive property. The charge-transfer resistance of the PIN composite (PAN/PIN), is much smaller than that of PAN because of the formation of a better charge-transfer complex, an increase in electrical conductivity and an increase in surface area (Aglan et al., 2014).

The electrochemical characteristic of those fiber samples were also compared with the spin-coated film samples (S1f, S2f and S3f). (Figure 2.9), (Figure 2.10) and (Table 2.2) shows the EIS results of the obtained samples at similar conditions. The Q_{dl} double layer capacitance values were found to decrease with increasing PIN content (Q_{dl}=6.82 $nS \cdot s^{-n} \cdot cm^{-2}$; n: 0.6911 for S1f, Q_{dl}=3.84 $nS \cdot s^{-n} \cdot cm^{-2}$; n: 0.7369 for S2f and Q_{dl}= 4.38 $nS \cdot s^{-n} \cdot cm^{-2}$; n: 0.7168 for S3f). The Bode phase plots (Figure 2.10) for S1f, S2f and S3f samples have a similar behavior with the S3 fiber sample. An analogous plateau region with 0^o at 100 Hz-10 kHz frequency region is observed, while a second region is also perceived at 100 mHz-1 Hz shifting to 10 Hz at high PIN content. Those results confirm that the sample S3 electrode surface shows similarity with the film coated S1f-S3f samples. The dense and high surface area generated by the low fiber diameter covers the ITOPET surface more accurately, rendering more difficult the diffusion of solvent molecules to the electrode surface.

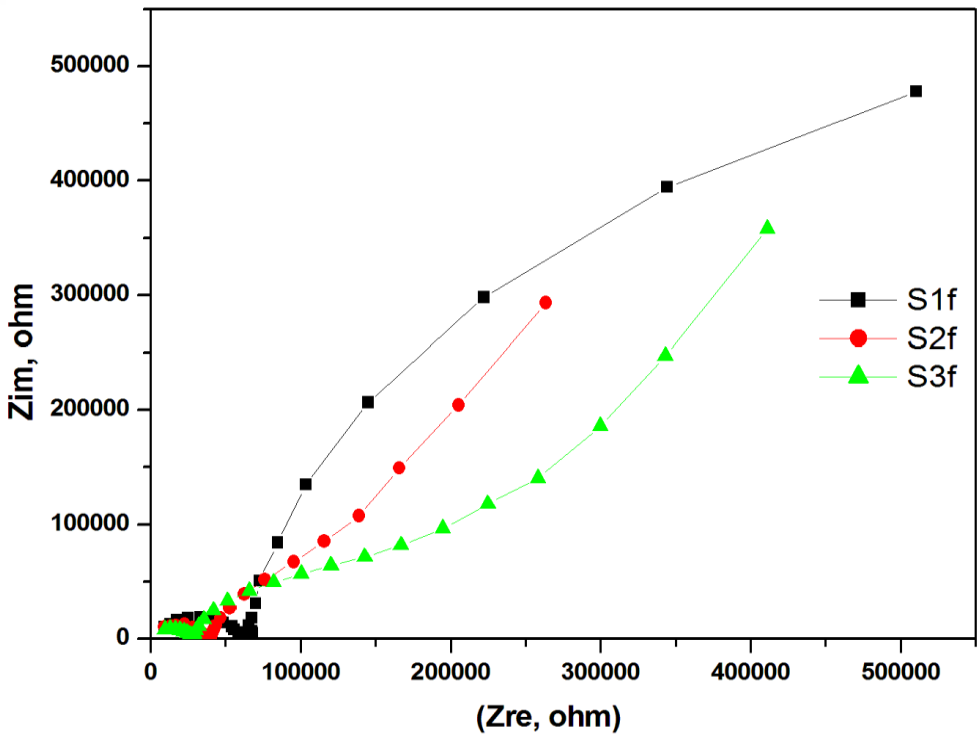

Figure 2.9 : Nyquist plots of S1f, S2f, S3f solvent cast films.

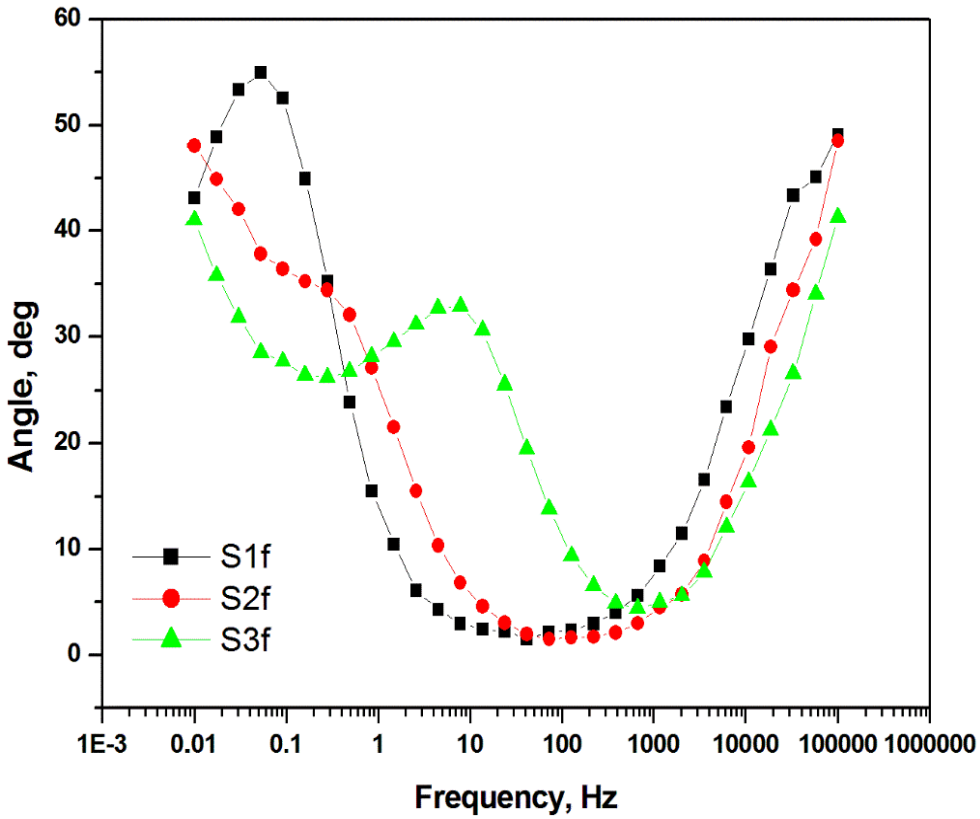

Figure 2.10 : Bode phase plots showing change in phase angle for S1f, S2f, S3f solvent cast films.

Table 2.3 : Surface Tension obtained for PIN and PAN/PIN solutions.

Concentration (mol.l^{-1})	0.0%PIN	0.2%PIN	0.5%PIN	1%PIN	2%PIN
10 wt% PAN/DMF (dyne.cm^{-2})	23.37	26.34	26.77	27.44	26.53
DMF (dyne.cm^{-2})	26.24	25.68	23.77	22.78	27.01

2.2.4 Surface tension and solution conductivity measurements

As it can be seen from the surface tension results given in (Table 2.3), PIN solutions shows a minimum at 1.0 wt% PIN content. This behavior is inversely confirmed with a maximum at 1.0 wt% PIN solution in the presence of 10 wt% PAN content and found to be in harmony with the solvent conductivity measurements (Figure 2.8). The fiber diameter also showed a similarity with a minimum at PAN/PIN (10/1.0) content.

Those behaviors could be elucidated by the interaction of DMF with PIN and PAN binary and ternary complexes occurring via the hydrogen bonding between the H and the N atoms. PIN showed a surface active emulsifier material behavior as it lowers the

surface tension by the increasing content. The surface tension lowers until 1.0 wt% PIN and increase at excess content showing a critical micelle concentration behavior in DMF. While, there is a linear correlation for DMF and PAN, as PAN is a surface inactive material (Table 2.3). On the other hand, by the addition of PAN to the PIN solution a new interaction is seen between DMF-PIN and PIN-PAN strands. The bond relations between PIN-PAN intensify, while the Van der Waals interaction between DMF-PIN diminishes. Those results by an increase in surface tension with increasing PIN content. But, the surface tension shows a decrease at 2.0 wt% PIN content as the surfaceactive PIN content overcome the PAN quenching behavior.This behavior observed with the surface tension had a direct impact on the fiber diameter. These properties were previously investigated by our group (Cetiner et al., 2010) and have shown their direct influence on the fiber diameter and in accordance on electrochemical behaviors.

2.2.5 Electrocatalytical activity of PIN fiber

2.2.5.1 Cyclic voltammogram results

The sensitivity of the manufactured electrodes against an internal standard chemical with electron redox ability such as Ferrocene, H_2O_2 or $K_3Fe(CN)_6/K_4Fe(CN)_6$ is a common method (Gagne, Koval, & Lisensky, 1980; W. Xu et al., 2014). The potential response of Fe(II) ions were examined to determine the electrochemical activity of the obtained fibers. A quasi-reversible peak is observed for sample S5, while no sensitivity was observed for PAN and ITO-PET electrodes as seen from the (Figure 2.11) inset. The oxidation peak currents were found to differ linearly with the scan rate in the range of 50-1000 mV/s ($r>0.9739$), which indicates a thin film formation of the reactant on the electrode solution interface (Figure 2.11).

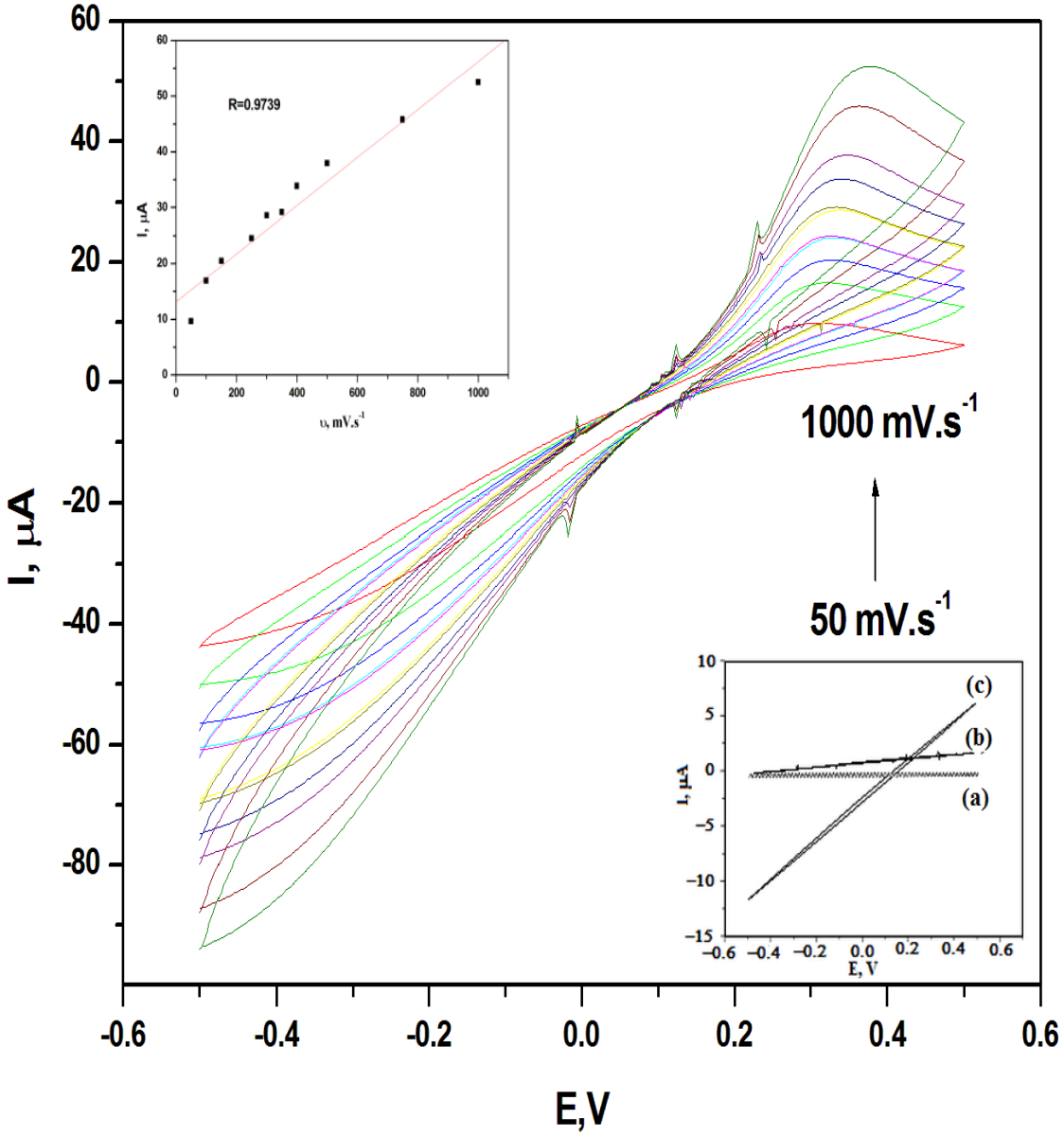

Figure 2.11 : Cyclic voltammograms of S5 fiber sample in 0.1 M $K_3Fe(CN)_6$ aqueous solution at different scan rates (insets: CV for (a) ITO bare electrode in aqueous solution, (b) S0 fiber electrode, and (c) ITO bare electrode in 0.1M $K_3Fe(CN)_6/K_4Fe(CN)_6$ aqueous solution).

2.2.5.2 Electrochemical Impedance Spectroscopy (EIS) results

EIS has been employed to study the interfacial properties of the modified electrodes in the presence of Fe(II) ions. Nyquist and Bode Phase plots were given for S5 electrode in the frequency range of 0.01 Hz to 10.0 kHz (Figure 2.12) and (Figure 2.13). The impedance spectra was recorded using 0.1 M $K_3Fe(CN)_6/K_4Fe(CN)_6$ (Merck Chemicals, USA) containing stock aqueous solution. All the impedance measurements were carried out using open circuit potential. The information regarding electron transfer kinetics and diffusion characteristics will be obtained from the shape

of the impedance spectrum. The semicircle portion and linear portion of the impedance spectra respectively correspond to the electron transfer limiting and diffusion limiting electrochemical processes. EIS of the S5 fiber sample electrocatalytic activity was investigated at different iron concentrations.

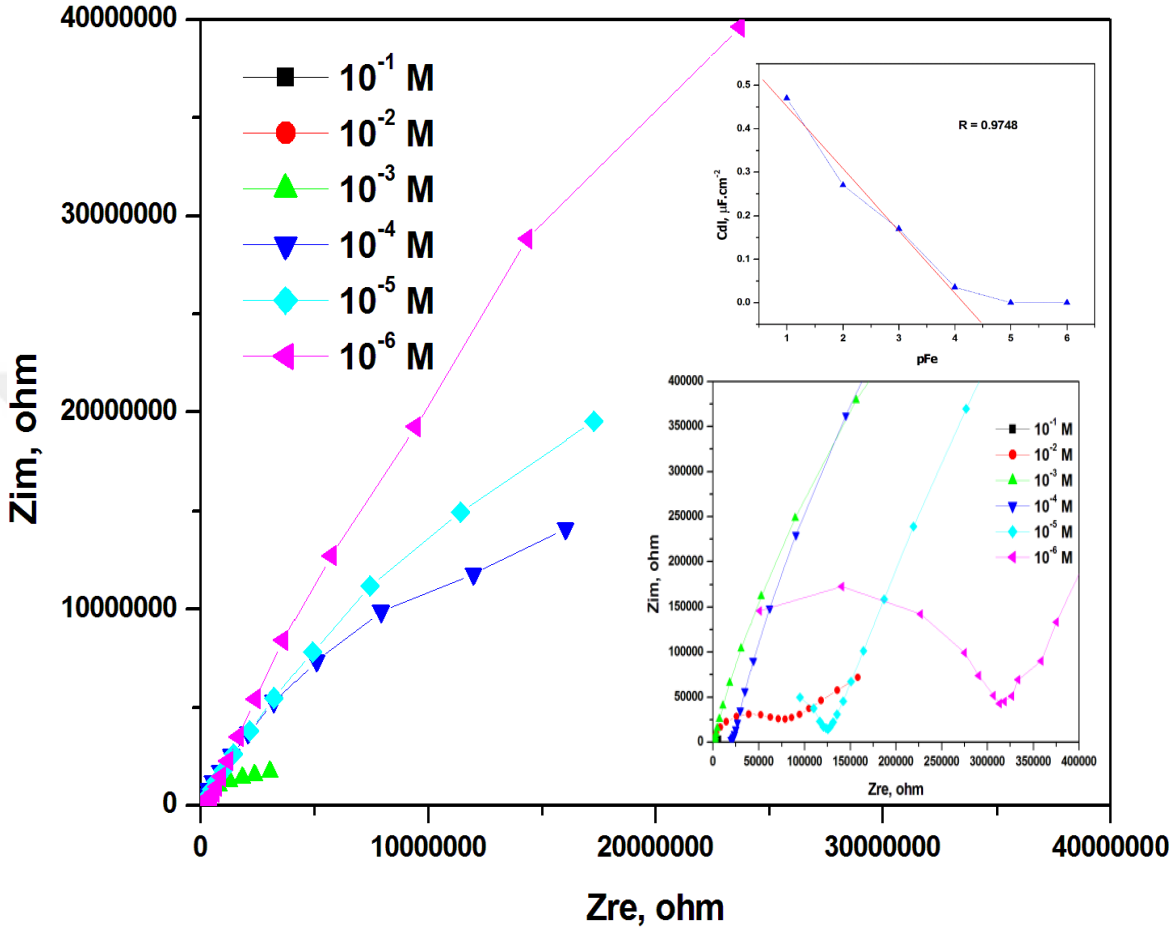

Figure 2.12 : Nyquist plots of S5 fiber at different $K_3Fe(CN)_6/K_4Fe(CN)_6$ concentrations, in aqueous solution. The enlarged data in (a) high frequency and (b) the double layer capacitance (C_{dl}) dependency with pFe (the reciprocal logarithm of $K_3Fe(CN)_6/K_4Fe(CN)_6$ concentrations, in aqueous solution are shown in inset. Symbols Zre and Zim refer to the real and imaginary components.

The simulated equivalent circuit model compared with experimental results is shown in (Table 2.4). The results showed a $R_{sol}(C_{dl}(R_{ct}(Q_{el}(R_{el}W_{el}))))$ equivalent circuit model, with χ^2 defined as the sum of the squares of the residuals minimized to ~10^{-4} error. R_{sol} decrease with the increasing iron ionic strength acting as supporting electrode. The C_{dl} and R_{ct} were affected inversely with the increasing iron concentration. The charge transfer resistance for S5 in aqueous solution shows a large semicircle with R_{ct} of 7.151×10^{6} $\Omega\cdot cm^{-2}$ indicating slow electron transfer process, while it decreased drastically (R_{ct}=6.09×10^{-4} $\Omega\cdot cm^{-2}$) at high ionic content.

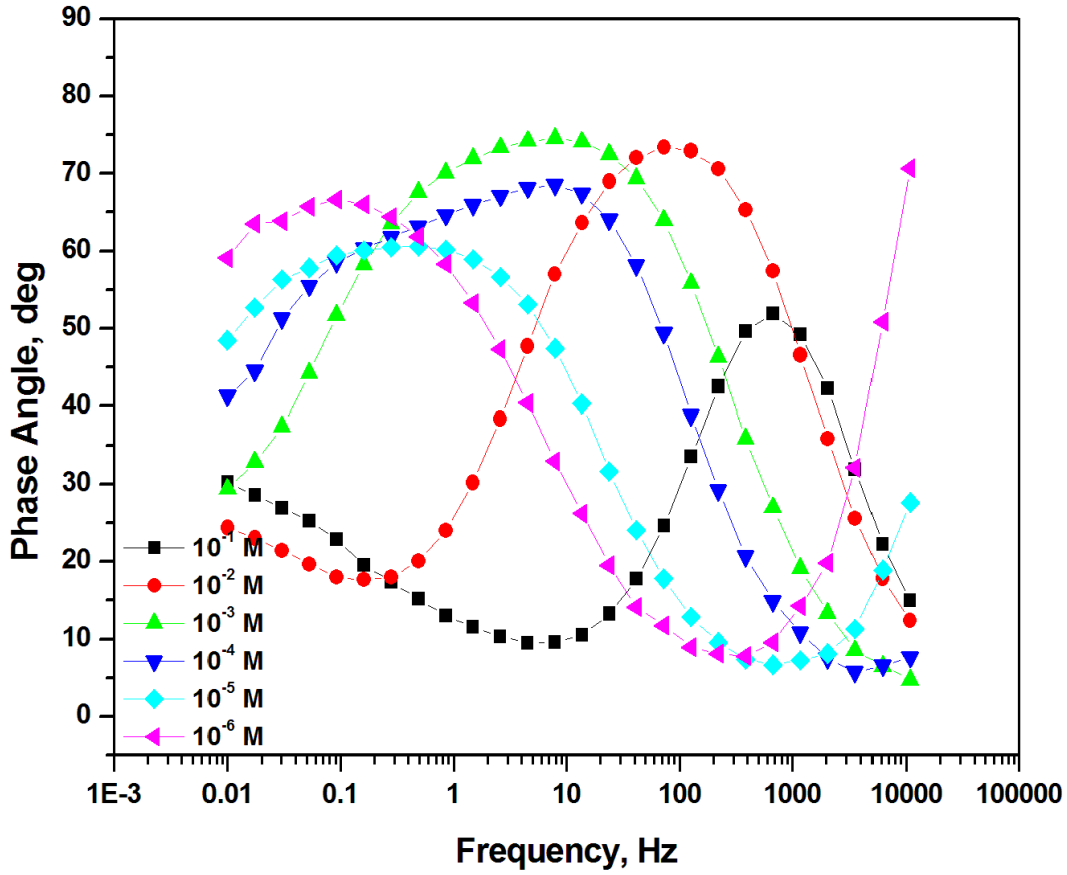

Figure 2.13 : Bode phase plots of S5 fiber at different $K_3Fe(CN)_6/K_4Fe(CN)_6$ concentrations, in aqueous solution.

On the other hand, Q_{el}, and W_{el} values were also found to increase while R_{el} decreases with the iron content. A graphical representation is given in (Figure 2.14) according to (Table 2.4), to show the close logarithmic relation of Fe(II) with R_{sol}, R_{ct} and C_{dl}.

The electron transfer process occurring on the fiber surface is a diffusion controlled process as seen by the presence of the Warburg element in the equivalent circuit. The plot of pFe concentration against C_{dl} showed a Nernstian linear correlation with r>0.9748 (Figure 2.12(b)).

The quantitation limit (QL) was determined by establishing the least concentration that can be measured according to the Q2(R1) equation as reported by the ICH (International Conference on Harmonization of Technical Requirements for Registration of Pharmaceuticals for Human Use) recommendations (López-Manchado & Arroyo, 2000), below which the calibration range is nonlinear. It was found to be 3.19×10^{-5}.

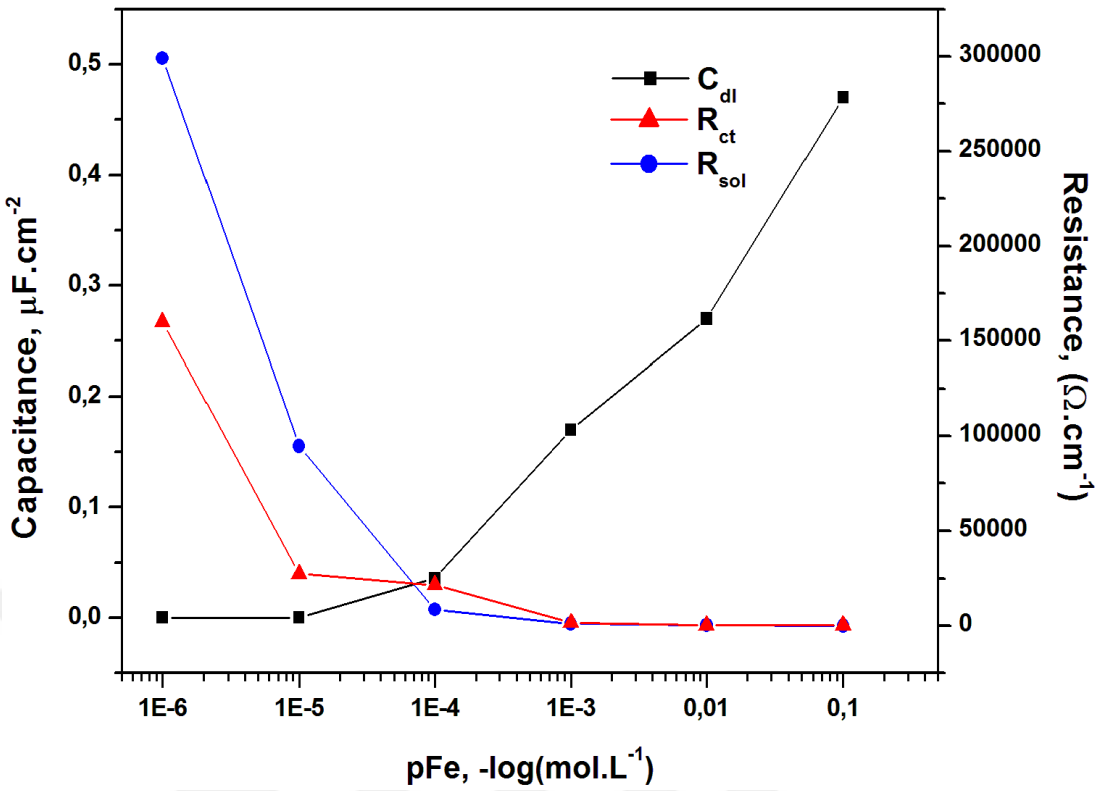

Figure 2.14 : R_{sol}, R_{ct} and C_{dl} vs pFe (the reciprocal logarithm of $K_3Fe(CN)_6/K_4Fe(CN)_6$ relation in aqueous solution.

The quantitation limit (QL) was determined by establishing the least concentration that can be measured according to the Q2(R1) equation as reported by the ICH (International Conference on Harmonization of Technical Requirements for Registration of Pharmaceuticals for Human Use) recommendations (López-Manchado & Arroyo, 2000), below which the calibration range is nonlinear. It was found to be 3.19×10^{-5}.

The detection limit (DL) was determined by evaluating the lowest concentration of the Fe(II) ion analyte that can be readily detected and was found to be 1×10^{-4} mol·l^{-1} for the S5 electrode. The QL and DL were calculated according to the following equations (ICH November 2005):

$$QL=10\sigma/S$$

$$DL=3.3\sigma/S$$

where σ is the standard deviation of the response and S is the slope of the calibration curve.

Table 2.4: EIS data simulations for S5 fiber against $K_3Fe(CN)_6/K_4Fe(CN)_6$ aqueous solution.

Conc. (mol.l^{-1})	R_{sol} ($\Omega.cm^{-2}$)	C_{dl} ($\mu F.cm^{-2}$)	R_{ct} ($\Omega.cm^{-2}$)	Q_{el} ($\mu S.s^{-n}.cm^{-2}$)	n	R_{el} ($\Omega.cm^{-2}$)	W_{el} ($\mu S.s^{-0.5}.cm^{-2}$)	χ^2 ($x10^{-4}$)
1.10^{-1}	151	0.47	$6.09x10^{-4}$	51.7	0.2459	2297	550.6	9.599
1.10^{-2}	277.3	0.27	347.2	0.93	0.7718	$7.38x10^{4}$	35.49	6.631
1.10^{-3}	1543	0.17	1108	0.73	0.7895	$2.989x10^{6}$	2.65	5.391
1.10^{-4}	$2.15x10^{4}$	$3.58x10^{-2}$	8591	0.18	0.6792	$3.92x10^{7}$	0.37	18.00
1.10^{-5}	$2.73x10^{4}$	$1.14x10^{-4}$	$9.48x10^{4}$	0.21	0.7371	$4.66x10^{7}$	0.14	4.312
1.10^{-6}	$1.60x10^{5}$	$1.02x10^{-4}$	$2.99x10^{5}$	0.16	0.7587	$3.48x10^{8}$	$3.45x10^{-2}$	9.461
0 M	7680	$4.746x10^{-2}$	$7.151x10^{6}$	0.05	0.7477	$1.00x10^{11}$	$2.43x10^{-2}$	15.29

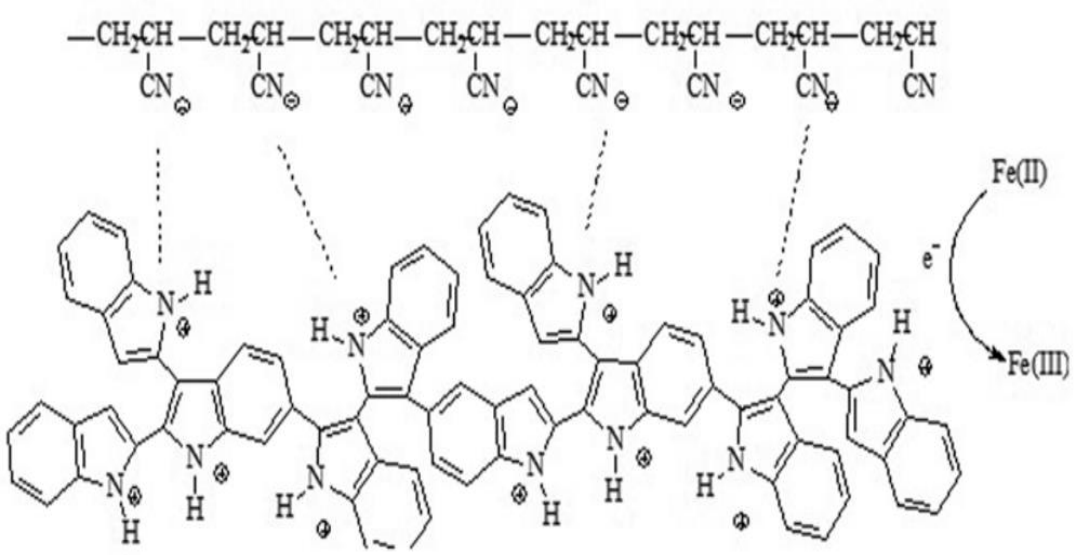

Figure 2.15 : Schematic electron transfer process for PAN-PIN fibers in the presence of Fe(II) ions.

2.3 Conclusion

PIN microfibers were prepared by electrospinning technique and characterized by different methods. The EIS and CV measurements were used to determine the electroactivity of the PAN/PIN fibers. The topological properties differed with the PIN content. The amount of PIN content has been found to have a direct impact on the fiber morphology, thermal properties and electrochemical behavior. The incorporation of PIN on the fiber structure showed a sensitivity to Fe(II)/Fe(III) electron transfer process. This may be due to the synthesis of PIN with $FeCl_3$ as initiator and the quasi self-dopant effect of PAN and PIN interaction (Figure 2.15) similar to the PEDOT:PSS interaction. Compared with polyindole film, polyindole fiber membrane shows significantly high specific surface areas and a more effective electronic conductivity.

3. OXIDATIVE STABILIZATION OF POLYACRYLONITRILE NANOFIBERS AND CARBON NANOFIBERS (CNFs) CONTAINING GRAPHENE OXIDE (GO): A SPECTROSCOPIC AND ELECTROCHEMICAL STUDY[2]

Carbon nanofibers are of great interest because of their chemical similarity to fullerenes and carbon nanotubes. Carbon nanofibers (CNFs) have promising electrochemical and mechanical properties and potential for various applications; such as supercapacitors, batteries, and also catalyst support materials. Polyacrylonitrile (PAN) is one of the well known precursor for obtaining carbon nanofibers that have diameters ranging between nanometers and micrometers and exhibit high surface area and high electrical conductivity.

Also, nanofibers can be used with polymeric structures to generate composite materials to improve the electrochemical properties of polymeric structures (Tamura & Kawakami, 2010; Vieira, Pham-Huu, Keller, & Ledoux, 2002; Wu, Xu, Yao, Liu, & Shi, 2010). Nanofiber-reinforced polymeric structures present improved mechanical properties because of the interaction between nanofibers and the matrix material (D. Li & Xia, 2004). CNFs can be used as reinforcing material inside the polymer composites thanks to their enhanced mechanical and physical properties (Green, Dean, Vaidya, & Nyairo, 2009; Sadeghian, Gangireddy, Minaie, & Hsiao, 2006; Tibbetts et al., 2007). The manufacturing of CNFs/polymer composites is challenging and the manufacturing processes need to be improved to obtain high-performance composite structures (A. J. Rodriguez, Guzman, Lim, & Minaie, 2011).

Oxidative stabilization is a crucial heat-treatment process for the production of carbon fibers from PAN fibers. PAN chains begin to cross-link during this process and the

[2] This chapter is based on "**Gergin, İ., Ismar, E., and Sarac, A. S.** (2017). Oxidative stabilization of polyacrylonitrile nanofibers and carbon nanofibers containing graphene oxide (GO): a spectroscopic and electrochemical study. *Beilstein journal of nanotechnology*, *8*(1), 1616-1628."

newly composed polymeric structure can endure the rigors of high-temperature processing (Ko, 1991; Shokuhfar, Sedghi, & Farsani, 2006; Yusof & Ismail, 2012). Oxidative stabilization is crucial to prevent melting or fusion of the fibers. Also, it minimizes volatilization of elemental carbon in the following carbonization step and maximizes the final carbon yield. Chemistry and mechanisms of complex oxidative stabilization reactions for PAN were reported (Dalton, Heatley, & Budd, 1999). Oxidative stabilization reactions mainly consist of dehydrogenations and cyclizations, i.e., cyclization of nitrile groups (C≡N) and crosslinking of chain molecules in the form of –C=N–C=N–. Moreover, this stabilization process depends on pyrolysis temperature, heating rate, tension of the fiber, total stabilization time and dwell time, air flow rate and pre-stabilization treatment (Faraji, Yardim, Can, & Sarac, 2017). Carbonization is the next step for the production of carbon fibers. The carbonization processes can be divided into low-temperature and high-temperature carbonization, and graphitization above 2000 °C (Arshad, Naraghi, & Chasiotis, 2011; de Almeida Coelho, Furtado, Pham-Huu, & Vieira, 2008; Rahaman, Ismail, & Mustafa, 2007). Carbonization should be conducted under nitrogen environment to prevent burning (Ismar & Sarac, 2016; Lee, Kim, Ku, et al., 2012; Morgan, 2005). During the carbonization process, the elimination of other elements (N_2, O_2, H_2) and structural impurities is accelerated and the carbon concentration is simultaneously increased inside the structure.

The most common co-monomers of acrylonitrile in the acrylonitrile copoymers are: vinyl acetate, itaconic acid, methylmetacrylate, and acrylic acid (Ismar & Sarac, 2016; Masson, 1995; Morgan, 2005). Co-monomers are mainly used is to improve the processability of acrylonitrile and to decrease the cyclization temperature (Devasia, Reghunadhan Nair, Sivadasan, Katherine, & Ninan, 2003; Kakida, Tashiro, & Kobayashi, 1996). For instance, the glass-transition temperature (T_g) of PAN homopolymer is reduced by the addition of a co-monomer to form P(AN-co-AA), thereby enhancing cyclization reactions and the formation of thermally stable aromatic ladder polymer chains (Ismar & Sarac, 2016). Acidic co-monomers (itaconic acid and acrylic acid) improve the hydrophilicity of the PAN precursor but also catalyze the cyclization of nitrile groups during the stabilization process by forming a ladder structure. In our previous studies, copolymers of AN have been synthesized by free radical polymerization and also electrospun nanofibers were obtained with different

AN co-polymers as carbon nanofiber precursors (Faraji et al., 2017; Ismar & Sarac, 2016).

Graphene has several desirable features, such as high surface area, high aspect ratio, and other properties comparable to those of carbon nanotubes. Thus, graphene attracts attention in science as a new class of material for polymer-based composites (Lee, Kim, Kim, Ku, & Joh, 2012). Graphene oxide has been synthesized from graphite with strong acids and oxidants (Karthika, Rajalakshmi, & Dhathathreyan, 2012; Yanwu Zhu et al., 2010). The oxidation level can be adjusted by modifying reaction conditions and systems, and the type of precursor. Moreover, oxygen functional groups increase wettability and capacitive property, but not all of the surface oxygen groups have the same effect. For enhancing the capacitance of a supercapacitor, an active electrode material with oxygen functional groups is necessary (Karthika et al., 2012). Furthermore, PAN cyclization temperature can be decreased in the presence of graphene oxide. The functional groups of graphene oxide initiate the PAN cyclization at lower temperature via ionic mechanisms. In addition, the performance of an electrochemical capacitor prepared from carbon nanotubes/carbon nanofiber (CNT/CNF) composites is influenced by the oxidation level. Increasing the O/C ratio improves the capacitance of CNT/CNF composites. According to the literature, a flexible and free standing composite paper comprising carbon nanofibers and graphene shows a higher specific capacitance than pure carbon nanofibers. Thus, the CNF/graphene combination can be a good candidate for a high-performance flexible capacitor applications (Tai, Yan, Lang, & Xue, 2012).

In this thesis, graphene oxide was used as an additive to increase the capacitance of oxidized PAN-based nanofibers. Further, GO addition was studied to improve electrochemical properties of CNF webs.

3.1 Experimental

3.1.1 Materials

Polyacrylonitrile (PAN, M_w 150.000 g/mol) was purchased from Sigma-Aldrich and was used as received. Dimethylformamide (DMF; Sigma-Aldrich), sulfuric acid (H_2SO_4, 98%; Sigma-Aldrich), acetonitrile (ACN; Sigma) were chosen as solvents and were used without any further purification. Graphene oxide (GO, purity 99%) was

purchased from Grafen Chemical Industries and used as received. The properties of the few-layered GO are: GO consists of a few layers (1–10 layers) and the average thickness of the layer is smaller than 4 nm. The specific surface area of GO is larger than 550 m^2/g. GO consists of 68.44 atom % C, 30.92 atom % O and 0.63 atom % S.

PAN dissolved in DMF and spinning solution was prepared for electrospinning process. The solution was fed into a 2 mL syringe. DMF evaporated under high voltage (around 15 kV) by applied electrical potantial. Thus, nanofiber formation was achieved onto the collector. Those nanofibers stacked and formed a web. Different collectors were used to fabricate PAN-based nanofiber webs via electrospinning. Before the electrospinning process, GO was also added to PAN/DMF solution to obtain PAN/GO nanofibers. After electrospinning of the PAN/GO nanofibers, PAN/GO samples underwent the same heat treatment (oxidation and carbonization) as PAN nanofibers. Rotating and fixed collectors were used to vary the samples and investigate physical and chemical changes.

Electrospinning solutions were prepared at different PAN/DMF ratios. Electrospinning parameters (e.g., viscosity, voltage, feeding ratio) effect the nanofiber diameter and homogeneity. Lower viscosity helps to produce finer nanofibers, and an increased polymer weight percentage results in higher viscosities. Thus, it is one of the significant parameters for electrospinning (Sarac, 2016).

In this study, graphene oxide was used as an additive to increase the capacitance of oxidized PAN-based nanofibers. Thus, the nanofibers were produced via electrospinning using mixture of PAN (10% w/v) and given amount of GO (at different weight-to-volume percentages) in DMF. The solutions were poured into a 2 mL syringe and delivered at a constant flow rate of 1.0 mL/h (New era, NE-300) to a needle with a blunt tip connected to a high-voltage power supply (Gamma high voltage research) producing 15 kV. Aligned nanofibers were deposited on the rotating drum collector at 21.50 Hz rotating frequency at a distance of 15 cm. After producing the nanofibers, oxidative stabilization was performed at 250 °C for 3 h in air atmosphere and carbonization was performed at 900 °C for 1 h under nitrogen atmosphere.

3.1.2 Characterization

Attenuated total reflectance Fourier transform infrared spectroscopy (ATR-FTIR) and Raman spectroscopy were used to record the characteristic peaks of the oxidized and

carbonized nanofibers. Mechanical properties of nanofiber webs were characterized by using a dynamic mechanical analyzer (DMA) (TA Q800 Dynamic Mechanical Analyser).

Thermal behavior of nanofiber webs was examined with thermogravimetric analysis (TGA, Q 50 from TA instruments). The structure of the nanofiber webs was characterized by attenuated total reflectance Fourier transform infrared spectroscopy (ATR-FTIR) (Perkin Elmer, Spectrum One, with a Universal ATR attachment with a diamond and ZnSe crystal). The microstructure of the carbonized nanofiber webs was investigated by Raman spectroscopy (DXR Raman spectrometer, Thermo Scientific, at 532 nm). The sample morphologies were characterized by scanning electron microscopy (Gemini Leo Supra 35 VP) and so samples were coated with thin gold film using a sputter coater to prevent the accumulation of charge on their surface.

Electrochemical performances of nanofibers were analyzed by using cyclic voltammetry (CV) and electrochemical impedance spectroscopy (EIS). Electrochemical measurements were performed by using potentiostat 2263 Electrochemical Analyser (Princeton Applied Research, Tennessee, USA). EIS data were simulated with the electrical equivalent circuit by ZSimpWin V.3.10 analysis program (Princeton Applied Research,Tennessee, USA). The surface topography of the fibers was observed by atomic force microscopy (AFM) with Nanosurf Easy-Scan2TM software. AFM analyses were performed with a noncontact mode by using NCLR-10 model Al-coating silicon tips with 7 μm thickness, 225 μm length, 38 μm width, 190 kHz resonance frequency and 48 N/m force constant. Surface morphology of the nanofibers was observed with transmission electron microscopy (TEM) and scanning electron microscopy (SEM) at Namık Kemal University. Fiber diameters were measured within electron micrographs from a population between forty and fifty nanofibers taken from each sample and then the average values were calculated by ImageJ software.

3.2 Results and Discussion

3.2.1 Oxidative stabilization of PAN nanofibers

Oxidative stabilization is a complex process and should be applied to the webs before carbonization. The mechanism plays an important role in the carbonization. Therefore,

a detailed understanding of the mechanism of oxidation has an important part in the success of the production of CNF.

Nanofiber webs are produced with different collectors to achieve fiber alignment. The results for webs of aligned and non-aligned nanofibers are compared. A rotating collector that produces aligned nanofiber webs reduces the nanofiber diameter as shown in SEM images in (Figure 3.1). Non-aligned PAN nanofibers diameter are in the range of 371.6 ± 36 nm; whereas the aligned PAN nanofibers diameter are decreased to 330.8 ± 27 nm.

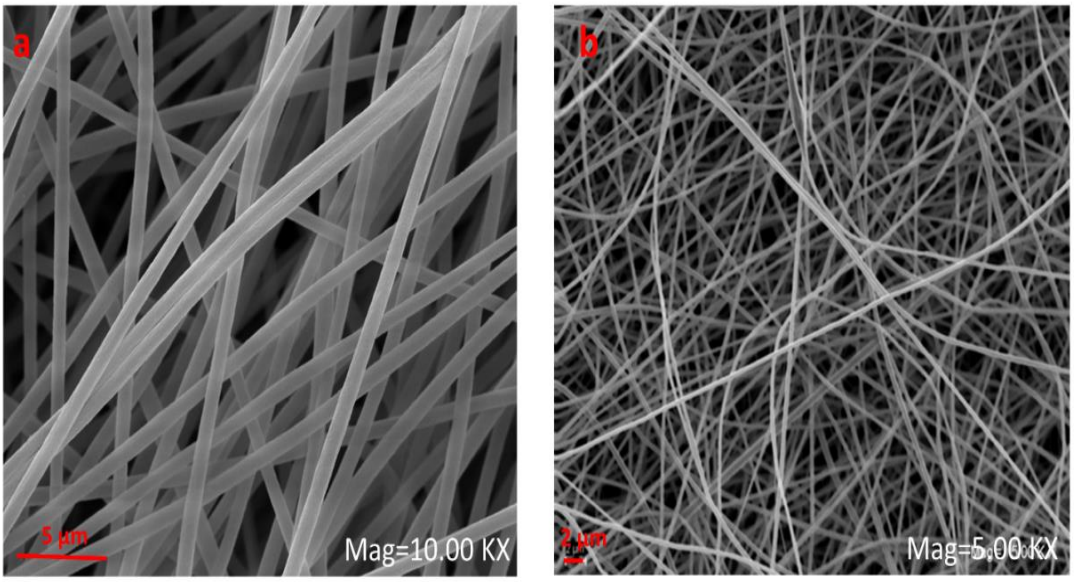

Figure 3.1 : a) Web of aligned PAN nanofibers produced with rotating collector and b) Web of PAN nanofibers produced with fixed collector.

The stress–strain curve obtained by DMA shows that fiber alignment increases the mechanical properties of the web. A directional orientation of the fibers definitely and expectedly has the effect of increasing modulus and reducing the strain to break (Fennessey & Farris, 2004; Ismar & Sarac, 2016; Naraghi, Arshad, & Chasiotis, 2011). Aligned nanofibers has a greater modulus than non-aligned ones (Dissertations & Fennessey, 2014; Fennessey & Farris, 2004; Ismar & Sarac, 2016; Zhou et al., 2009). Also, our previous work (Ismar & Sarac, 2018) exhaustively explains the effects of rotating collector and fixed collector. Rotational movement helps to orient the nanofibers and obtain thinner fibers compared to the fixed collector. Webs of aligned nanofibers present superior mechanical properties in terms of modulus. Stress–strain plots of aligned and non-aligned PAN nanofibers is shown in (Figure 3.2).

According to the plots, the elastic modulus of PAN-nanofiber web increases with fiber orientation from 63 MPa to 159 MPa. Thus, rotating collectors were chosen to obtain nanofibers with better mechanical and morphological properties.

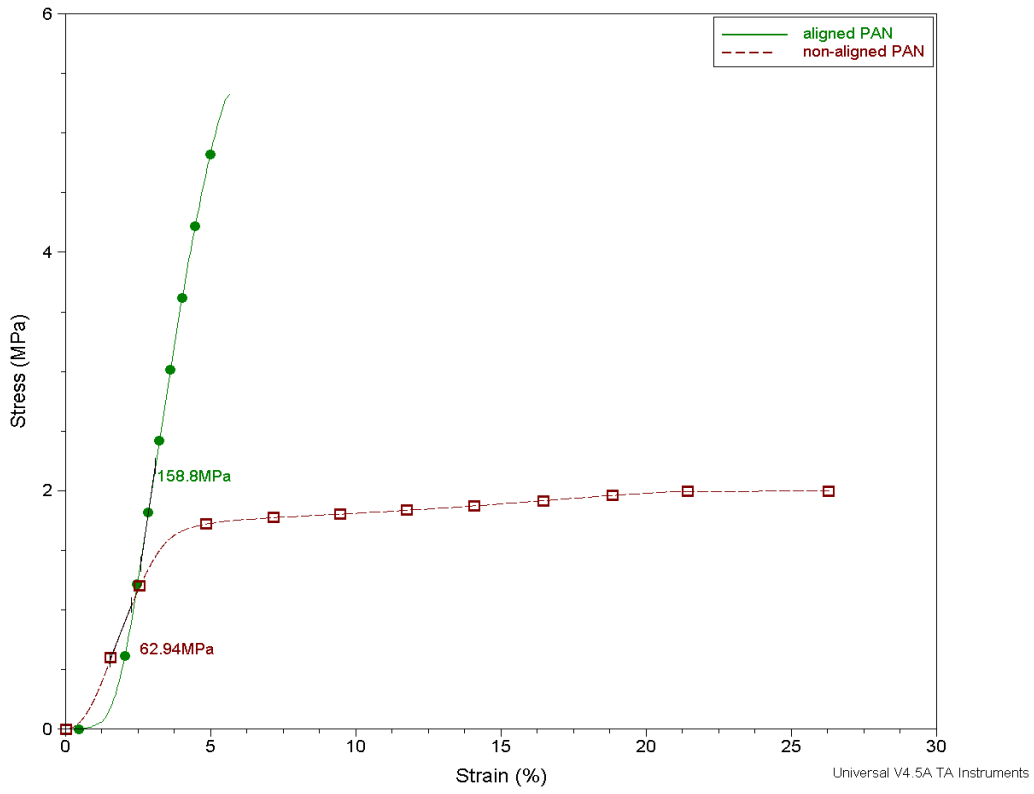

Figure 3.2 : Stress–strain plots of webs of aligned and non-aligned PAN nanofibers.

3.2.2 ATR-FTIR spectroscopy results

The oxidation process including conversions of C≡N bonds to C=N and also dehydrogenation leading to aromatic and supramolecular structures was studied (Sai Ma et al., 2016). Structural changes during the oxidation process can be tentatively expressed as in (Figure 3.3), and the oxidation route was explained through cyclization and dehydrogenation reactions. Peaks around 2243 cm^{-1} represent the absorption of C≡N bond (Kakida et al., 1996; Lee, Kim, Ku, et al., 2012; Ouyang, Cheng, Wang, & Li, 2008). Those around 1590 cm^{-1} can be assigned to a combined effect of C=N, C=C, N–H groups (Arshad et al., 2011; Dalton et al., 1999; Lee, Kim, Ku, et al., 2012; J. Liu et al., 2009; Ouyang et al., 2008), and the broad peak at around 3000 cm^{-1} is connected to C–H bonds (Farsani, Raissi, Shokuhfar, & Sedghi, 2009; T. J. Xue, McKinney, & Wilkie, 1997). ATR-FTIR results are given in (Figure 3.4). The oxidation temperature is too low to eliminate all C≡N bonds. This means that cyclization reactions can not

be completed. A schematic description is given in (Figure 3.3). However, the intensity of the C≡N bonds is decreased after oxidation (Dalton et al., 1999; J. Liu et al., 2009; Ogawa & Saito, 1995). A weight loss is not observed during the cyclization process, contrary to dehydrogenation (T. J. Xue et al., 1997). During the dehydrogenation a new peak appears at around 800 cm^{-1} because of the formation of =C−H bonds (Clarke & Bailey, 1973; Farsani et al., 2009; Mittal, Bahl, Mathur, & Sandle, 1994). In the presence of oxygen =C−H groups were created during the aromatization by the removal of H atoms in the form of H_2O (Farsani et al., 2009). Also, an increased temperature increases the intensity of the =C−H peak.

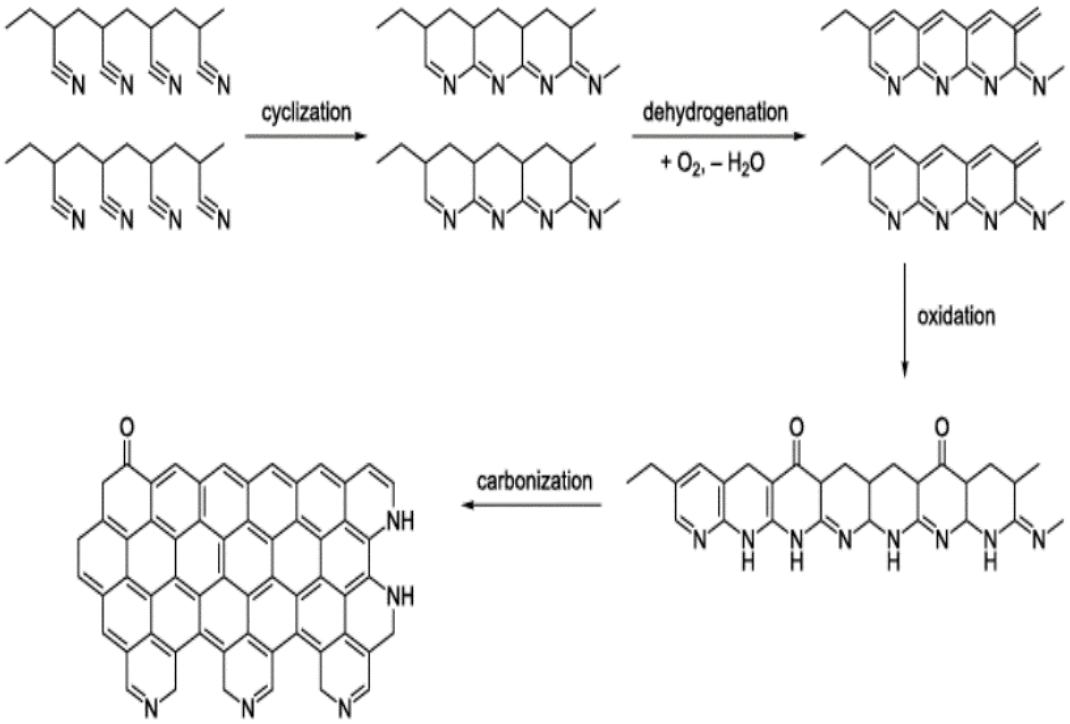

Figure 3.3 : Schematic description of carbonization process starting from polyacrylonitrile.

The oxidation ratio can be calculated from the absorbance ratio obtained from ATR-FTIR results (Dalton et al., 1999; Mittal et al., 1994; Ogawa & Saito, 1995). The inset in (Figure 3.4) represents the oxidation ratio as a function of the oxidation temperature by evaluating the ratio between the mixed signals of C=N, C=C, N–H groups and the signal of C≡N bonds. Oxidation temperatures at 250 °C and 270 °C, the oxidation ratios are quite close contrary to that of the oxidation at 235 °C. During the oxidation process, C≡N triple bonds are damaged and C=N double bonds are created. Thus the ratios of these peaks from ATR-FTIR can help to calculate the oxidation ratio. GO-containing samples are marked in (Figure 3.4 inset). At 250 °C, the addition of GO to

the PAN nanofiber web causes a deviation in the oxidation ratio values compared to pure PAN. GO acts via ionic mechanism in the oxidation step and improves the conversion of C≡N bonds to C=N, C=C and N–H (Fu et al., 2014; Ouyang et al., 2008; O. K. Park et al., 2012).

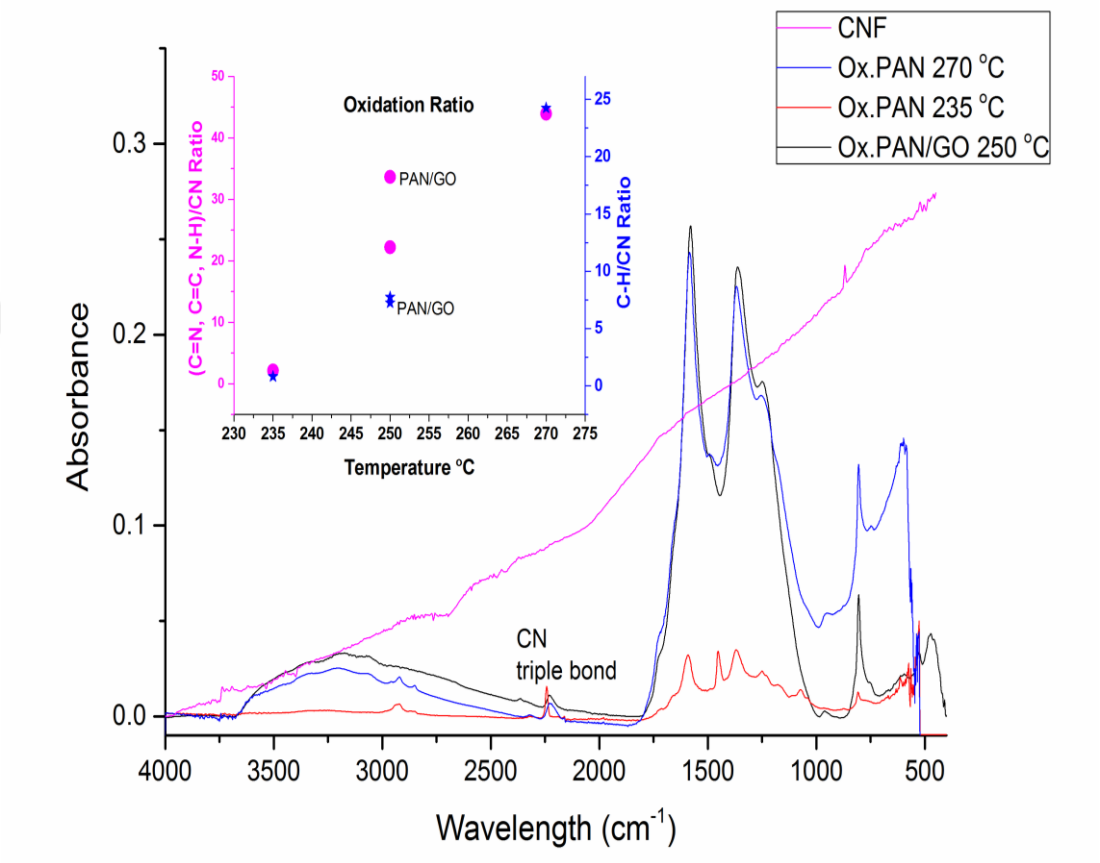

Figure 3.4 : ATR-FTIR results of oxidized webs with GO and of the carbon nanofiber web. The inset represents the oxidation ratio of the webs as a function of the temperature according to absorbance ratios of (C=N, C=C, N–H)/C≡N and the newly occurred =C−H/C≡N ratio. (C=N, C=C, N–H) represents the mixture of the corresponding absorbances.

During the stabilization process, the cyclization of the nitrile groups and cross-linking of the chain molecules is followed by dehydrogenation (Farsani et al., 2009). This reaction promotes the creation of a ladder structure from the linear molecule (Bashir, 1991; Farsani et al., 2009; J. Liu et al., 2009). Ladder structure polymers are thermally more stable than linear polymers, because the structure prevents them from melting at higher temperatures (Farsani et al., 2009) (Joseph C. Salamone, 1998). Weight loss starts at around 100 °C with the removal of moisture and continues with increasing duration and temperature. However, it is not much significant for the oxidation process

(Dalton et al., 1999; Ismar & Sarac, 2016; C. Q. Li et al., 2015). Weight loss as a function of temperature and time was recorded with TGA. There is a region in which there is no weight loss, and this region can be explained by cyclization reactions (T. J. Xue et al., 1997). Both TGA curves (in N_2 and in O_2 atmosphere) exhibit the same trend. However, the region with no weight loss is shifted in N_2 atmosphere because of N_2 suppresses the reactions compared to O_2, according to TGA measurements, PAN polymer stays stable up to ca. 300 °C. This stable phase can be explained by cyclization reactions (T. J. Xue et al., 1997). Above this temperature, weight loss begins to increase because of the dehydrogenation reactions (Farsani et al., 2009; T. J. Xue et al., 1997). In O_2 atmosphere, weight loss starts above 100 °C, after a stable cyclization phase, dehydrogenation in O_2 atmosphere is observed between 100 °C and 140 °C. This temperature shifts to 300°C–400 °C in N_2 atmosphere. The reaction propagation is faster under O_2 atmosphere compared to N_2.

The same conditions as in the oxidation procedure were applied during TGA. A 5 °C/min ramp was applied till the samples reached the desired oxidation temperature (235 °C, 250 °C, 270 °C and 300 °C). After the samples reached the oxidation temperature, TGA was carried out for further 300 minutes. It can be seen from the TGA curves that the 300 °C/300 min oxidation process shows the highest weight loss. For the TGA measurement of nanofiber webs in oxygen environment the curves are similar to those of the PAN polymer. However, the temperature ranges are shifted because of the presence of oxygen. In the presence of reactive atmospheres, such as air or oxygen, the oxidation process is faster at lower temperatures (Chand, 2000). At temperatures above 100 °C weight loss was recorded. A sudden reduction of weight was recorded during dehydrogenation reactions in which hydrogen and oxygen formed H_2O, which was released from the structure (Farsani et al., 2009; T. J. Xue et al., 1997). (Figure 3.5) shows that at the oxidation temperature of 300 °C a weight loss of around 14.5% is observed after 300 min. During 300 min of oxidation, the weight loss varies between 4.9% and 14.5% for increased temperatures (235 °C, 250 °C and 270 °C). The weight loss is recorded as 14.5% at 300 °C. The energy applied to the sample depends on temperature and duration which they promote bond breakage together, thus the weight loss of the samples increases with temperature. Also, using a co-polymer instead of a homopolymer can strengthen the fiber structure and lead to a higher heat stability (Faraji et al., 2017; Ismar & Sarac, 2016). A dramatic weight loss (around

45%) is recorded during the low-temperature carbonization process with increasing elimination of other elements (N, H, O) (Farsani et al., 2009; Mittal, Konno, Inagaki, &Bahl,1998).

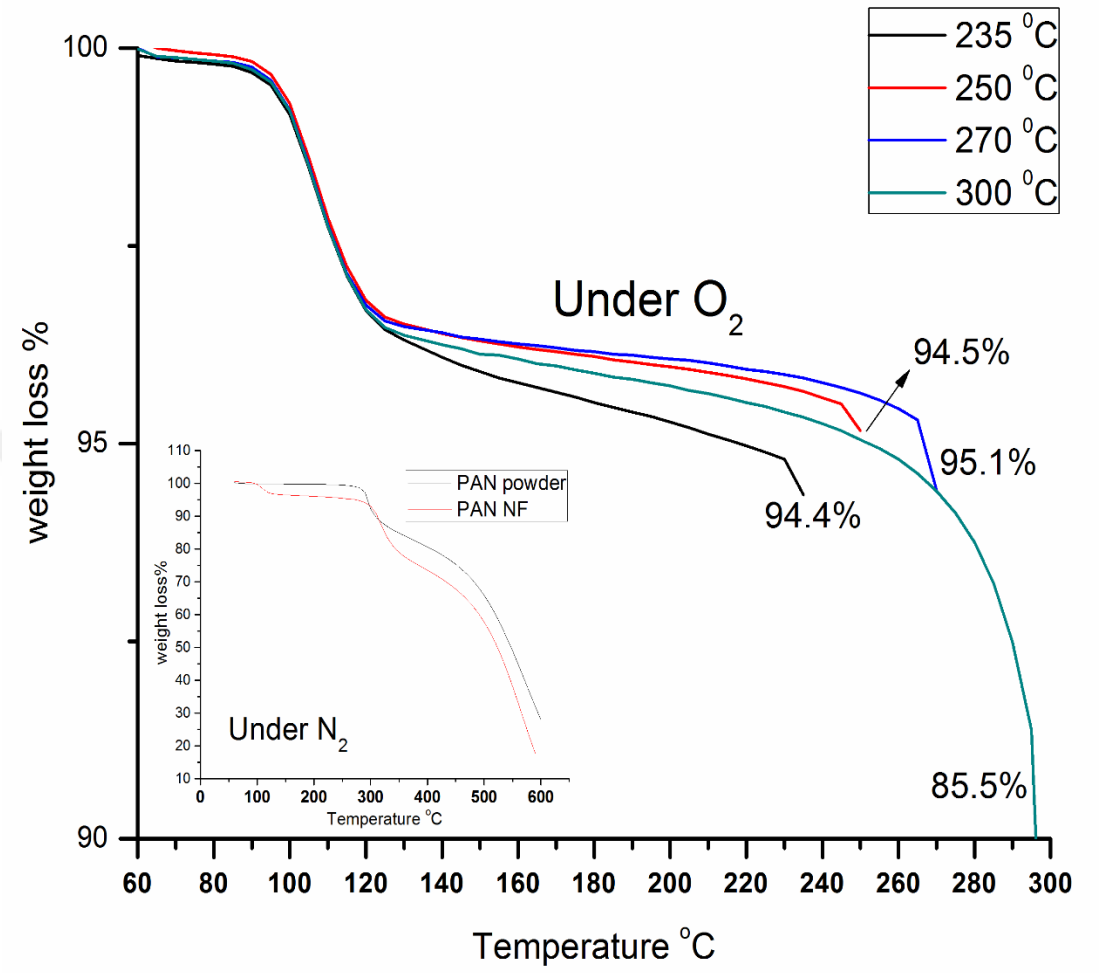

Figure 3.5 : TGA curves representing the experimental conditions of oxidation for 300 min of different oxidation temperatures for webs of aligned PAN nanofibers (under air). The inset represents the TGA of PAN polymer under inert (nitrogen) atmosphere.

3.2.3 Electrochemical impedance measurements of oxidized PAN nanofibers

Electrochemical properties of oxidized PAN nanofibers were analyzed by using electrochemical impedance spectroscopy (EIS). EIS measurements were performed in 0.5 M H_2SO_4 electrolyte in the frequency range of 100 mHz to 100 kHz at open circuit potential with an AC perturbation of 10 mV. A standard three-electrode cell was used to study the electrochemical performances of PAN nanofibers which were stabilized at 250 °C for 1 h in air. Oxidized PAN nanofiber mats were used as free standing working electrodes, a platinum wire was used as counter electrode, and a silver wire

was used as pseudo-reference electrode. EIS data were simulated with electrical equivalent circuit by using the ZSimpWin V.3.10 analysis program.

Experimental and calculated measurements were fitted by equivalent circuit modelling. EIS plots with measured and calculated data are shown in (Figure 3.6). An excellent agreement between experimental results and simulation was found with $\chi^2 \approx 5 \cdot 10^{-4}$ (χ^2 is function defined as the sum of the squares of the residuals). R_s is the ohmic resistance of the solution, R_{ct} represents the charge-transfer resistance between nanofiber electrodes and electrolyte interface and Q_{dl} (constant phase element (CPE)) is the double-layer CPE, a frequency-dependent element.

The Nyquist plot in (Figure 3.6(a)) consists of a semicircle related to the electron-transfer process. The charge-transfer resistance (R_{ct}) can be calculated from measuring the diameter of the semicircle. According to the Bode phase plot in (Figure 3.6(b)), the phase angle of the sample was 10° around 80 Hz. In the Bode magnitude plot, the absolute values of impedance are plotted as a function of the frequency. The impedance values between low-frequency region and high-frequency region do not change drastically compared to the GO-containing PAN nanofibers (see below in (Figure 3.14)). Addition of GO to PAN nanofibers changes the homogeneity of the electrode. Thus, the penetration of electrolyte ions varies with frequency.

The values of R_s, R_{ct} and Q_{dl} were determined as 552 Ω, 340 Ω and $2 \cdot 10^{-2}$ μS·s^n according to the Randles circuit model for non-ideal electrodes described as $R_s(Q_{dl}R_{ct})$ in short hand. The CPE (Q_{dl}) can also be attributed to the double-layer capacitance (C_{dl}) in the non-homogeneous systems (Engin Sagirli, Kayali, & Sarac, 2016). Double-layer capacitance occurs at the electrode/electrolyte interface of materials with especially high surface area. The electrical charge is stored based on the separation of charged species in an electrolytic double layer across the interface of electrode/solution. This capacitance value is proportional to the surface area of the electrode and inversely proportional to the thickness of the double layer (Qu & Shi, 1998).

The impedance of the non-ideal electrode is defined by

$$Z_{CPE} = T_{CPE}(j\omega)^{-n},$$

where j is the imaginary unit $\sqrt{-1}$, ω is the angular frequency, and T_{CPE} and n are frequency-independent experimental constants; T_{CPE} relates to the size, thickness, and

materials properties,while *n* relates to the degree of energy dissipation andmeasures the arc depression, which is frequency-independent. Moreover, *n* is a parameter describing the deviation from an ideal capacitor and arises from the slope of the log *Z* versus log*f* plot. The values for *n* vary from 0 to 1, and *n* = 1 describes an ideal capacitor, while *n* = 0 describes the behavior of a resistor.The *n* value of oxidized PAN was equal to 0.83.

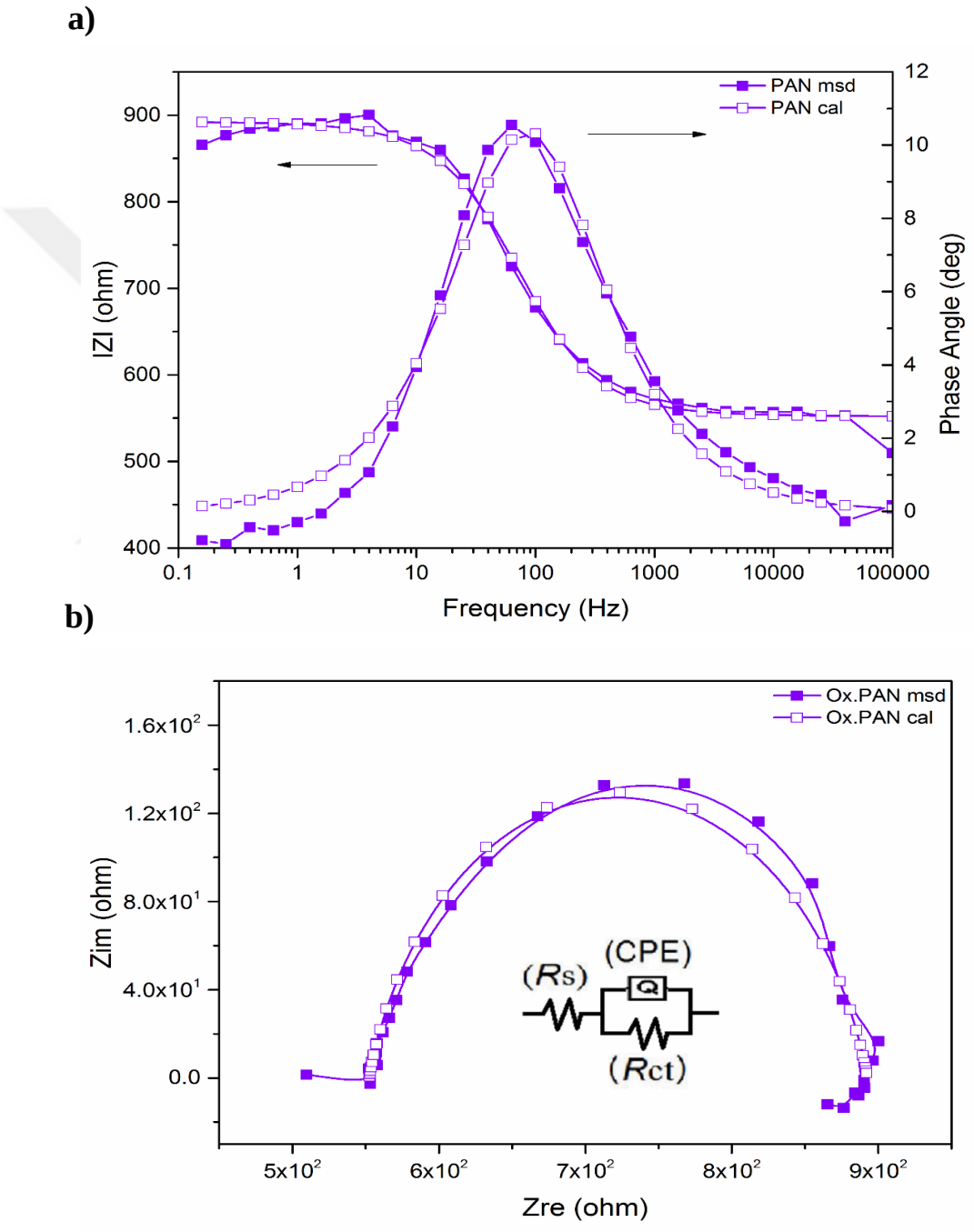

Figure 3.6 : a) Nyquist plots of webs of oxidized PAN nanofibers. Inset: Randles circuit model. b) Bode magnitude and Bode phase plots of PAN nanofiber webs.

3.2.4 Oxidative stabilization of PAN/GO nanofibers and CNF

The Raman spectroscopic measurements show characteristic peaks of carbon materials, namely D band and G band at around 1360 cm^{-1} and 1580 cm^{-1}–1600 cm^{-1}, respectively (Ferrari, 2007; Qu & Shi, 1998) (Figure 3.7). Oxidation and carbonization contributed to the conversion of PAN fibers into a graphitic form via fraction of disordered sp^2-hybridized C–C bonds (Y. Wang, Serrano, & Santiago-Aviles, 2002). The ratio of the D and G bands provides an information about the crystallinity of the carbonaceous material (Jawhari, Roid, & Casado, 1995; Kim, Park, et al., 2004). The G band (1590 cm^{-1}) represents ordered graphitic crystallites (Kim, Park, et al., 2004), while the D band around 1350 cm^{-1} is related to disordered turbostratic structures (N. M. Rodriguez, 1993). The measured intensity ratio between D band and G band ($R = I_D/I_G$) indicates structurally ordered graphite crystallites (Jawhari et al., 1995; Zhou et al., 2009). The R value of CNF is around 0.9. A lower R value means a more crystalline material with higher conductivity (Sharma, Katepalli, Sharma, & Madou, 2011). Position and intensity of D and G band demonstrate the electronic structure and electron–phonon interactions of the material (Ferrari, 2007).

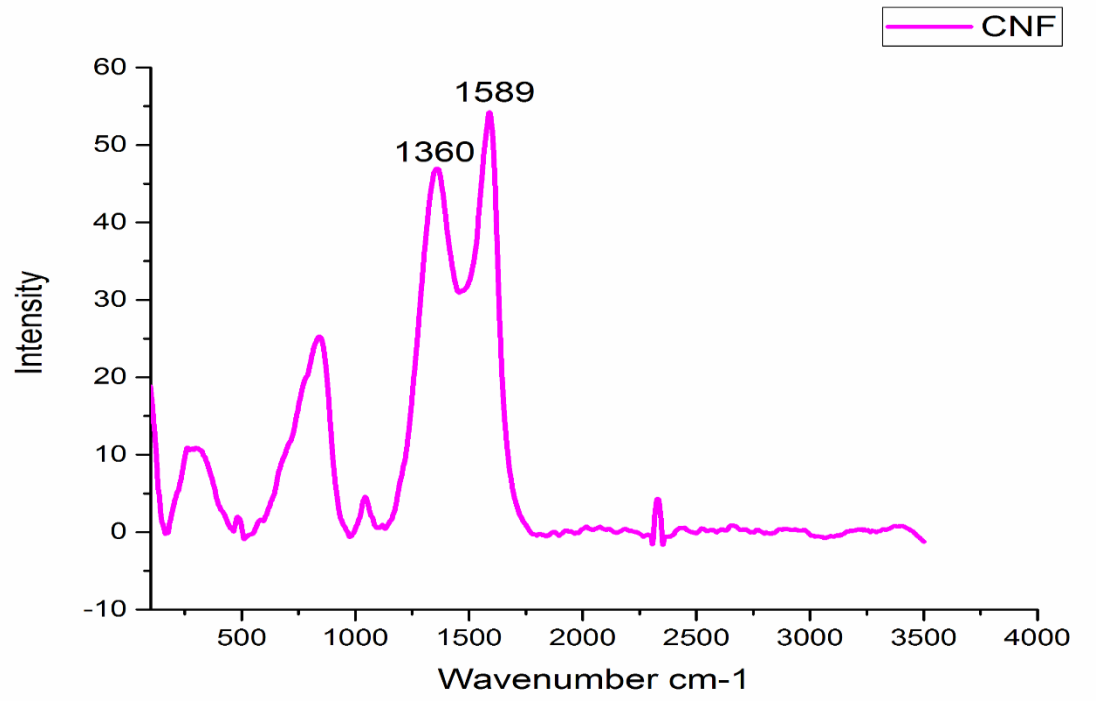

Figure 3.7 : Raman spectrum of carbon nanofiber webs.

3.2.5 ATR-FTIR spectroscopy of oxidized PAN/GO nanofibers

The ATR-FTIR results show a broad OH stretching peak of GO around 3300 cm^{-1} (Gong, Li, Fu, & Pan, 2015) and the C–H vibrations of the CH, CH_2 and CH_3 structures of oxidized polyacrylonitrile around 2920 cm^{-1} (Farsani et al., 2009; Mittal et al., 1994). Through the carbonization process most of the bonds are damaged and eliminated. The ladder structure of carbon atoms becomes more dominant and it is not always possible to follow further structural changes of carbonaceous materials with FTIR. Also, ATR-FTIR results of carbonized nanofibers (Figure 3.4) are not clear not only because of the changing bond structure of PAN but also because of the black color of the carbon nanofiber webs. A photo of GO-containing PAN-based electrospun, oxidized and carbonized nanofibers are shown in (Figure 3.8). The colors of the nanofibers change from white to brown after oxidation and then from brown to black after carbonization.

Figure 3.8 : GO-containing PAN-based electrospun, oxidized and carbonized nanofibers.

3.2.6 Morphological studies

The surface of the nanofibers is not smooth and has pores, which can be related to graphene oxide content. This can be seen very clearly from the AFM, TEM and SEM images in (Figure 3.9), (Figure 3.10) and (Figure 3.11) respectively. AFM was performed to observe the topography of nanofibers. Oxidized PAN nanofibers formed with GO nanosheets can be seen in AFM image (Figure 3.9). The nanofibers have rough surfaces with flaky shapes attributed to GO. The morphology of GO is also shown in Figure (3.10(a)). Layers of GO can be seen in the SEM image. Also, some

layer edges of GO and the interspaces of the layers can be observed in the SEM image. GO-containing electrospun nanofibers are seen in (Figure 3.10 (b,c)). GO nanosheets that are formed with PAN nanofibers are observed on the structure in (Figure 3.10 (b)). A rough surface with a kind of joints is presented in the image. Distance between two nodes in the structure is around 50 nm calculated by ImageJ Software.

The morphology of PAN nanofibers with smooth surfaces is presented in (Figure 3.1) and (Figure 3.11(a)) for comparison with GO-containing PAN nanofibers. When GO is included into PAN nanofibers rough surface can be seen. Furthermore, the porous structure of carbon nanofibers with GO is shown in (Figure 3.10 (b,c)). The porous surface of oxidized PAN/GO nanofibers is shown in (Figure 3.11 (b)) and also the pore distribution chart is added on the SEM image. It can be seen from (Figure 3.11) that addition of GO makes the nanofiber surface porous and these pores are well distributed on the fibers. The morphological property of the porous carbon electrodes such as the surface and pore size distributions are the factor that influences the double-layer capacitance. Therefore, the pore size distribution of porous carbons also affect the performance of carbon-based electrochemical capacitors (Abdul Manaf, Amin Bistamam, & Azam, 2013).

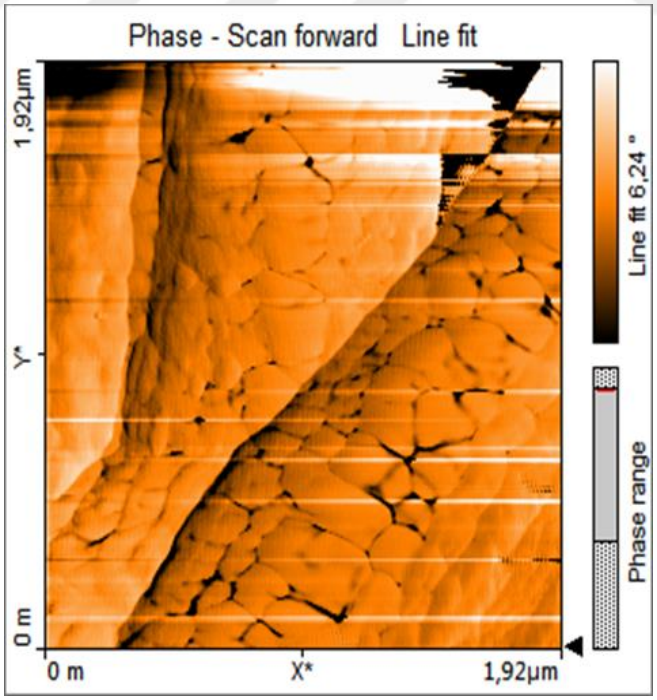

Figure 3.9 : AFM image of GO-containing oxidized PAN nanofiber webs.

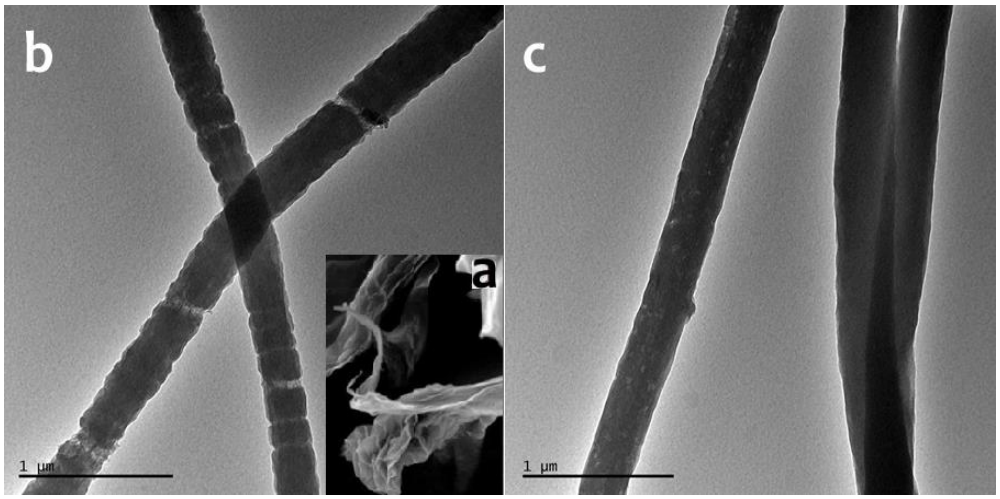

Figure 3.10 : a) SEM image of GO; b) TEM images of GO-containing PAN nanofibers; c) carbon nanofibers.

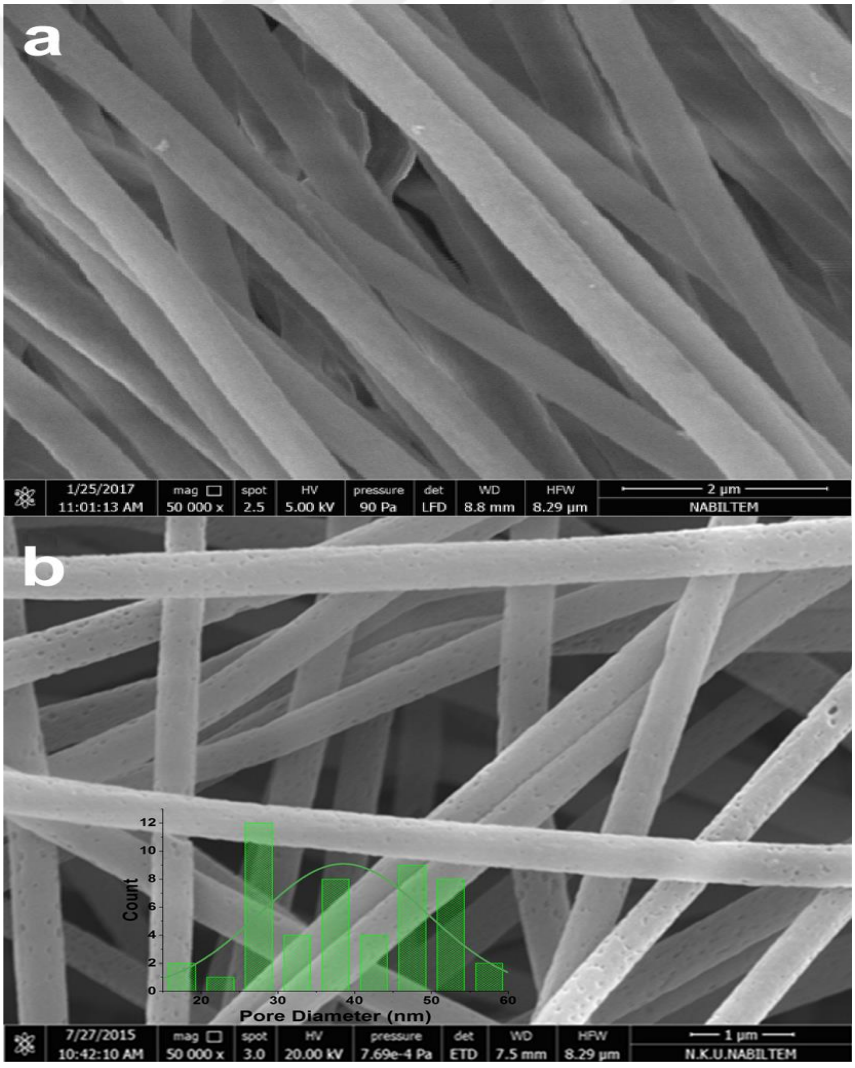

Figure 3.11 : SEM images of (a) oxidized PAN nanofiber webs and (b) GO-containing oxidized PAN nanofiber webs with pore distribution chart.

According to SEM images (Figure 3.11b) pore size on the nanofibers were measured as 38.5 ± 11 nm. All morphological characterizations prove the porous structure of GO containing nanofibers.

In supercapacitors that use nanoporous electrodes to store large amounts of charge, ions penetrate into the pores of the electrode. Raymundo-Piñero et al. considered that an adequate pore size is more important than a high surface area and reported optimum pore sizes as 0.7 nm and 0.8 nm in aqueous and organic media, respectively (Raymundo-Piñero, Kierzek, Machnikowski, & Béguin, 2006). Graphene oxide shows high specific capacitive performance because of layered graphene sheets in the structure (Karthika et al., 2012).

3.2.7 Electrochemical impedance studies of PAN and GO-containing PAN-based nanofibers

A standard three-electrode cell was used to study electrochemical performances of nanofibers by using cyclic voltammetry (CV) and electrochemical impedance spectroscopy (EIS). Carbonized nanofibers were used as free standing electrodes whereas oxidized nanofibers were deposited on fluorine-doped tin oxide (FTO) glass to use as working electrodes. EIS analysis were investigated in 0.1 M $NaClO_4$/ACN electrolyte in a frequency range of 10 mHz to 100 kHz at open circuit potential with an AC perturbation of 10 mV. The samples of oxidized nanofibers are designated as Ox.PAN, Ox.PAN/GO(1) and Ox.PAN/GO(2) indicating concentration of 0, 1.25 and 2.5% graphene oxide relative to PAN, respectively.

Nyquist plots in (Figure 3.12) represent a semicircle in the high to medium frequency range. The inclined line corresponding to diffusion processes at low frequencies region appears only in PAN/GO(1). The charge-transfer resistances (R_{ct}) were evaluated by using equivalent circuit modelling. R_{ct} is attributed to the pore size of the electrodes. The values of R_{ct} of Ox.PAN, Ox.PAN/GO(1) and Ox.PAN/GO(2) were equal to 1180 kΩ, 119700 kΩ and 182800 kΩ, respectively, R_{ct} increases with GO content.

According to the Bode phase plots, the sample of Ox.PAN/GO(1) and Ox.PAN/GO(2) show similar properties while Ox.PAN behaves differently (Figure 3.13). After adding GO to the nanofibers the phase angle increases linearly and exhibits larger plateau regions. This indicates the capacitive behavior.

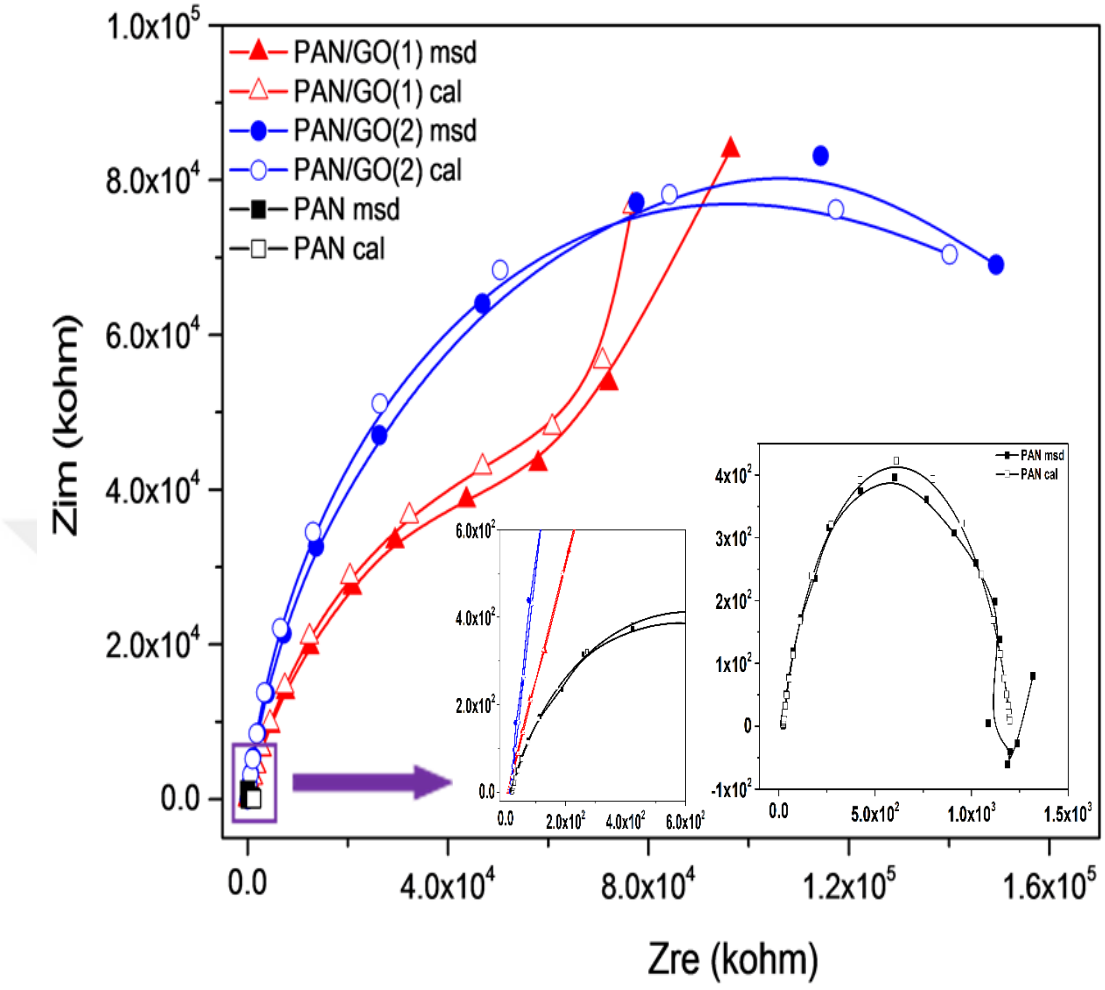

Figure 3.12 : Nyquist plots of oxidized PAN and GO-containing oxidized PAN nanofiber webs (inset: Nyquist plots of oxidized nanofiber webs at high frequencies and Ox.PAN nanofiber webs up to 100 kHz).

The Bode magnitude plots exhibit two different shapes for high and low frequencies (Figure 3.14). At high frequencies, the impedance values of Ox.PAN and Ox.PAN/GO nanofibers do not change significantly and this is attributed to the disability of the electrolyte ions to penetrate into the electrode. The solution resistance (R_s) of the electrochemical system changes very slightly, which can be seen in (Table 3.1). On the other hand, the impedance of Ox.PAN/GO nanofibers is very high due to the penetration of ions into the electrode surfaces at low frequencies (Karthika et al., 2012).

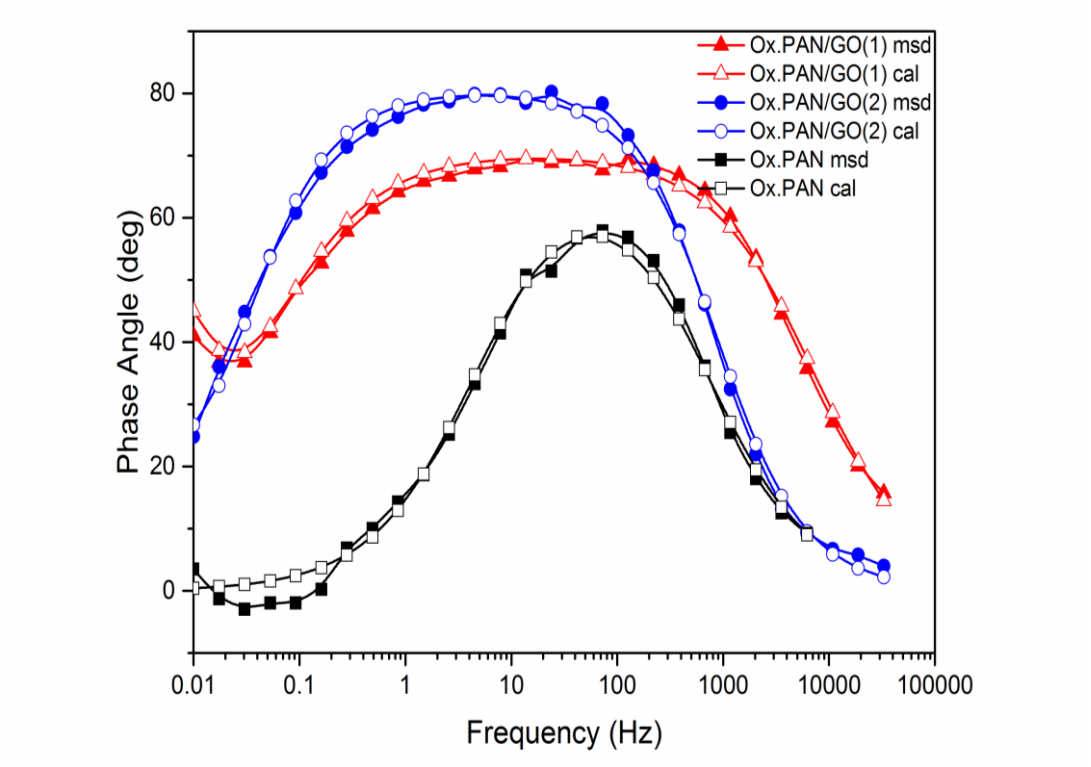

Figure 3.13 : Bode phase plots of oxidized PAN nanofiber webs and GO-containing oxidized PAN nanofiber webs.

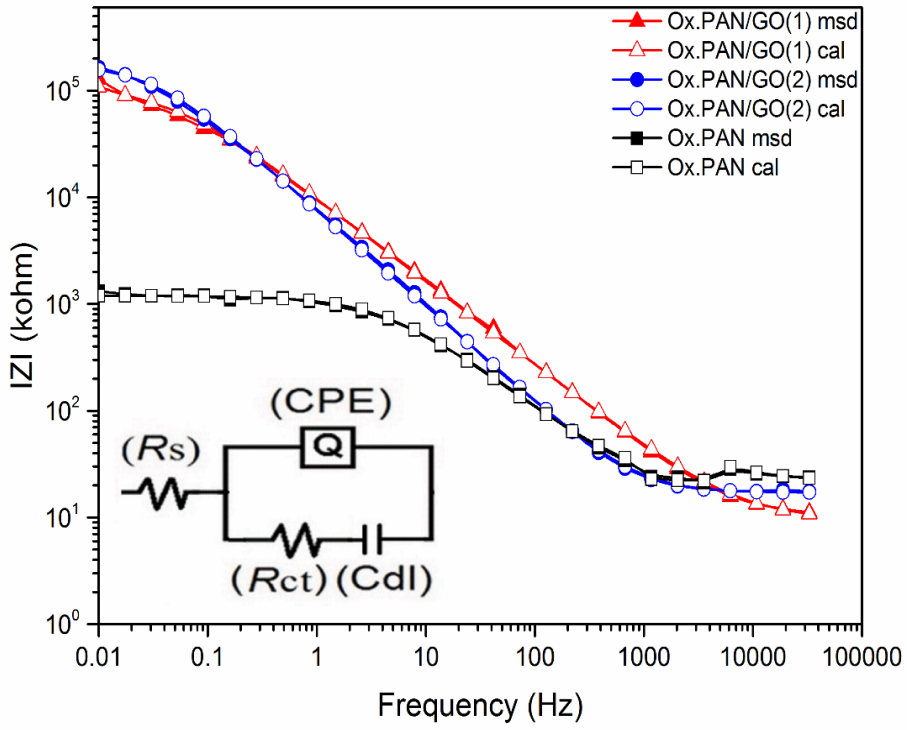

Figure 3.14 : Bode magnitude plots of oxidized PAN nanofiber webs and GO-containing oxidized PAN nanofiber webs (inset shows the electrochemical equivalent circuit).

The parameters of the simulated equivalent circuit models obtained from the Nyquist and Bode phase plots are given in (Table 3.1). Fitting with equivalent circuit modelling exhibited a good correlation between the calculated and experimental values with χ^2 values around 10^{-3}. The result shows two different models. $R_s(Q_{el}R_{ct})$ circuit modeling was compatible with Ox.PAN, while a $R_s(Q_{el}(R_{ct}C_{dl}))$ circuit modelling was chosen for Ox.PAN/GO(1) and Ox.PAN/GO(2).

Table 3.1 : Fitting values for the equivalent circuit elements by simulation of the impedance spectra of oxidized nanofibers**.**

Sample	R_s (kΩ)	Q_{el}(CPE) (μS.s^n)	n	C_{dl}(μF)	R_{ct} (kΩ)	χ^2 (10^{-3})
Ox.PAN[a]	21.80	0.060	0.79	-	1180	5.54
Ox.PAN/GO(1)	9.55	0.024	0.78	0.190	119700	4.72
Ox.PAN/GO(2)	17.05	0.025	0.90	0.600	182800	3.99

[a]An $R_s(Q_{el}R_{ct})$ equivalent circuit model has shown a better correlation with this sample.

R_s corresponds to the solution resistance, R_{ct} corrresponds to the charge-transfer resistance of electrode surface and solution interface, and Q_{el} corrresponds to the combined capacitance of nanofibers and FTO glass electrode. R_{ct} and C_{dl} change linearly with the amount of GO and n values of Ox.PAN and Ox.PAN/GO(1) are very similar (Table 3.1). After increasing the GO content in the nanofibers, n value increases and exhibits nearly ideal capacitive behavior for Ox.PAN/GO(2). The C_{dl} of Ox.PAN/GO(2) is 3.16 times higher than that of Ox.PAN/GO(1). CPE is generally used in heterogeneous systems associated with non-ideal capacitive behavior resulting from electrode roughness, inhomogeneous conductivity, or even diffusion (Rubinson & Kayinamura, 2009). CPE is also related to the composition of the nanofibers. The proposed model is consistent with charge-transfer processes taking place at interior pores filled with electrolyte.

Heat treatment was applied to Ox.PAN and Ox.PAN/GO nanofibers to produce carbon nanofibers (CNF) and GO-containing carbon nanofibers (CNF/GO). CNF and CNF/GO, which include very small amount of graphene oxide (1.25% relative to PAN) were used as free standing working electrodes during cylic voltammetry. CV of CNF and CNF/GO electrodes are shown in (Figure 3.15) at a scan rate of 50 $mV \cdot s^{-1}$ between

−0.5 V and 1.2 V in 0.1 M $NaClO_4$/ACN electrolyte. It can be seen that CNF/GO electrode exhibits a larger CV area than the CNF electrode, indicating a higher specific capacitance compared to CNF. Adding GO increases the O/C ratio, which could result in an enhanced capacitive behavior of the carbon nanofibers.

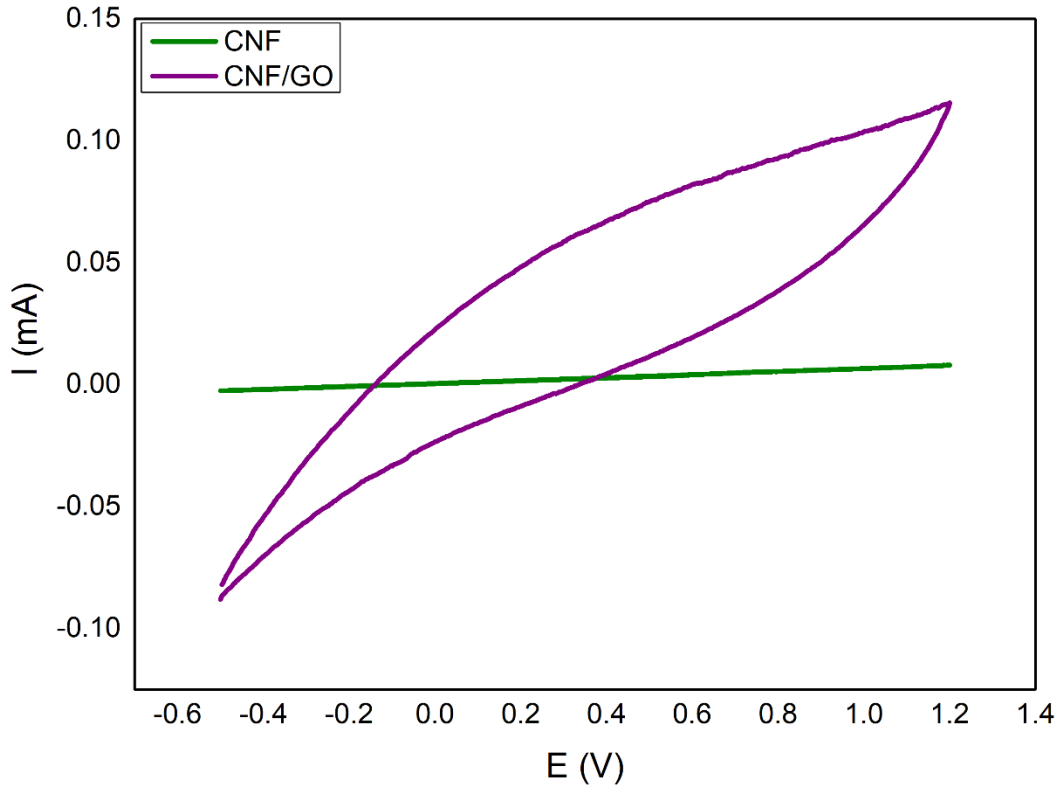

Figure 3.15 : Cyclic voltammograms of carbon nanofibers and GO-containing carbon nanofiber webs at scan rate of 50 $mV \cdot s^{-1}$ (PAN-based nanofibers with and without GO, first oxidized then carbonized).

3.3 Conclusion

In this study, CNF webs and GO-containing CNF webs were successfully fabricated. Nanofiber webs were fabricated via electrospinning. Nanofiber alignment was achieved with a rotating collector, which also had the definite and expected effect of increasing modulus and reducing the strain to break of the webs. Different oxidation temperatures were studied and 250 °C was selected as optimum temperature for this study. Increased the oxidation temperature increases the oxidation level of the sample. However, thermal oxidation between 200 °C and 300 °C was not enough to eliminate all C≡N triple bonds. GO-containing oxidized nanofibers have a rough surface. Nanopores of around 38.5 ± 11 nm pore size on the nanofiber surface can help to store large amounts of charge. GO addition into PAN makes a significant change on the EIS

results, i.e., the capacitive behavior increases with the increase in the C_{dl} value of GO-containing oxidized nanofibers. The C_{dl} value of Ox.PAN/GO(2) is the highest as being 0.600 μF. Individual layered sheets of GO with high surface area are supposedly exposed to the electrolyte, which can result in the increase of the double layer capacitance. GO functional groups enhance the capacitance performance of CNF webs. As a result, CNF/GO can be a potential candidate for capacitive applications.

4. THERMALLY TREATED GRAPHENE OXIDE/POLYACRYLONITRILE BASED ELECTROSPUN CARBON NANOFIBER PRECURSOR[3]

Nanoparticles exhibit a variety of special properties relative to bulk forms; in particular nanoparticles have different properties due to their increased surface area, reactivity and strength. Graphene has great attention recently because of its unique properties such as electronic, optical, magnetic, thermal, and mechanical as well as large specific surface area (Bhuyan, Uddin, Islam, Bipasha, & Hossain, 2016). Graphene Oxide (GO) has especially some distinguishing properties such as high surface area and a honeycombed carbon based structure (Yanwu Zhu et al., 2010). It exhibits 2-D graphene layers decorated with oxides that reduce the conductivity. Therefore, GO needs to be chemically reduced or thermally treated to improve its electrical performance before it can be applied (L. Q. Xu, Liu, Neoh, Kang, & Fu, 2011). Although oxygen functional groups make GO hydrophilic and electrically insulating (Toh, Loh, Kartom Kamarudin, Ramli, & Daud, 2014), in contrast to graphene, GO sheets are more compatible with organic polymers. Pristine graphene is not compatible with organic polymers and does not form homogeneous composites. As a result, GO has attracted considerable attention as a nanofiller for polymer nanocomposites (Das & Prusty, 2013). Furthermore, reduced graphene oxide (rGO) obtained from GO by thermal treatment possesses higher degree of graphitic structure and consequently outstanding electrical properties (Bai, Huang, Yu, & Kang, 2014). rGO acts as a conducting filler with addition into the polyacrylonitrile (PAN) film. Electrical resistivity of PAN/Graphene Oxide (PAN/GO) composite films decrease because of the thermal reduction of GO by applied appropriate temperature (Lee, Kim, Kim, et al., 2012). Therefore, PAN/GO composite nanofibers structure give a chance to develop carbon nanofibers which includes GO as a nano filler.

Polyacrylonitrile (PAN) and its copolymers are widely used as precursors in the manufacturing carbon fiber materials with interesting mechanical, electrical and

[3] This chapter is based on "**Gergin, I., Micusik, M., Ismar, E., Omastova, M., and Sarac, A.S.** (2020). Thermally Treated Graphene Oxide/Polyacrylonitrile Based Electrospun Carbon Nanofiber Precursor. *Journal of nanoscience and nanotechnology*, *20*(6), 3448-3459."

magnetic properties and high thermal, chemical resistance (Faraji et al., 2017; Ismar & Sarac, 2016). These materials are found in a wide range of applications in the aircraft and automotive industries, including in electronics and filters. Nanoparticles and polymeric composites are sophisticated materials which exhibits variety of benefits. Unlike their bulk forms, nanoparticles have different properties due to their increased surface area, reactivity and strength. Electrospinning is an useful method for fabricating submicron and nanosized fibers (Huang et al., 2003). During the electrospinning process, voltage difference between the collector/ground and needle push the polymeric solution, solvent can be evaporated by forming a Taylor cone and polymer in the fiber form can be collected on the collector (Nataraj, Yang, & Aminabhavi, 2012). Submicron fibers and especially nanofibers exhibit significant properties such as high surface area, high aspect ratio, and light weight.

Carbon nanofibers (CNF) are of increasing interest due to their unique properties in addition to their high-surface areas, electrical conductivity and mechanical properties. The main research areas of carbon nanofiber usage are catalyst support materials, Li-ion batteries, supercapacitors, fuel cells, sensors and applications in composite materials (De Jong & Geus, 2000). Carbon nanofiber production from PAN nanofibers consists of oxidative stabilization and carbonization steps. Oxidation and carbonization studies should be carefully conducted to obtain the desired properties for CNF. Oxidation process has a key role, which helps to prevent melting and fusing of nanofibers during the carbonization (Ismar, Karazehir, Ates, & Sarac, 2018). Thermally stable and well organized cyclic molecular structures of pyrolysis products of PAN are produced by processing with an appropriate thermal treatment at lower temperatures than carbonization; this is defined as stabilization of the process. Stabilization is carried out in the presence of oxygen whereas pyrolysis conditions consist of inert atmosphere. Oxidation prevents polymer decomposition during carbonization at high temperature (Biedunkiewicz, Figiel, & Sabara, 2011). Through the carbonization of PAN fibers/nanofibers, thermal stabilization has a key role to achieve the desired properties for the end product.

The thermal stabilization process can be considered in two separate steps: oxidation and dehydrogenation (Ismar & Sarac, 2018; Ogawa & Saito, 1995; W. X. Zhang, Wang, & Sun, 2007). During thermal stabilization, linear PAN chain can be attacked by the oxygen and due to the oxidation process at high temperature following structural

changes can be realized; triple CN bonds break and convert to CN double bond while oxygen uptake is increased and –HCN starts to be eliminated from the PAN and nitrogen content of the structure is decreased. Thermal oxidation process is a series of complex and un-ordered reactions thus; it is identified as a complex mechanism.

Oxidative stabilization of PAN and micron sized fiber and their composites is already studied to understand the complex reaction mechanism. There is lack of study given in the literature about thermal stabilization of GO containing PAN nanofibers analyzed by EIS and XPS in detail.

In this study, thermal stabilization (oxidation) process is applied to both PAN nanofibers and compared to PAN/GO composite nanofibers to obtain further information especially, electrochemical properties on the oxidation structure and in a certain extent in the mechanism. Therefore, PAN/GO composite nanofibers were prepared by electrospinning and then treated at various temperatures for up to 3 hours. XPS, FTIR-ATR spectroscopical measurements and EIS studies were analyzed for characterization of the thermally treated samples. The results obtained provide insight into the change in the chemical structure of PAN and PAN/GO during oxidation process so the effect of GO on the final structure. XPS is a powerful tool to understand the detailed structure by giving information about the presence of C, O, N bonds in the materials surface. These newly formed bonds during thermal oxidation and stabilization steps play an essential role on the intermediate form of PAN based Carbon nanofiber structures and make important contributions to the carbonization process.

4.1 Experimental

4.1.1 Materials and methods

Polyacrylonitrile (PAN) with an average M_W 150.000 g/mol and N,N-Dimethylformamide (DMF) reagent grade were purchased from Sigma Aldrich and were used as received. Graphene oxide (GO, purity 99%) was purchased from Grafen Chemical Industries and used as received. GO composite nanofibers were prepared by electrospinning method using mixture of PAN (10 wt/v%) and dispersing given amount of GO blend (1.25 wt/v% graphene oxide relative to PAN) in DMF solution. The solution was mixed with a magnetic stirrer for 24 hours at room temperature.

Fabrication of the nanofibers was achieved via electrospinning technique which is equipped with a rotating collector to improve the fiber alignment. Electrospinning solution fed into the syringe and parameters were set as follows: 1.0 ml/h feeding ratio, 15 kV, 15 cm (tip to collector distance) and 400 rpm was the rotational speed of collector. Thermal oxidative stabilization of samples was performed under an oxygen atmosphere for 1 h and 3 h, at changing temperatures (250 °C , 280 °C , and 300 °C).

The chemical structure of the samples was characterized by Fourier Transform Infrared Attenuated Total Reflectance (FTIR-ATR) Spectroscopy (Perkin Elmer, Spectrum One, with a Universal ATR attachment with a diamond and ZnSe crystal). XPS signals were recorded using a Thermo Scientific K-Alpha compact XPS system (Thermo Fisher Scientific, UK) equipped with a microfocused, monochromatic Al Kα X-ray source (1486.6 eV).The spectra were acquired in the constant analyzer energy mode with the pass energy of 200 eV for the survey. Narrow regions were collected with the pass energy of 50 eV. Charge compensation was achieved with the system Ar flood gun. Thermo Scientific Avantage software, version 5.9904 (Thermo Fisher Scientific), was used for digital acquisition and data processing. Spectral calibration was determined using the automated calibration routine and the internal Au, Ag and Cu standards supplied with the K-Alpha system. The surface compositions (in atomic %) were determined by considering the integrated peak areas of detected atoms and the respective sensitivity factor. Surface morphology of nanofibers was investigated with an FEI Quanta FEG 250 scanning electron microscopy (SEM) with 15 kV accelerating voltage after being coated with Gold using Ion Sputter Metal Coating Device (MCM-100 Model). Electrochemical Impedance Spectroscopic (EIS) measurements were conducted with Potensiostat 2263 Electrochemical Analyzer (Princeton Applied Research, USA) in 0.1 M $NaClO_4$/ACN electrolyte in a frequency range of 10 mHz to 100 kHz at open circuit potential with an AC perturbation of 10 mV.

4.2 Results and Discussion

4.2.1 Morphologic characterization of oxidized nanofibers

Homogeneity and homogeneous distribution of nanofibers were checked by SEM measurements and fiber diameters were obtained from the SEM results as well. Nanofiber formations are presented in (Figure 4.1). According to SEM images, the

diameter of the nanofibers increases with increasing GO addition to the PAN structure in (Figure 4.1(a, b)). The inclusion of GO results in a porosity in the nanofiber surface with an average diameter of 38.5±11 nm which is reported in our previous study and TEM measurements also prove the porous structure of GO containing PAN nanofibers (Gergin, Ismar, & Sarac, 2017). This porous structure affects the electrochemical performance of nanofibers that can help to store large amounts of charge.

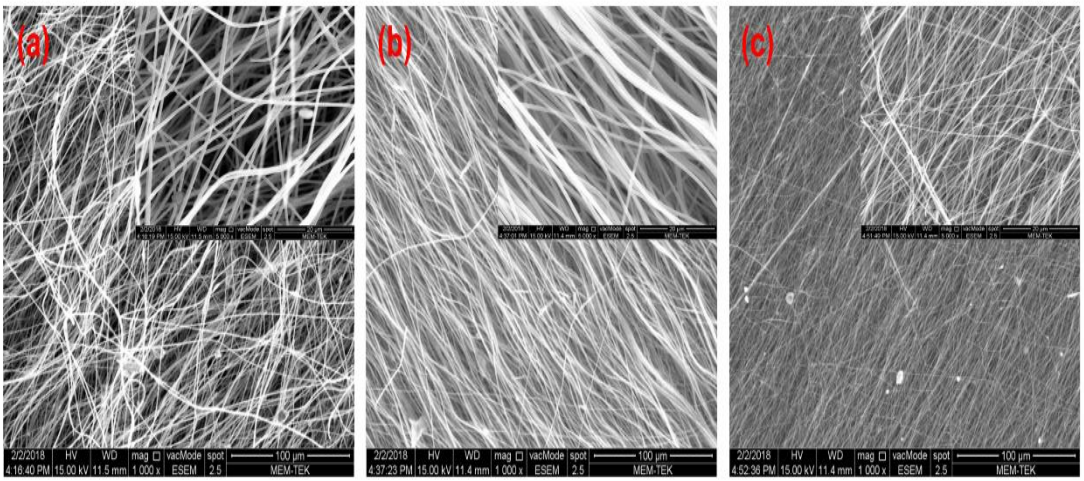

Figure 4.1 : SEM images of oxidized nanofiber webs at 280 ^{0}C with 5 kx and 1 Kx magnification; (a) PAN/GO-1 h, (b) PAN/GO-3 h, (c) PAN-3 h.

4.2.2 Surface properties of oxidized nanofibers

Oxidation reaction mechanism of PAN is complex and the cyclization process for PAN fibers (homopolymer) occurs by a free radical initiation stage followed by oxidative reactions. The cyclization of nitrile pendant groups of PAN which give polyimine type structure is well accepted as the main reaction during stabilization (Avilés et al., 2002). These imine sequences are postulated to be three to six units long. The presence of polar groups C=O, OH and COOH in the chains facilitates the initiation of the cyclization process through a nucleophilic attack and accelerates the subsequent oxidative ring closure reactions.

Production of carbon form from PAN, a linear polymer is changed to a graphitic structure, and so the main question can be when the cyclization occurs (Bashir, 1991). There are still some uncertainties on the order of the chemical reactions in between cyclization and dehydrogenation. In the most accepted mechanism, cyclization goes through the opening of C≡N triple bond to C=N double bond and crosslinking. In

addition, the appearance of the C=C group is a consequences of dehydrogenation. The final, thermally stable and strong product becomes ready for high temperature carbonization process (Nataraj et al., 2012). Firstly, CN triple bonds break and convert to CN double bond, but CN triple bonds still exist with a low amount in the structure where it can be observed from (Figure 4.2) between ~280 °C-300 °C by the application of heat. C≡N bonds gradually decrease during the cyclization reaction. The decrease in the rate of C≡N bond % which is also related to cyclization rate for the PAN/GO-3h sample is faster than PAN/GO-1h and PAN-3h samples (Figure 4.2). A more linear relationship can be seen where the reaction still proceeds for PAN/GO-1h samples between ~280 °C-300 °C temperature region compared to others.

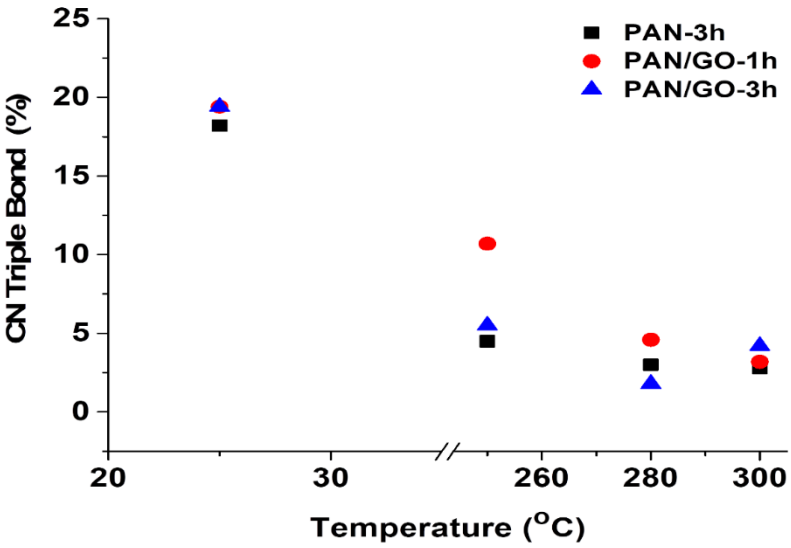

Figure 4.2 : Dependence of C≡N at.% (from N1s) obtained from XPS results versus temperature for PAN and PAN/GO nanofibers.

Thermal stabilization of PAN was explained with the four leading reactions: shaping of the ladder like polymer structure with the formation of cyclized C=N structures, crosslinking of intermolecular nitrile units, azomethine crosslinking, and hydrogen elimination (Bashir, 1991). During the oxidation, two types of structural conversion are seen; one is the conversion of C≡N bonds to C=N which promotes the cyclic structure and other is dehydrogenation which leads the aromatic and supramolecular structures (S. Ma et al., 2016).

According to FTIR-ATR spectroscopic results shown in (Figure 4.3(a)), an absorption band around 2243 cm^{-1} was assigned as C≡N bond (Kakida et al., 1996; Lee, Kim, Ku, et al., 2012; Ouyang et al., 2008) and a band at 1580 cm^{-1} was assigned to C=N bond

(Ogawa & Saito, 1995), (Ouyang et al., 2008), (Lee, Kim, Ku, et al., 2012), (Arshad et al., 2011; Dalton et al., 1999; J. Liu et al., 2009; Standage & Matkowsky, 1971). During the oxidation step C≡N bonds start to become C=N and C—N bonds, however C≡N bonds are never eliminated completely during the oxidation. By way of explanation, nitrile group in the sample change to C=N and C—N groups through the cyclized structure and naphthyridine type rings were seen by heating (Brandrup & Peebles, 1968; Ouyang et al., 2008). FTIR-ATR spectra of oxidized PAN and PAN/GO nanofibers are very similar as are seen in (Figure 4.3). Since the addition amount of GO into PAN matrix is very low, GO effect on PAN nanofibers show a very little change as can be seen inset of (Figure 4.3(a)). GO containing samples have shoulder-like peaks at 1714 cm^{-1} and 1662 cm^{-1} which may be attributed to oxygen uptake reaction, can be probably explained due to C=O stretching vibration of a free ketone and a conjugated ketone (Fu et al., 2014).

Further understanding of the mechanism of cyclization of PAN-GO nanofibers the absorbance ratio of C≡N groups to C=N bond according to FTIR-ATR spectroscopic and XPS analysis were performed . FTIR-ATR measurements are essential in terms of obtaining the absorbance ratio between the mixed signals of C=N, C=C, N–H groups and the signal of C≡N bonds which is the indication of the oxidation level as it is expected the increase this ratio during the oxidation reaction. According to (Figure 4.3(b)), (C=N, C=C, N-H)/C≡N absorption ratio of PAN/GO nanofiber webs with 1 hour oxidation duration time linearly increases which means the reaction continues in that temperature interval by the formation of corresponding groups. Also, PAN and PAN/GO nanofiber webs with 3 hours oxidation duration time have a deviation at high temperature which can be related to the isomerization of C=N in the cyclic structures (Y. Xue, Liu, & Liang, 2013).

The increase in C=N bond amount and a decrease in C≡N bond amount reveals that the cyclization process takes place in the structure. According to (Figure 4.3(c)), C=N/C≡N ratios increases linearly with temperature, however, after 280 °C it decreases. This can be explained by the isomerization and other reactions which become the main reactions for PAN/GO nanofibers after undergoing 280 °C thermal treatment with 3 hours duration time. This temperature value and oxidation duration time would be considered as the terminations of the cyclization as a major reaction. It is obvious that 300 °C with 3 h for this sample has an excessive amount of energy for

oxidation process which probably causes the termination of cyclization and provides the occurrence of the isomerization and other reactions on the nanofiber structure which is supported by FTIR-ATR results shown in (Figure 4.3(b)).

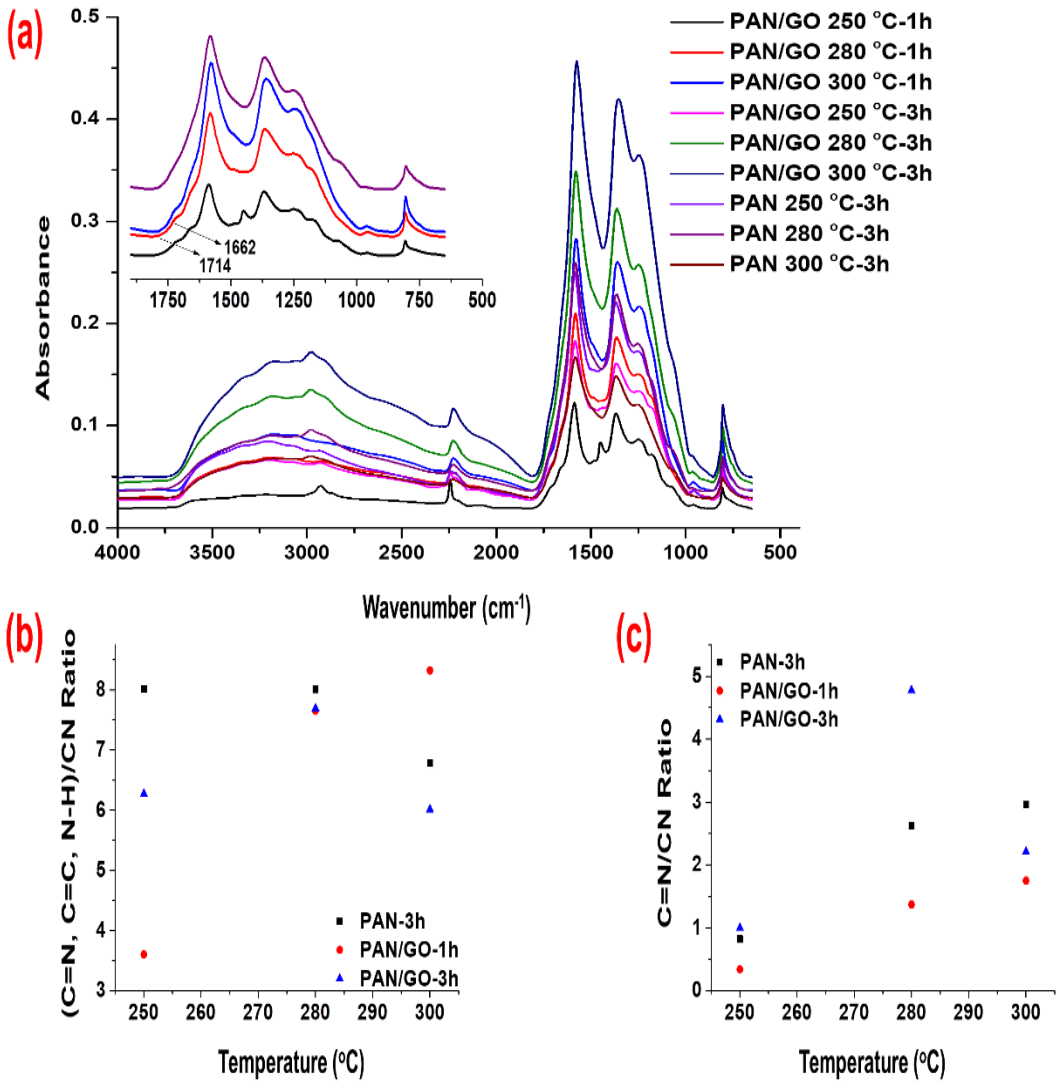

Figure 4.3 : FTIR-ATR results of oxidized PAN and PAN/GO nanofiber webs (a) for different temperatures and oxidation duration time, (b) absorption ratio of (C=N, C=C, N–H)/C≡N and, (c) C=N/C≡N ratios according to FTIR-ATR measurements.

In our previous studies, it has been indicated that the optimum oxidation temperature should be below 300 °C (Ismar & Sarac, 2018). PAN/GO composite structure should be also treated bellow 300 °C.

XPS results also support the FTIR-ATR measurements in terms of increasing the signal ratio between the mixed signals of (C=N, C=C, N–H) groups and the signal of C≡N bonds which is the indication of increased oxidation level. All over the oxidation

process, the carbon content is decreased on the other hand it is increased during the carbonization process.

GO consists of honeycombed carbon structure which also includes oxygen atoms. Although the addition of GO amount into PAN matrix is very low, GO still exhibits an important role on the oxidation process of polyacrylonitrile. This result can be very clearly seen by XPS and EIS measurements. The functional groups of graphene oxide initiate the PAN cyclization at lower temperature via ionic mechanisms (Nataraj et al., 2012). Thus, during the oxidation stage of PAN, GO plays a key role. Schematic representation of the interaction of GO flakes and oxidized PAN is seen in (Figure 4.4).

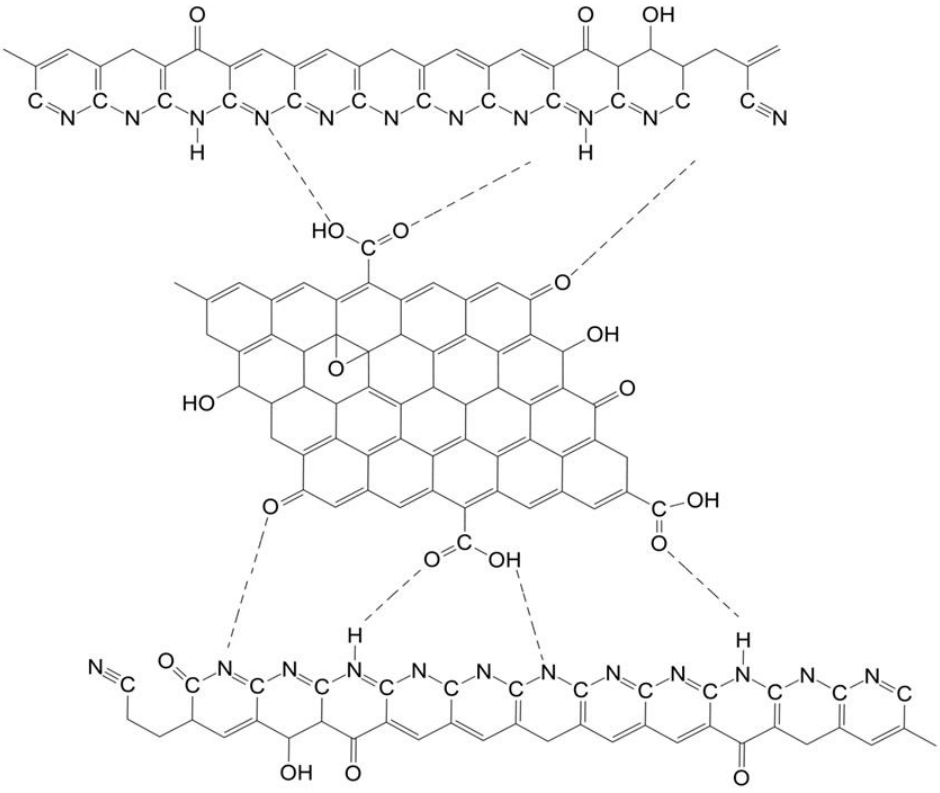

Figure 4.4 : Interaction of GO flakes and oxidized PAN.

The XPS results in (Figure 4.5) indicates that while carbon content is almost linearly decreasing, the oxygen content is increasing and nitrogen content also slowly decreasing and not much change was observed for the nitrogen content as expected. The main reaction can occur between adjacent nitrile groups within a polymer chain to form the ladder-like structure so that nitrogen content shows a small change (Takahagi, Shimada, Fukuhara, Morita, & Ishitani, 1986) (Figure 4.5(c)). There is not

much carbon atom elimination during the thermal oxidation of PAN, only the amount of newly formed carbon bonds is changed. When carbon content is evaluated according to XPS results, the percentage of carbon slightly decreased due to the changing of the total content of PAN. Elimination of other atoms and O_2 uptake causes to the change in the percentage of the carbon content over the total content of the structure (Figure 4.5(b, d)).

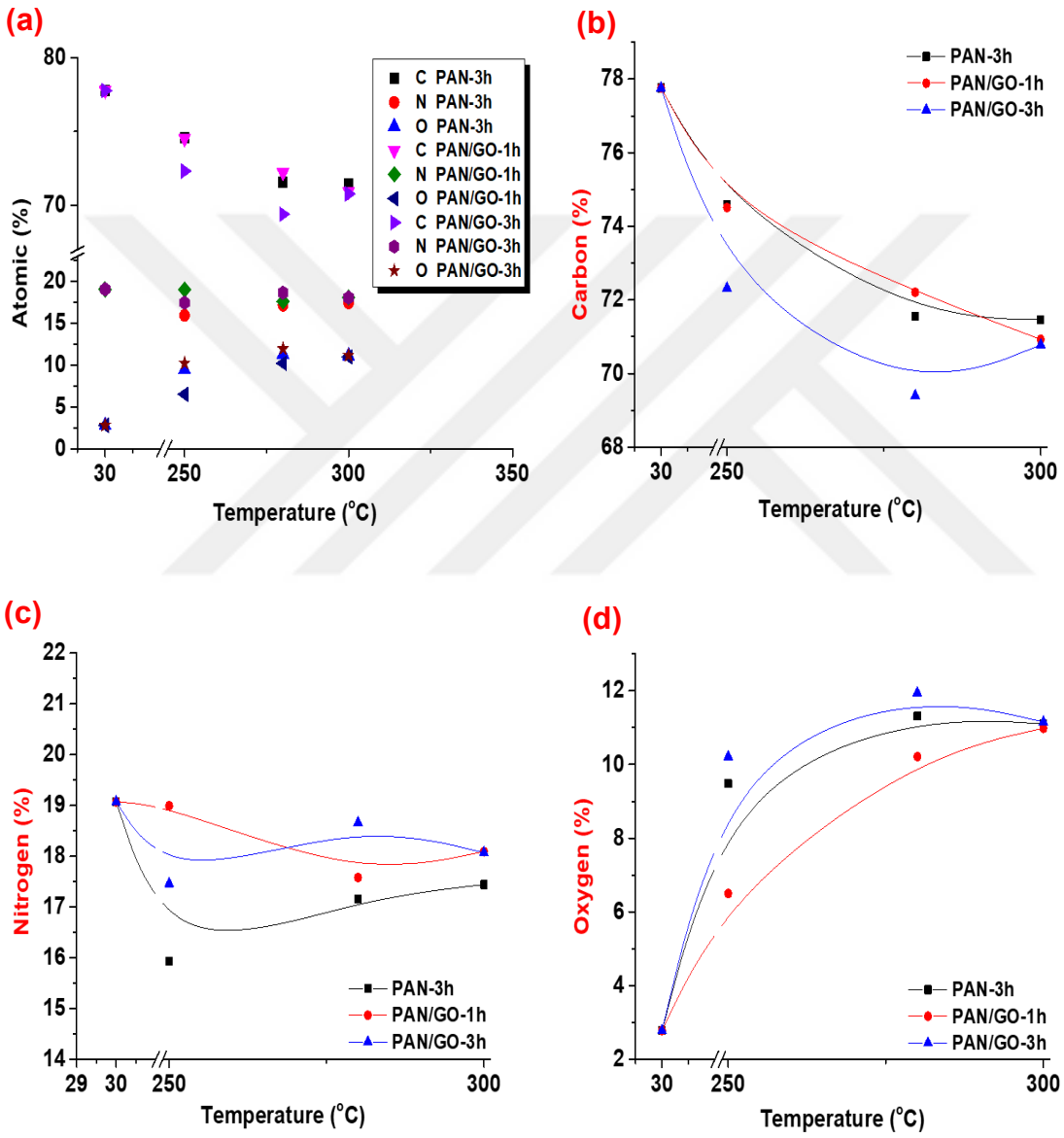

Figure 4.5 : (a) XPS results of oxidized PAN nanofibers for different temperatures and duration, (b) carbon (%) content, (c) nitrogen (%) content, (d) oxygen (%) content comparison between non-treated NF, oxidized PAN and PAN/GO nanofibers according to XPS results.

XPS results of Polyacrylonitrile based nanofibers [PAN, PAN/GO] treated at different temperatures (25 °C, 250 °C, 280 °C and 300 ºC) for different treatment time (0 h, 1 h

and 3 h) indicate that oxygen uptake is increased through the time and temperature however, 300 °C is too much for the samples for expected cyclization.

During the heat treatment for the cyclization and dehydrogenation steps, the cyclization goes through the opening of C≡N bond to C=N bond firstly and then C-N (even after carbonization at ∼1000 °C to C–C bonds). Through the complex thermal oxidation process, nitrogen content decreases and –HCN is removed from the structure, and a slight decrease in carbon content is balanced with oxygen uptake (Figure 4.5) while strong nitrile bonds are more or less stay stable during the low thermal oxidation stages (Morgan, 2005). Higher temperatures are needed for more elimination of nitrogen from the structure which occurs almost completely during carbonization dependingon applied temperature (Edie, 1998; Rahaman et al., 2007). The decrease in the CH_2 results with the presence and increase of the=C-H groups is indicative of aromatization of the structure under the oxygen atmosphere (Mittal et al., 1994; Ogawa & Saito, 1995).

XPS results show in (Figure 4.6) the deconvolution of C1s of pure PAN with typical ratio of C1 (at ~ 285.5 eV), C2 (at ~ 286.4 eV) and C3 (at ~ 287.0 eV) carbon signal (see the structure inset in (Figure 4.6(a)) with some adventitious carbon (at ~ 284.7 eV) and some surface oxidation (NC=O at ~ 288.8 eV) (Beamson & Briggs, 1992). The typical peaks of PAN are overlapping with the peaks from oxidation (C1 with increasing C-C signal at ~ 285.1 eV, C2 with C-O at ~ 286.2 eV, C3 with C=O at ~ 287.3 eV), but the ratio of these signals is clearly changing and with the overall higher oxygen content also new oxidation peaks appeared (OC=O at ~ 289.9 eV) (see Figure 4.6(b)).

After heat treatment there is a clear change in C1s spectra from virgin PAN to the oxidized form, also sp^2 carbon is developed, what confirms sp^2 signal at 284.4 eV and Pi–Pi* at 291 eV (Figure 4.6 (a,b)). The presence of GO probably accelerates the oxidation and development of the final structure and even at 250 °C has the C1s spectrum shape of that of PAN 280 °C–3 h and PAN-300 °C–3 h (see comparison (Figure 4.6 (c, d))). At shorter heat treatment time in the case of PAN/GO-1 h 250 °C the C1s shape shows the less oxidized form and the typical peaks C1, C2, C3 for pure PAN is still present in the similar ratio as in the case of virgin PAN. This can be followed also by the increase of imine (-C=N) groups of the N1*s* signal, which increase with the temperature and time has visible effect only in the case of 250 °C as discussed

above see (Figure 4.7). After heat treatment also new peak at 400.5 eV appeared, this could be assigned to some oxidized structures as CO–N–CO. Signal labeled as N^+ at ~402 eV could be also some graphitic nitrogen.

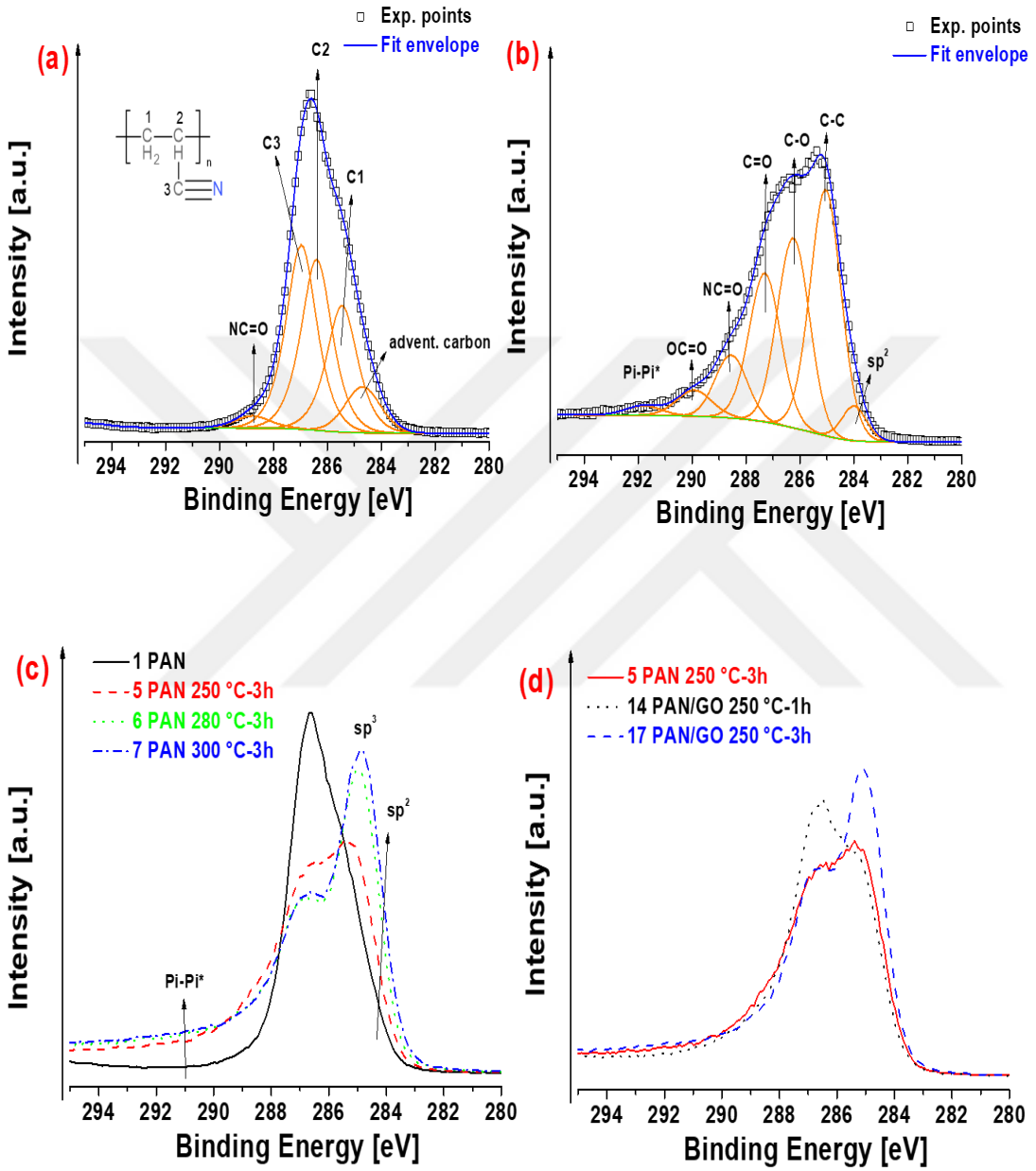

Figure 4.6 : XPS C1*s* region of (a) PAN before heat treatment, (b) PAN 250 °C –3 h, (c) C1*s* comparison of PAN and PAN treated 3 h at 250 °C, 280 °C, and 300 °C ; (d) PAN 250 °C –3 h, PAN/GO 250 °C –1 h, PAN/GO 250 °C–3 h.

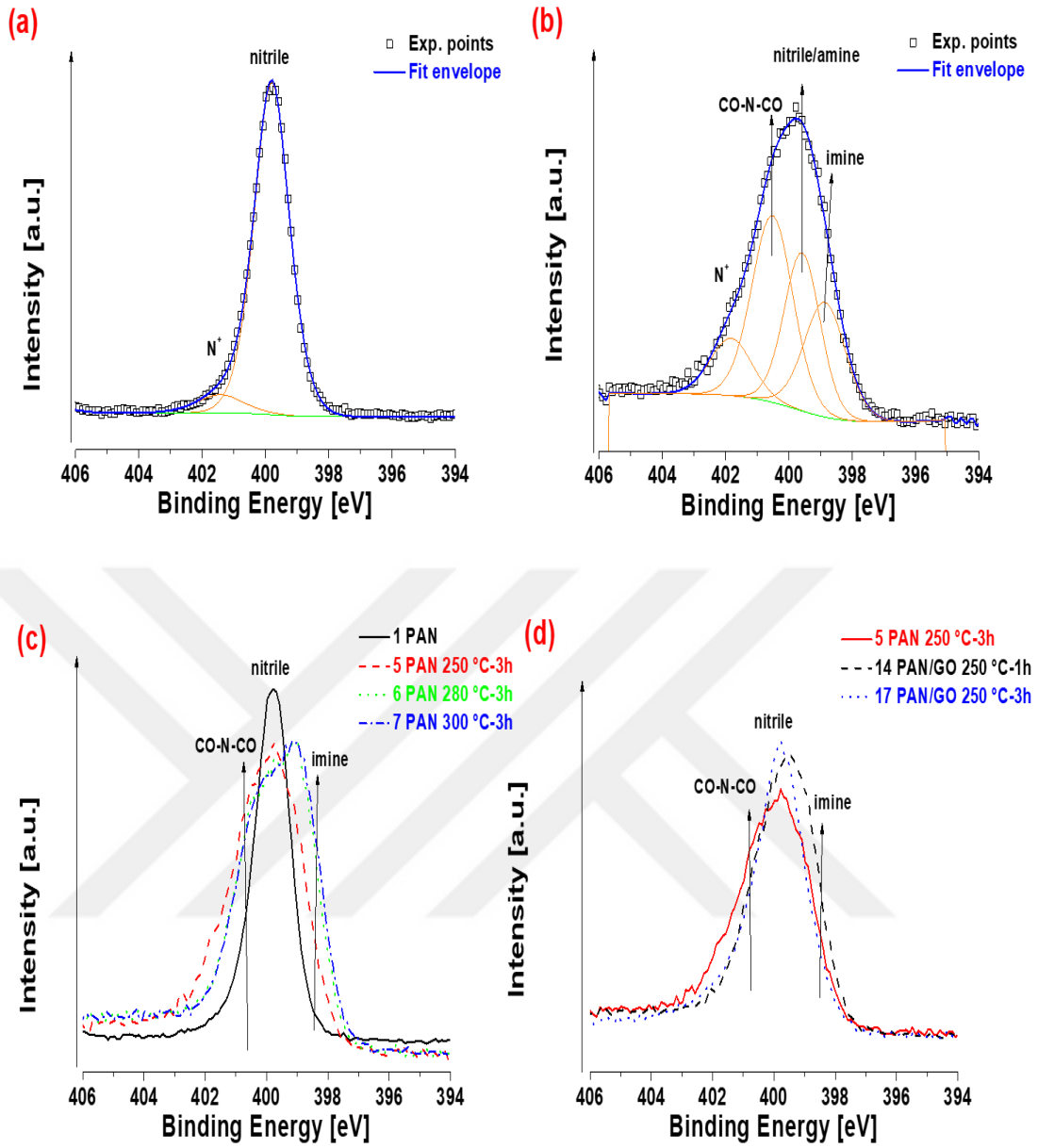

Figure 4.7 : XPS N1s region of (a) PAN before heat treatment, (b) PAN 250 °C–3 h, (c) C1s comparison of PAN and PAN treated 3 h at 250 °C, 280 °C, and 300 °C; (d) PAN 250 °C–3 h, PAN/GO 250 °C–1 h, PAN/GO 250 °C–3 h.

4.2.3 Electrochemical impedance spectroscopic (EIS)analysis of oxidized nanofibers

Electrochemical performance of nanofibers was analyzed by Electrochemical Impedance Spectroscopy. The EIS measurements were performed with a three electrode system consisting of platinum wire as a counter electrode, silver wire as a pseudo reference electrode and oxidized nanofiber free standing webs as working electrode in 0.1 M $NaClO_4$/ACN solutions. An equivalent circuit for the simulation of

the EIS spectra of nanofibers was performed with the ZSimp Win programme (v.3.10). Experimental and calculated measurements were fitted by equivalent circuit modeling. EIS plots with measured and calculated data are shown in (Figure 4.8) and (Figure 4.9).

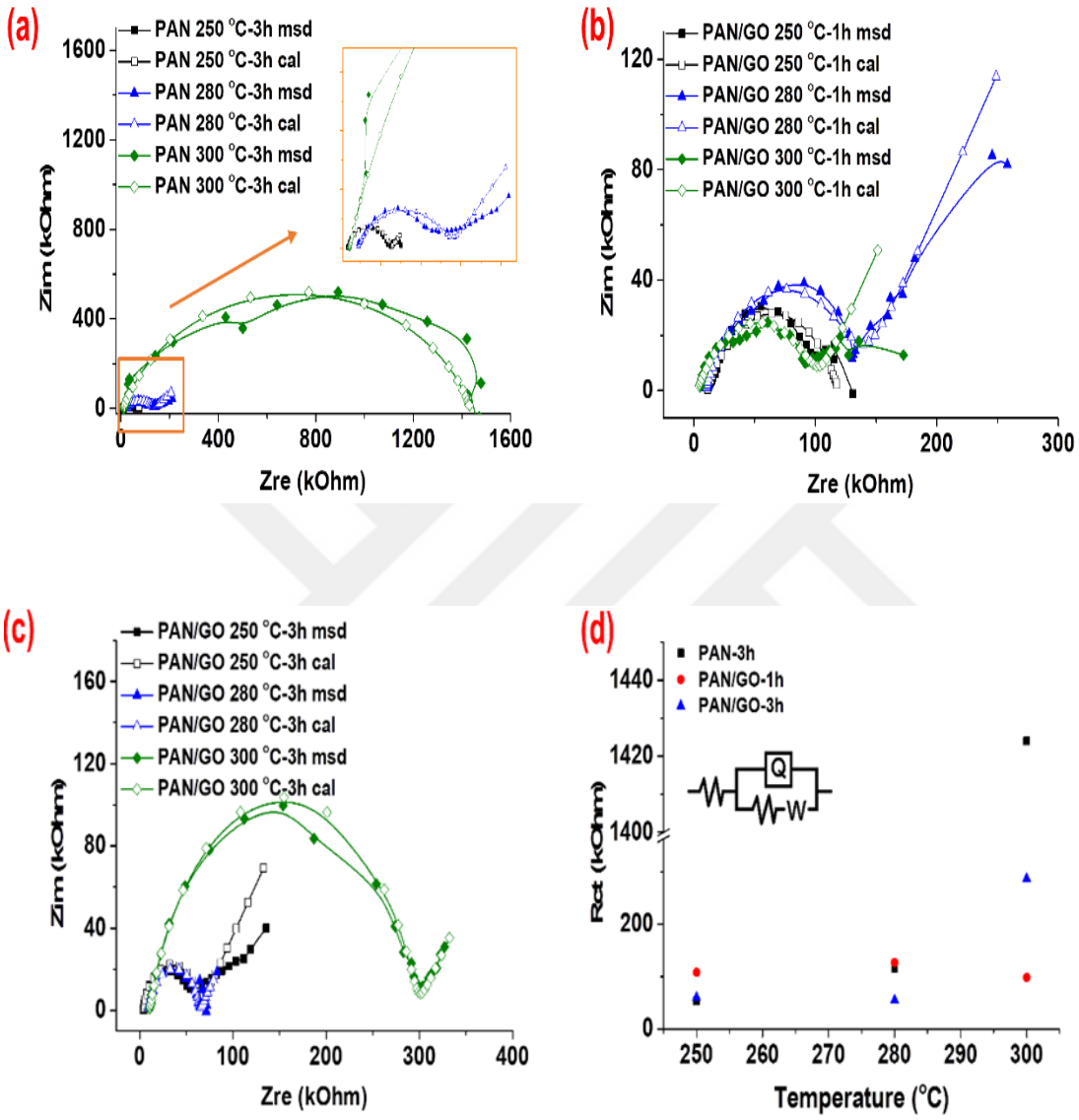

Figure 4.8 : Nyquist plots of (a) PAN-3 h, (b) PAN/GO-1 h, (c) PAN/GO-3 h, measured and calculated values at 250 °C, 280 °C, and 300 °C, (d) R_{ct} versus temperature plots with equivalent circuit model as *R(Q(RW))* inset.

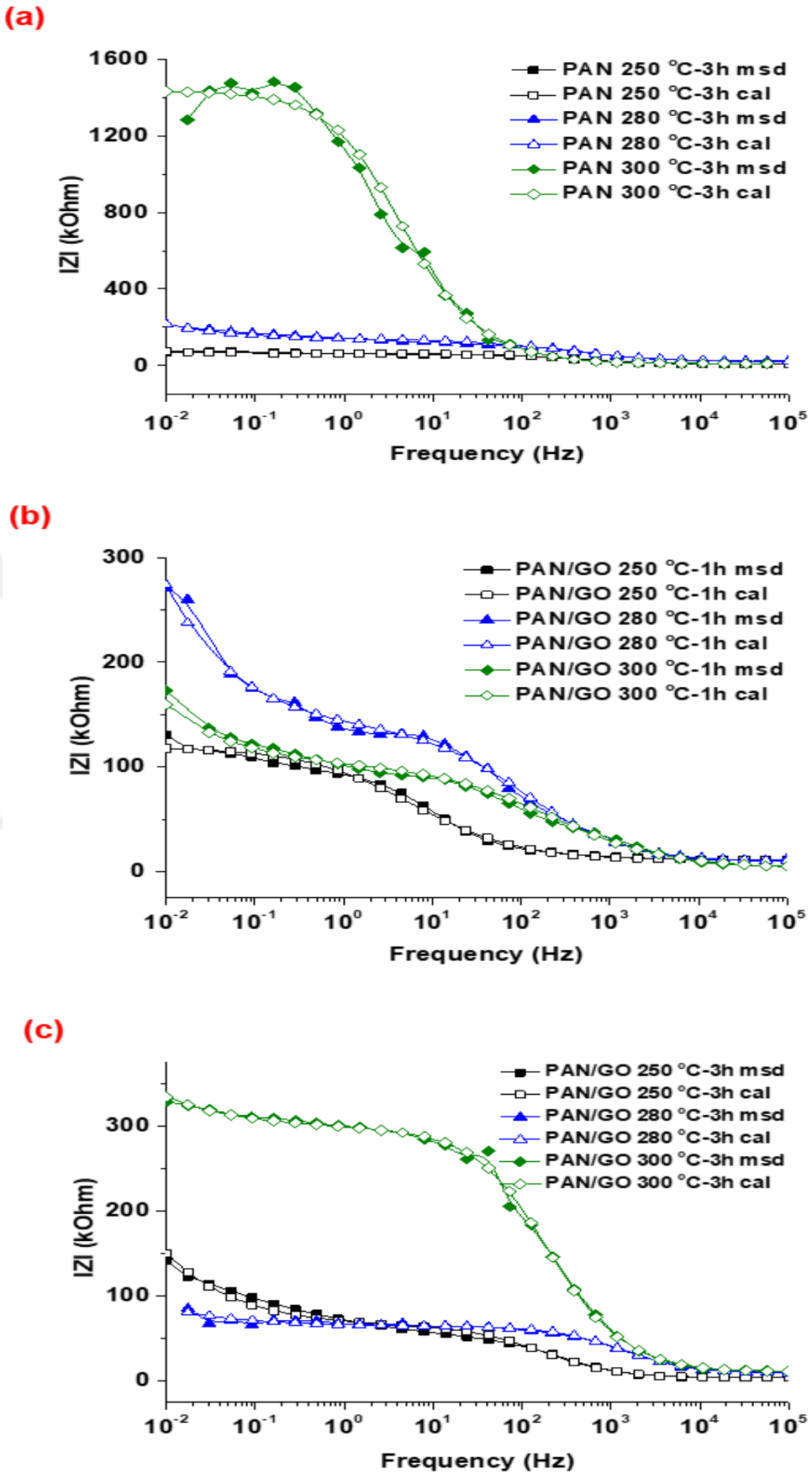

Figure 4.9 : Bode magnitude plots of (a) PAN-3 h, (b) PAN/GO-1 h, (c) PAN/GO-3 h, measured and calculated values.

A good agreement between experimental results and simulation was found with $\chi^2 \approx 10^{-3}$ (χ^2 is a function defined as the sum of the squares of the residuals). The Nyquist plot in (Figure 4.8(a)–(c)) consists of semicircles related to the electron-transfer process. Charge transfer resistance (R_{ct}) is correlated inversely with the electrochemical activity of nanofiber web surfaces and solution interface. The charge transfer resistance can be calculated from measuring the diameter of the semicircle. R_{ct} values of electrodes which are obtained by equivalent circuit modeling are given in (Figure 4.8(d)). The results showed an R_s (Q_{dl}(R_{ct}W)) model was fitted better to the data which can be seen in (Figure 4.8(d)) inset. R_s , R_{ct} , Q_{dl}, and W corresponded to solution resistance, charge transfer resistance, double layer constant phase element, and Warburg impedance element, respectively. Solution resistance (R_s) corresponds to the behavior of electrolyte and interface. Warburg impedance (W) represented diffusion properties. The 45° high-frequency intercept which can be seen in the Nyquist plot is a characteristic of the Warburg impedance (Murray, Tsai, & Barnett, 1998).

According to (Figure 4.8(d)), R_{ct} values increase exponentially with applied temperature for PAN and PAN/GO samples with 3 hours oxidation duration time. The highest value of R_{ct} was obtained 1424 kΩ for oxidized PAN nanofiber webs at 300 °C in 3 hours. It also reflected to Bode Magnitude plots in (Figure 4.9). The most resistive nanofibers are PAN samples at 300 °C in 3 h oxidation duration time. These results could be explained by degradation of PAN nanofibers at highest temperature with long oxidation duration time. The magnitude of IZI value of PAN/GO nanofibers smaller than PAN nanofibers at 0.01 Hz with 280 °C and 300 °C in 3 h oxidation time. It can be related to the partial reduction of GO in the PAN nanofibers with long duration time in high temperature. PAN composite films can be stabilized in air at 250 °C for 3 h and led to get a simultaneous partial reduction of GO (Lee, Kim, Kim, et al., 2012). GO has some oxygen functional groups on the surface such as 1,2-epoxide and alcohol groups on the basal planes, and carboxyl and ketone groups at the edges. These groups make the GO as an insulator. Significant amounts of these oxygen functional groups can be removed by various reduction methods to make the structure conductive (S. Park et al., 2011). Therefore, it is expected to reduce the resistivity of the structure with partial reduction of GO.

Constant phase elements (CPE) often used to improve to fit a model to impedance data. CPE is defined by:

$$Z_{CPE} = T_{CPE}(jw)^{-n}$$

where T_{CPE} and n are frequency-independent constants; ω is the angular frequency. The exponent n is a correction factor related to the roughness of electrode. The values for n are ranging between 0 and 1. n = 1 denotes the CPE (Q) element is an ideal capacitor, while n =0 and 0.5, denotes a resistance and Warburg behavior, respectively (Guan, Fan, Zhang, & Qu, 2010). As seen from (Figure 4.10), the value of Q_{dl} is very close to each other in the same samples with the different applied temperatures except a few nanofibers.As oxidation temperature decreased, the Q_{dl} values of PAN/GO-1 h samples increased and reached the highest value of 1.246 $\mu S.s^n$. GO containing PAN samples show much capacitive behavior than the pure PAN nanofibers.

GO addition into the matrice makes the surface more heterogeneous because of the individual layered sheets of GO. The microstructure of the nanofibers with active surface area and porosity makes a huge change in the EIS results (Gülercan, Gergin, & Sarac, 2018). These capacitive behaviors can be explained by the porous structure of nanofibers. The porous structure of the PAN/GO fibers explains such capacitive behavior (Gergin et al., 2017). On the other hand, the double layer capacitance decreases during long oxidation duration time which may be related to the partial thermal reduction of GO (Nataraj et al., 2012). During the oxidation process, a complex mechanism can happen due to the reduction of graphene oxide and the elimination of some of the oxygen containing groups at around 200 °C (G. Wang et al., 2008).

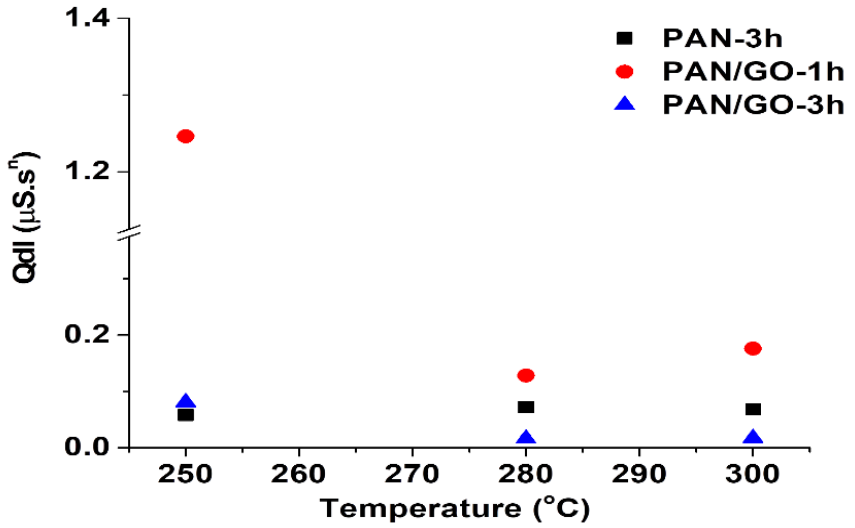

Figure 4.10 : Effect of temperature on Q_{dl} of PAN and PAN/GO nanofibers.

As seen in (Figure 4.11), C=O double bond % in the nanofiber webs is increased and C≡N bond % is decreased inversely by applied temperature which is indicative of the oxidation and cyclization reactions, respectively. The isomerization of resultant groups would take place when the cyclization, dehydrogenation and/or oxidation proceed to certain degrees. Therefore, the isomerization in oxidized PAN leads to the amount of resultant groups first increasing and then decreasing. Furthermore, two significant intermediate oxidized products (hydroxyl pyridine and pyridone structures) may be produced during the process of isomerization. The reaction mechanism indicates that the absorbance tendency of resultant groups (-C-N, C=C and C=O) first increasing and then decreasing may be due to the tautomeric isomerization among quasi-pyridone, hydroxyl pyridine and pyridone structures subsequent to critical reactions (Y. Xue et al., 2013).

Electrochemical impedimetric examinations are correlated with the XPS results in terms of R_{ct} which is obtained from the equivalent circuit model and C, O content which are obtained from the XPS measurements. R_{ct} has reached the highest value of 1424 kohm for PAN 300 °C in 3 hours. PAN/GO composite nanofibers represent lower R_{ct} value. Oxidized nanofiber webs show the similar behavior for both R_{ct} values and C=O % in (Figure 4.12). R_{ct} values and C=O % of PAN/GO-3h sample shows a small decrease at 280 °C compared to the others according to the partial reduction of GO during the oxidation process. After this temperature the values getting an increase which is caused by side reactions during the process.

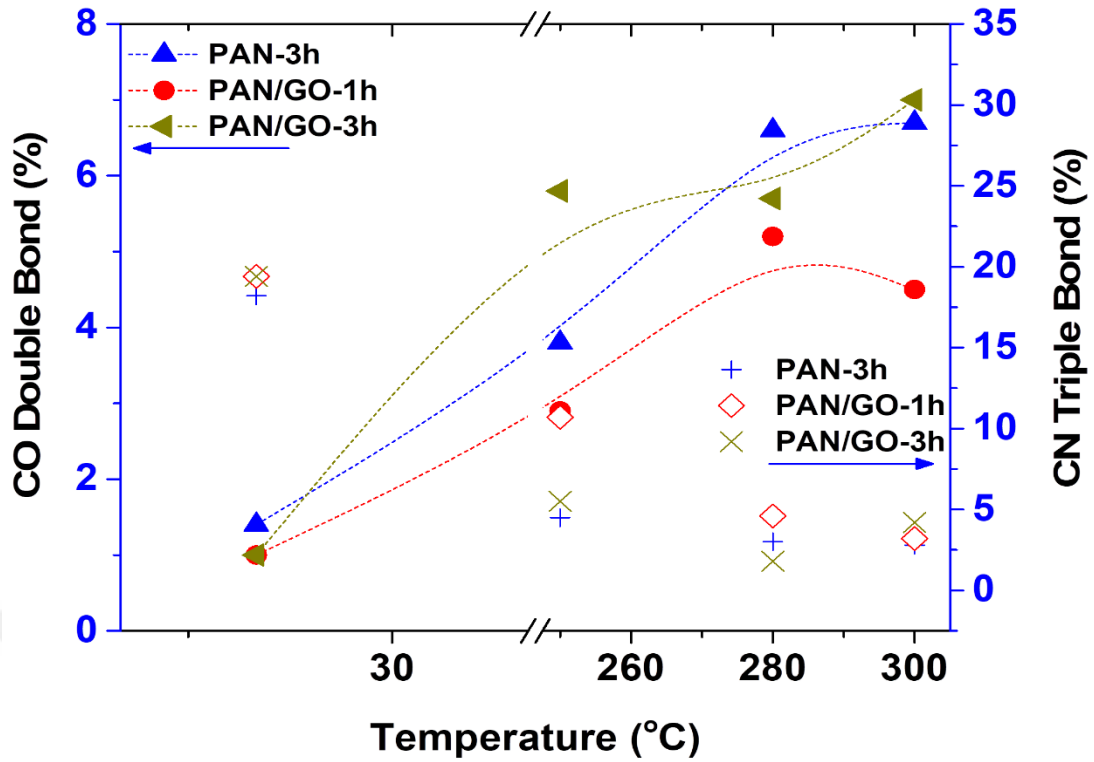

Figure 4.11 : C=O from O1s amounts and C≡N from N1s amounts were plotted to show the inverse ratio of the C=O and C≡N bonds during the oxidation process.

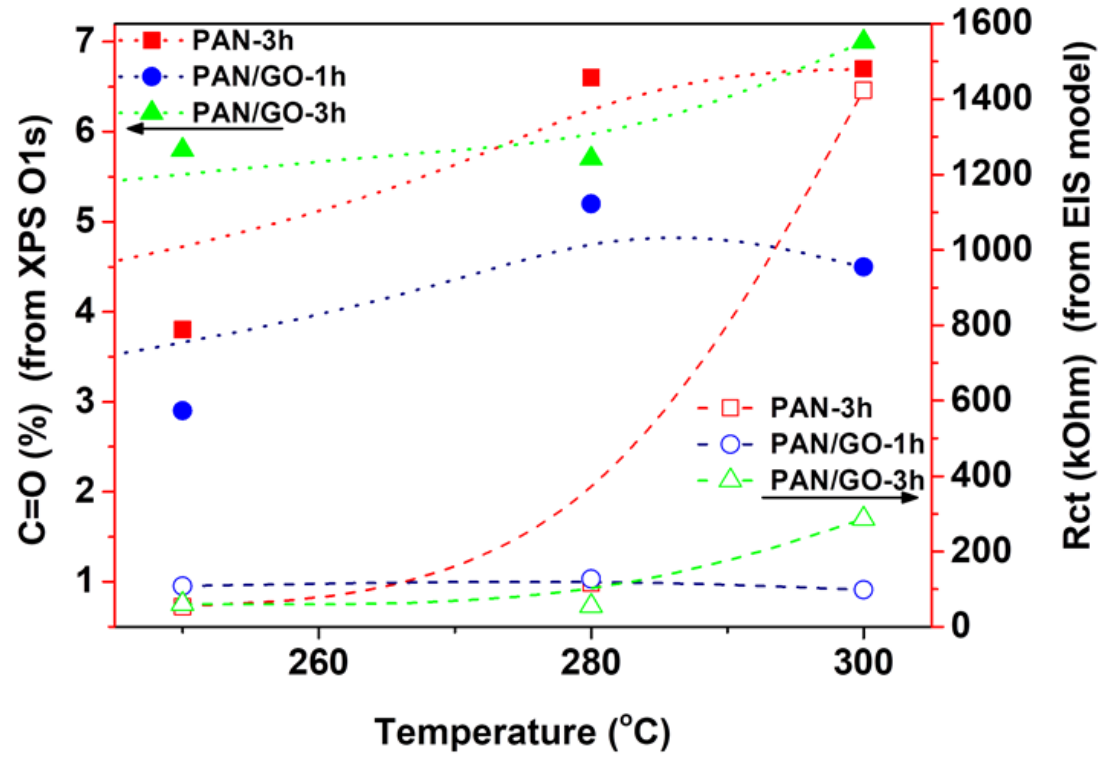

Figure 4.12 : Correlation between R_{ct} values from equivalent circuit model and C=O (%) amount from XPS analysis.

4.3 Conclusion

PAN and PAN/GO composite nanofibers were produced by electrospinning method. Nanofiber webs were oxidized with different temperature and duration time. During the oxidation, the chemical structure of PAN based nanofibers was changed especially from C≡N to C=N groups. Oxidation ratio and possible route of oxidation of these nanofibers were analyzed by FTIR-ATR and XPS measurements. It has been found that nanofiber webs were significantly affected by long oxidation duration time at a high temperature which has a direct impact to EIS analysis and easy to detect with EIS. 300 °C during 3 h has an excessive amount of energy for the oxidation process that cyclization reaction can be replaced by isomerization and other reactions on the nanofiber structure. On the other hand, it has been determined that GO has a crucial effect on the oxidation process. The presence of GO in the PAN nanofiber induces the oxidation process at a low temperature in a short duration of time which aids to develop the final, stabilized structure. Intermolecular nitrile polymerization leading to non-cyclic conjugated C=N structures is also possible. In addition to the imine sequences with three to six units long, the presence of polar groups C=O, OH and COOH in the chains facilitates the initiation of the cyclization process through a nucleophilic attack and accelerates the subsequent oxidative ring closure reactions. The cyclization of nitrile pendant groups of PAN forming polyimine type structure is the main reaction occurs during the stabilization.

Both inter and intramolecular reactions contribute to the observed changes in the polymer structure, which are firstly thermal stability, colouration, insolubility, and flame resistance properties. Stabilized PAN and PAN/GO composite nanofibers can be used in advanced flame resistant resin systems for reinforced composite applications, i.e., automotive, aviation, marine (shipboard) applications. Due to their excellent thermal stability and chemical resistance of oxidized electrospun PAN and PAN/GO composite nanofibers can be used in further industrial applications i.e., heat-protective, and flame-retardant textile, for industrial seals and packaging where protection from fire and heat are required by having a high surface area to volume ratio providing a light weight.

5. CONCLUSIONS

In this thesis, Polyacrylonitrile based composite nanofibers containing polyindole and graphene oxide were produced, characterized and also, graphene oxide containing nanofibers were oxidized, carbonized and characterized.

The thesis was consisted of three main chapters except the introduction part. The second chapter describes to produce of PAN/PIN fibers. First of all, PIN was synthesized chemically by $FeCl_3$. PAN (10 wt/v %) and PIN (at different wt/v %) were dissolved in DMF in order to obtain electrospun fibers. Electrospun fibers were successfully fabricated by 15 kV potential, 0.5-2.0 ml/h constant flow rate and 19 cm distance. Morphological analysis has been studied by SEM and AFM. The topological properties differed with the PIN content. The average diameter of the population of fifty fibers was calculated by ImageJ Programme. It was found that the diameter of fibers consistently increased up to 694 nm with PIN content except 1.0 wt/v % PIN content sample. This deviation from the linearity was confirmed by the surface tension results of polymer solution. Surface tension had a direct impact on the fiber diameter. Thus, it also affected the electrochemical behavior of the fibers. PAN showed a close interaction with indole moieties which was shown in DSC measurements. Electrospun fibers were deposited on the ITOPET surface to study on electrochemical characterization by EIS and CV measurements. The amount of PIN content has been found to have a direct impact on the fiber morphology, thermal properties and electrochemical behavior. The potential response of Fe(II) ions were examined to determine the electrochemical activity of the obtained fibers. A quasi-reversible peak is observed for sample S5 (contains 2.0 wt/v% PIN) which indicated electrochemical activity behaviour while no sensitivity was observed for PAN. EIS has been employed to study the interfacial properties of the modified electrodes in the presence of different iron concentrations. The simulated equivalent circuit model compared with experimental results showed a $R_{sol}(C_{dl}(R_{ct}(Q_{el}(R_{el}W_{el}))))$ equivalent circuit model, with χ^2 minimized to $\sim 10^{-4}$ error. The detection limit (DL) was determined by calculating the lowest concentration of Fe(II) ion analyte and was found to be 1×10^{-4}

mol·l^{-1} for the S5 electrode. These findings indicate that the electronegative N atom of polyindole attracts iron ions, and doping of polyindole matrix with iron ion where the doped ions can act as counter ion dopant which enhance the electronic conductivity of polymer chain and function as redox active site. This facilitate the redox mechanism of polymer composite fiber for p-doping-dedoping process during the cycling. Polyacrylonitrile (PAN) and its copolymers are widely used as precursor for manufacturing carbon fibers. There are two very important stages in carbon fiber production, oxidation and carbonization. The oxidation step determines the structure of the final product, the carbon nanofiber. Graphene Oxide (GO) exhibits two dimensional graphene layers with high surface area and honeycombed carbon structure.

In the last parts of the thesis, GO containing PAN composite nanofibers were produced give a chance to develop carbon nanofibers which includes GO as a nano filler. For this purpose, aligned PAN/GO nanofibers fabricated by 15 kV potantial, 1.0 ml/h constant feed rate, 15 cm distance and 21.50 Hz rotating frequency with a rotating collector. The inclusion of GO resulted porosity in the nanofiber surface which was measured with ImageJ Programme with an average diameter of 38.5±11 nm. Also, porous structure of GO containing PAN nanofibers were proved by TEM analysis. This porous structure affected the electrochemical performance of nanofibers that can help to store large amounts of charge. These results was also confirmed by the EIS analysis. The capacitive value increased to 600 µF with the highest amount inclusion of GO in the composite. Individual layered sheets of GO with high surface area are supposedly exposed to the electrolyte, which can resulted in the increase of the double layer capacitance (C_{dl}). Oxidation process were applied to nanofibers at 250 °C. During the oxidation process, C≡N bonds at 2243 cm^{-1} are damaged and C=N bonds are created at 1590 cm^{-1}. Also, during the dehydrogenation =C−H bonds appeared at around 800 cm^{-1}. Thus the ratio of these peaks were calculated from ATR-FTIR spectra. It was found that addition of GO to the PAN nanofiber web causes a deviation in the oxidation ratio values compared to pure PAN. As a result, it was found that GO acts via ionic mechanism in the oxidation step and improves the conversion of C≡N bonds to C=N bond. In addition, carbonization were aplied to oxidized PAN based nanofibers at 900 °C during 1h at inert atmosphere. Carbonized nanofibers were used as free standing electrode during CV measurements. It was seen that GO containing

carbon nanofiber exhibits a larger area under CV curve indicating high specific capacitance. GO functional groups enhanced the capacitive performance of carbon nanofibers. Consequently, GO containing carbon nanofibers can be a potential candidate for capacitive applications.

In the final part of the thesis, electrospun PAN based composite containing GO nanofibers were produced and then oxidized at 250 °C, 280 °C, and 300 °C during 1 and 3h time interval. Thus, the effect of temperature and time on oxidation process of composite nanofibers was investigated. Oxidation ratio and possible route of oxidation of these nanofibers were analyzed by FTIR-ATR and XPS measurements in detail. It has been found that nanofiber webs were significantly affected by long oxidation duration time at high temperature which has direct impact to EIS analysis. The highest R_{ct} value was obtained 1424 kΩ for oxidized PAN nanofiber webs at 300 °C in 3 hours. 300 °C during 3 h has an excessive amount of energy for the oxidation process that cyclization reaction can be replaced by isomerization and possible other reactions on the nanofiber structure. On the other hand, it has been determined that GO has a crucial issue on the oxidation. The presence of GO in the PAN nanofiber induces the oxidation process at a low temperature in a short duration of time which aids to develop the final, stabilized structure. The presence of polar groups C=O, OH and COOH in the chains facilitates the initiation of the cyclization process through a nucleophilic attack by these polar groups become easier. Also, these groups accelerate the subsequent oxidative ring closure reactions. The main reaction by during stabilization is cyclization of nitrile pendant groups of PAN forming polyimine type structure.

The recommended future work can be based on oxidation and carbonization study of different composites of Polyacrylonitrile nanofibers. In the future study, it can be possible improving the capacitance properties of new composite nanofibers by using suitable both fillers, i.e.,GO and conjugate polymer (polyindole) under optimum oxidation conditions with an aim of producing novel materials for capacitor applications.

REFERENCES

Abdul Manaf, N. S., Amin Bistamam, M. S., & Azam, M. A. (2013). Development of high performance electrochemical capacitor: A systematic review of electrode fabrication technique based on different carbon materials. *ECS Journal of Solid State Science and Technology*, Vol. 2. https://doi.org/10.1149/2.014310jss

Agend, F., Naderi, N., & Fareghi-Alamdari, R. (2007). Fabrication and electrical characterization of electrospun polyacrylonitrile-derived carbon nanofibers. *Journal of Applied Polymer Science*, *106*(1), 255–259. https://doi.org/10.1002/app.26476

Aglan, R. F., Rizk, M. S., Mohamed, G. G., El-Wahy, A. H., & Mohamed, H. A. (2014). Preparation and Properties of a New Carbon Paste Iron Selective Electrodes and Their Applications. *American Journal of Analytical Chemistry*, *5*, 140–148. https://doi.org/10.4236/ajac.2014.52017

Arjomandi, J., Nematollahi, D., & Amani, A. (2014). Enhanced electrical conductivity of polyindole prepared by electrochemical polymerization of indole in ionic liquids. *Journal of Applied Polymer Science*, *131*(8). https://doi.org/10.1002/app.40094

Arshad, S. N., Naraghi, M., & Chasiotis, I. (2011). Strong carbon nanofibers from electrospun polyacrylonitrile. *Carbon*, *49*(5), 1710–1719. https://doi.org/10.1016/j.carbon.2010.12.056

Avilés, M. A., Ginés, J. M., Del Rio, J. C., Pascual, J., Pérez-Rodríguez, J. L., & Sánchez-Soto, P. J. (2002). Thermal analysis of acrylonitrile polymerization and cyclization in the presence of N,N-dimethylformamide. *Journal of Thermal Analysis and Calorimetry*, *67*(1), 177–188. https://doi.org/10.1023/A:1013706501882

Bai, Y., Huang, Z. H., Yu, X. L., & Kang, F. (2014). Graphene oxide-embedded porous carbon nanofiber webs by electrospinning for capacitive deionization. *Colloids and Surfaces A: Physicochemical and Engineering Aspects*, *444*, 153–158. https://doi.org/10.1016/j.colsurfa.2013.12.053

Bajaj, P., Sreekumar, T. V., & Sen, K. (2001). Thermal behaviour of acrylonitrile copolymers having methacrylic and itaconic acid comonomers. *Polymer*, *42*(4), 1707–1718. https://doi.org/10.1016/S0032-3861(00)00583-8

Baqeri, M., Abolhasani, M. M., Mozdianfard, M. R., Guo, Q., Oroumei, A., & Naebe, M. (2015). Influence of processing conditions on polymorphic behavior, crystallinity, and morphology of electrospun poly(VInylidene fluoride) nanofibers. *Journal of Applied Polymer Science*, *132*(30). https://doi.org/10.1002/app.42304

Bashir, Z. (1991). A critical review of the stabilisation of polyacrylonitrile. *Carbon*, *29*(8), 1081–1090. https://doi.org/10.1016/0008-6223(91)90024-D

Beachley, V., & Wen, X. (2009). Effect of electrospinning parameters on the nanofiber diameter and length. *Materials Science and Engineering C*, *29*(3), 663–668. https://doi.org/10.1016/j.msec.2008.10.037

Beamson, G., & Briggs, D. (1992). High Resolution XPS of organic polymers , The Scienta ESCA 300 database John Wiley & Sons. In *Biomaterials* (Vol. 15).

Berger, C., Song, Z., Li, X., Wu, X., Brown, N., Naud, C., … De Heer, W. A. (2006). Electronic confinement and coherence in patterned epitaxial graphene. *Science*, *312*(5777), 1191–1196. https://doi.org/10.1126/science.1125925

Bhardwaj, N., & Kundu, S. C. (2010). Electrospinning: A fascinating fiber fabrication technique. *Biotechnology Advances*. https://doi.org/10.1016/j.biotechadv.2010.01.004

Bhuyan, M. S. A., Uddin, M. N., Islam, M. M., Bipasha, F. A., & Hossain, S. S. (2016). Synthesis of graphene. *International Nano Letters*, *6*(2), 65–83. https://doi.org/10.1007/s40089-015-0176-1

Biedunkiewicz, A., Figiel, P., & Sabara, M. (2011). Pyrolysis and Oxidation of PAN in Dry Air. Thermoanalytical Methods. *Materials Science* , *17*(1), 38–42. https://doi.org/10.5755/J01.MS.17.1.246

Billaud, D, Maarouf, E. B., & Hannecart, E. (1994). An investigation of electrochemically and chemically polymerized indole. *Materials Research Bulletin*, *29*(12), 1239–1246. https://doi.org/10.1016/0025-5408(94)90147-3

Billaud, D, Maarouf, E. B., & Hannecart, E. (1995). Chemical oxidation and polymerization of indole. *Synthetic Metals*, *69*(1–3), 571–572. https://doi.org/10.1016/0379-6779(94)02573-H

Billaud, Denis, Humbert, B., Thevenot, L., Thomas, P., & Talbi, H. (2003). Electrochemical properties and Fourier transform-infrared spectroscopic investigations of the redox behaviour of poly(indole-5-carboxylic acid) in LiClO4-acetonitrile solutions. *Spectrochimica Acta - Part A: Molecular and Biomolecular Spectroscopy*, *59*(1), 163–168. https://doi.org/10.1016/S1386-1425(02)00150-6

Bognitzki, M., Czado, W., Frese, T., Schaper, A., Hellwig, M., Steinhart, M., … Wendorff, J. H. (2001). Nanostructured Fibers via Electrospinning. *Advanced Materials*, *13*(1), 70–72. https://doi.org/10.1002/1521-4095(200101)13:1<70::AID-ADMA70>3.0.CO;2-H

Brandrup, J., & Peebles, L. H. (1968). On the Chromophore of Polyacrylonitrile. IV. Thermal Oxidation of Polyacrylonitrile and Other Nitrile-Containing Compounds. *Macromolecules*, *1*(1), 64–72. https://doi.org/10.1021/ma60001a012

Cai, J.-J., Zuo, P.-J., Cheng, X.-Q., Xu, Y.-H., & Yin, G.-P. (2010). Nano-silicon/polyaniline composite for lithium storage. *Electrochemistry Communications*, *12*(11), 1572–1575. https://doi.org/10.1016/J.ELECOM.2010.08.036

Cai, Z., & Yang, G. (2010). Synthesis of polyindole and its evaluation for Li-ion battery applications. *Synthetic Metals*, *160*(17–18), 1902–1905. https://doi.org/10.1016/j.synthmet.2010.07.007

Cetiner, S., Kalaoglu, F., Karakas, H., & Sarac, A. S. (2010). Electrospun Nanofibers of Polypyrrole-Poly(Acrylonitrile-co-Vinyl Acetate). *Textile Research Journal*, *80*(17), 1784–1792. https://doi.org/10.1177/0040517510365953

Chakrabarti, K., Nambissan, P. M. G., Mukherjee, C. D., Bardhan, K. K., Kim, C., & Yang, K. S. (2006). Positron annihilation spectroscopy of polyacrylonitrile-based carbon fibers embedded with multi-wall carbon nanotubes. *Carbon*, *44*(5), 948–953. https://doi.org/10.1016/j.carbon.2005.10.014

Chand, S. (2000). Carbon fibers for composites. *Journal of Materials Science*, *35*(6), 1303–1313. https://doi.org/10.1023/A:1004780301489

Chen, Q. (1989). *Microelements and Health*. Beijing: Peking University Press.

Chen, S., He, G., Carmona-Martinez, A. A., Agarwal, S., Greiner, A., Hou, H., & Schröder, U. (2011). Electrospun carbon fiber mat with layered architecture for anode in microbial fuel cells. *Electrochemistry Communications*, *13*(10), 1026–1029. https://doi.org/10.1016/j.elecom.2011.06.009

Chung, G. S., Jo, S. M., & Kim, B. C. (2005). Properties of carbon nanofibers prepared from electrospun polyimide. *Journal of Applied Polymer Science*, *97*(1), 165–170. https://doi.org/10.1002/app.21742

Clarke, A. J., & Bailey, J. E. (1973). Oxidation of acrylic fibres for carbon fibre formation. *Nature*, *243*(5403), 146–150. https://doi.org/10.1038/243146a0

Dalton, S., Heatley, F., & Budd, P. M. (1999). Thermal stabilization of polyacrylonitrile fibres. *Polymer*, *40*(20), 5531–5543. https://doi.org/10.1016/S0032-3861(98)00778-2

Das, T. K., & Prusty, S. (2013, March). Graphene-Based Polymer Composites and Their Applications. *Polymer - Plastics Technology and Engineering*, Vol. 52, pp. 319–331. https://doi.org/10.1080/03602559.2012.751410

de Almeida Coelho, N. M., Furtado, J. L. B., Pham-Huu, C., & Vieira, R. (2008). Carbon nanofibers: A versatile catalytic support. *Materials Research*, *11*(3), 353–357. https://doi.org/10.1590/s1516-14392008000300020

De Jong, K. P., & Geus, J. W. (2000). Carbon Nanofibers: Catalytic Synthesis and Applications. *Catalysis Reviews - Science and Engineering*, *42*(4), 481–510. https://doi.org/10.1081/CR-100101954

Deitzel, J. M., Kleinmeyer, J. D., Hirvonen, J. K., & Beck Tan, N. C. (2001). Controlled deposition of electrospun poly(ethylene oxide) fibers. *Polymer*, *42*(19), 8163–8170. https://doi.org/10.1016/S0032-3861(01)00336-6

Deitzel, J. M., Kleinmeyer, J., Harris, D., & Beck Tan, N. C. (2001). The effect of processing variables on the morphology of electrospun nanofibers and textiles. *Polymer*, *42*(1), 261–272. https://doi.org/10.1016/S0032-3861(00)00250-0

Devasia, R., Reghunadhan Nair, C. P., Sivadasan, P., Katherine, B. K., & Ninan, K. N. (2003). Cyclization reaction in poly(acrylonitrile/itaconic acid) copolymer: An isothermal differential scanning calorimetry kinetic study. *Journal of Applied Polymer Science*, *88*(4), 915–920. https://doi.org/10.1002/app.11706

Devaux, E., Koncar, V., Kim, B., Campagne, C., Roux, C., Rochery, M., & Saihi, D. (2007). Processing and characterization of conductive yarns by coating or bulk treatment for smart textile applications. *Transactions of the Institute of Measurement and Control*, *29*(4), 355–376. https://doi.org/10.1177/0142331207081726

Dimiev, A. M., & Tour, J. M. (2014). Mechanism of graphene oxide formation. *ACS Nano*, *8*(3), 3060–3068. https://doi.org/10.1021/nn500606a

Ding, J., Zhang, J., Li, J., Li, D., Xiao, C., Xiao, H., … Chen, X. (2019, March 1). Electrospun polymer biomaterials. *Progress in Polymer Science*, Vol. 90, pp. 1–34. https://doi.org/10.1016/j.progpolymsci.2019.01.002

Dissertations, D., & Fennessey, S. F. (2014). *Continuous carbon nanofibers prepared from electrospun polyacrylonitrile precursor fibers.* Retrieved from https://scholarworks.umass.edu/dissertations_1

Doshi, J., & Reneker, D. H. (1995). Electrospinning process and applications of electrospun fibers. *Journal of Electrostatics*, *35*(2–3), 151–160. https://doi.org/10.1016/0304-3886(95)00041-8

Edie, D. D. (1998). The effect of processing on the structure and properties of carbon fibers. *Carbon*, *36*(4), 345–362. https://doi.org/10.1016/S0008-6223(97)00185-1

Engin Sagirli, F. Z., Kayali, E. S., & Sarac, A. S. (2016). Electrochemical impedance spectroscopic study on Polypyrrole/Barium Titanate/Poly(acrylonitrile-co-methylacrylate) nanoparticles. *Journal of the Electrochemical Society*, *163*(3), H205–H212. https://doi.org/10.1149/2.0681603jes

Eraldemir, Ö., Sari, B., Gök, A., & Ünal, H. I. (2008). Synthesis and characterization of polyindole/poly(vinyl acetate) conducting composites. *Journal of Macromolecular Science, Part A: Pure and Applied Chemistry*, *45*(3), 205–211. https://doi.org/10.1080/10601320701839890

Faraji, S., Yardim, M. F., Can, D. S., & Sarac, A. S. (2017). Characterization of polyacrylonitrile, poly(acrylonitrile-co-vinyl acetate), and poly(acrylonitrile-co-itaconic acid) based activated carbon nanofibers. *Journal of Applied Polymer Science*, *134*(2). https://doi.org/10.1002/app.44381

Farsani, R. E., Raissi, S., Shokuhfar, A., & Sedghi, A. (2009). FT-IR study of stabilized pan fibers for fabrication of carbon fibers. *World Academy of Science, Engineering and Technology*, *38*, 434–437.

Feng, L., Li, S., Li, H., Zhai, J., Song, Y., Jiang, L., & Zhu, D. (2002). Super-hydrophobic surface of aligned polyacrylonitrile nanofibers. *Angewandte Chemie - International Edition*, *41*(7), 1221–1223. https://doi.org/10.1002/1521-3773(20020402)41:7<1221::AID-ANIE1221>3.0.CO;2-G

Fennessey, S. F., & Farris, R. J. (2004). Fabrication of aligned and molecularly oriented electrospun polyacrylonitrile nanofibers and the mechanical behavior of their twisted yarns. *Polymer*, *45*(12), 4217–4225. https://doi.org/10.1016/j.polymer.2004.04.001

Ferrari, A. C. (2007). Raman spectroscopy of graphene and graphite: Disorder, electron-phonon coupling, doping and nonadiabatic effects. *Solid State Communications*, *143*(1–2), 47–57. https://doi.org/10.1016/j.ssc.2007.03.052

Fu, Z., Gui, Y., Cao, C., Liu, B., Zhou, C., & Zhang, H. (2014). Structure evolution and mechanism of polyacrylonitrile and related copolymers during the stabilization. *Journal of Materials Science*, *49*(7), 2864–2874. https://doi.org/10.1007/s10853-013-7992-3

Fung, Y. S., & Fung, K. W. (1977). Determination of Iron(III) with a Copper Selective Electrode. *Analytical Chemistry*, *49*(3), 497–499. https://doi.org/10.1021/ac50011a040

Gagne, R. R., Koval, C. A., & Lisensky, G. C. (1980). Ferrocene as an Internal Standard for Electrochemical Measurements. *Inorganic Chemistry*, Vol. 19, pp. 2854–2855. https://doi.org/10.1021/ic50211a080

Gergin, I., Ismar, E., & Sarac, A. S. (2017). Oxidative stabilization of polyacrylonitrile nanofibers and carbon nanofibers containing graphene oxide (GO): A spectroscopic and electrochemical study. *Beilstein Journal of Nanotechnology*, *8*(1). https://doi.org/10.3762/bjnano.8.161

Goel, S., Mazumdar, N. A., & Gupta, A. (2010). Fabrication of polyindene and polyindole nanostructures. *Applied Surface Science*, *256*(14), 4426–4433. https://doi.org/10.1016/J.APSUSC.2010.01.010

Gong, Y., Li, D., Fu, Q., & Pan, C. (2015). Influence of graphene microstructures on electrochemical performance for supercapacitors. *Progress in Natural Science: Materials International*, *25*(5), 379–385. https://doi.org/10.1016/j.pnsc.2015.10.004

Green, K. J., Dean, D. R., Vaidya, U. K., & Nyairo, E. (2009). Multiscale fiber reinforced composites based on a carbon nanofiber/epoxy nanophased polymer matrix: Synthesis, mechanical, and thermomechanical behavior. *Composites Part A: Applied Science and Manufacturing*, *40*(9), 1470–1475. https://doi.org/10.1016/j.compositesa.2009.05.010

Gu, B. K., Ismail, Y. A., Spinks, G. M., Kim, S. I., So, I., & Kim, S. J. (2009). A linear actuation of polymeric nanofibrous bundle for artificial muscles. *Chemistry of Materials*, *21*(3), 511–515. https://doi.org/10.1021/cm802377d

Guan, H., Fan, L. Z., Zhang, H., & Qu, X. (2010). Polyaniline nanofibers obtained by interfacial polymerization for high-rate supercapacitors. *Electrochimica Acta*, *56*(2), 964–968. https://doi.org/10.1016/j.electacta.2010.09.078

Guerrero-Bermea, C., Rajukumar, L. P., Dasgupta, A., Lei, Y., Hashimoto, Y., Sepulveda-Guzman, S., … Terrones, M. (2017). Two-dimensional and three-dimensional hybrid assemblies based on graphene oxide and other layered structures: A carbon science perspective. *Carbon*, *125*, 437–453. https://doi.org/10.1016/J.CARBON.2017.09.082

Gülercan, D., Gergin, İ., & Sarac, A. S. (2018). Preparation and Electrochemical Performances of Graphene Oxide/PEDOT and Reduced Graphene Oxide/PEDOT Nanofibers and Nanocomposites. *Fibers and Polymers*, *19*(10), 2178–2187. https://doi.org/10.1007/s12221-018-8393-7

He, J. H. (2004). Allometric scaling law in conductive polymer. *Polymer*, *45*(26), 9067–9070. https://doi.org/10.1016/j.polymer.2004.10.024

Hohnholz, D., MacDiarmid, A. G., Sarno, D. M., & Jones, W. E. (2001). Uniform thin films of poly-3,4-ethylenedioxythiophene (PEDOT) prepared by in-situ deposition. *Chemical Communications*, *23*, 2444–2445. https://doi.org/10.1039/b107130k

Huang, Z. M., Zhang, Y. Z., Kotaki, M., & Ramakrishna, S. (2003). A review on polymer nanofibers by electrospinning and their applications in nanocomposites. *Composites Science and Technology*, *63*(15), 2223–2253. https://doi.org/10.1016/S0266-3538(03)00178-7

Ismar, E., Karazehir, T., Ates, M., & Sarac, A. S. (2018). Electrospun carbon nanofiber web electrode: Supercapacitor behavior in various electrolytes. *Journal of Applied Polymer Science*, *135*(4), 1–10. https://doi.org/10.1002/app.45723

Ismar, E., & Sarac, A. S. (2016). Synthesis and characterization of poly (acrylonitrile-co-acrylic acid) as precursor of carbon nanofibers. *Polymers for Advanced Technologies*, *27*(10), 1383–1388. https://doi.org/10.1002/pat.3807

Ismar, E., & Sarac, A. S. (2018). Oxidation of polyacrylonitrile nanofiber webs as a precursor for carbon nanofiber: aligned and non-aligned nanofibers. *Polymer Bulletin*, *75*(2), 485–499. https://doi.org/10.1007/s00289-017-2043-x

Jawhari, T., Roid, A., & Casado, J. (1995). Raman spectroscopic characterization of some commercially available carbon black materials. *Carbon*, *33*(11), 1561–1565. https://doi.org/10.1016/0008-6223(95)00117-V

Jia, W., Li, Z., Wu, Z., Wang, L., Wu, B., Wang, Y., … Li, J. (2017). Graphene oxide as a filler to improve the performance of PAN-LiClO4 flexible solid polymer electrolyte. *Solid State Ionics*, *315*, 7–13. https://doi.org/10.1016/j.ssi.2017.11.026

Jiang, H., Fang, D., Hsiao, B., Chu, B., & Chen, W. (2004). Preparation and characterization of ibuprofen-loaded poly(lactide-co-glycolide)/poly(ethylene glycol)-g-chitosan electrospun membranes. *Journal of Biomaterials Science, Polymer Edition*, *15*(3), 279–296. https://doi.org/10.1163/156856204322977184

Joseph C. Salamone. (1998). Concise Encyclopedia, Materials. *CRC Press*, 1–2.

Joshi, L., & Prakash, R. (2012). Polyindole-Au nanocomposite produced at the liquid/liquid interface. *Materials Letters*, *66*(1), 250–253. https://doi.org/10.1016/J.MATLET.2011.08.087

Kakida, H., Tashiro, K., & Kobayashi, M. (1996). Mechanism and kinetics of stabilization reaction of polyacrylonitrile and related copolymers I. Relationship between isothermal DSC thermogram and FT/IR spectral change of an acrylonitrile/methacrylic acid copolymer. *Polymer Journal*, *28*(1), 30–34. https://doi.org/10.1295/polymj.28.30

Karthika, P., Rajalakshmi, N., & Dhathathreyan, K. S. (2012). Functionalized Exfoliated Graphene Oxide as Supercapacitor Electrodes. *Soft Nanoscience Letters*, *2*, 59–66. https://doi.org/10.4236/snl.2012.24011

Kim, C., Jeong, Y. Il, Ngoc, B. T. N., Yang, K. S., Kojima, M., Kim, Y. A., … Lee, J. W. (2007). Synthesis and characterization of porous carbon nanofibers with hollow cores through the thermal treatment of electrospun copolymeric nanofiber webs. *Small*, *3*(1), 91–95. https://doi.org/10.1002/smll.200600243

Kim, C., Kim, Y. J., & Kim, Y. A. (2004). Fabrication and structural characterization of electro-spun polybenzimidazol-derived carbon nanofiber by graphitization. *Solid State Communications*, *132*(8), 567–571. https://doi.org/10.1016/j.ssc.2004.08.035

Kim, C., Park, S. H., Cho, J. I., Lee, D. Y., Park, T. J., Lee, W. J., & Yang, K. S. (2004). Raman spectroscopic evaluation of polyacrylonitrile-based carbon nanofibers prepared by electrospinning. *Journal of Raman Spectroscopy*, *35*(11), 928–933. https://doi.org/10.1002/jrs.1233

Kim, C., Yang, K. S., Kojima, M., Yoshida, K., Kim, Y. J., Kim, Y. A., & Endo, M. (2006). Fabrication of electrospinning-derived carbon nanofiber webs for the anode material of lithium-ion secondary batteries. *Advanced Functional Materials*, *16*(18), 2393–2397. https://doi.org/10.1002/adfm.200500911

Ko, T. -H. (1991). Influence of continuous stabilization on the physical properties and microstructure of PAN-based carbon fibers. *Journal of Applied Polymer Science*, *42*(7), 1949–1957. https://doi.org/10.1002/app.1991.070420719

Kozlov, A. V., Yegorov, D. Y., Vladimirov, Y. A., & Azizova, O. A. (1992). Intracellular free iron in liver tissue and liver homogenate: Studies with electron paramagnetic resonance on the formation of paramagnetic complexes with desferal and nitric oxide. *Free Radical Biology and Medicine*, *13*(1), 9–16. https://doi.org/10.1016/0891-5849(92)90159-E

Largeot, C., Portet, C., Chmiola, J., Taberna, P. L., Gogotsi, Y., & Simon, P. (2008). Relation between the ion size and pore size for an electric double-layer capacitor. *Journal of the American Chemical Society*, *130*(9), 2730–2731. https://doi.org/10.1021/ja7106178

Lazzaroni, R., De Pryck, A., Debaisieux, C., Riga, J., Verbist, J., Brédas, J. L., … André, J. M. (1987). Electronic structure of conducting polymers from heteroaromatic bicyclic compounds. *Synthetic Metals*, *21*(1–3), 189–195. https://doi.org/10.1016/0379-6779(87)90085-3

Lee, S., Kim, J., Ku, B.-C., Kim, J., & Joh, H.-I. (2012). Structural Evolution of Polyacrylonitrile Fibers in Stabilization and Carbonization. *Advances in Chemical Engineering and Science*, *2*, 275–282. https://doi.org/10.4236/aces.2012.22032

Lee, S., Kim, Y. J., Kim, D. H., Ku, B. C., & Joh, H. I. (2012). Synthesis and properties of thermally reduced graphene oxide/ polyacrylonitrile composites. *Journal of Physics and Chemistry of Solids*, *73*(6), 741–743. https://doi.org/10.1016/j.jpcs.2012.01.015

Li, C. Q., Xiao, Y., Zhao, H. J., Chen, X., He, Z. W., & Xu, L. H. (2015). Effect of oxidized structure on thermal stability of pre-oxidized polyacrylonitrile fiber. *Cailiao Rechuli Xuebao/Transactions of Materials and Heat Treatment*, *36*(5), 35–38.

Li, D., & Xia, Y. (2004, July 19). Electrospinning of nanofibers: Reinventing the wheel? *Advanced Materials*, Vol. 16, pp. 1151–1170. https://doi.org/10.1002/adma.200400719

Lieu, P. T., Heiskala, M., Peterson, P. A., & Yang, Y. (2001, February 4). The roles of iron in health and disease. *Molecular Aspects of Medicine*, Vol. 22, pp. 1–87. https://doi.org/10.1016/S0098-2997(00)00006-6

Liu, C. K., Feng, Y., He, H. J., Zhang, J., Sun, R. J., & Chen, M. Y. (2015). Effect of carbonization temperature on properties of aligned electrospun polyacrylonitrile carbon nanofibers. *Materials and Design*, *85*, 483–486. https://doi.org/10.1016/j.matdes.2015.07.021

Liu, C. K., Lai, K., Liu, W., Yao, M., & Sun, R. J. (2009, December). Preparation of carbon nanofibres through electrospinning and thermal treatment. *Polymer International*, Vol. 58, pp. 1341–1349. https://doi.org/10.1002/pi.2669

Liu, G., Ding, J., Qiao, L., Guo, A., Dymov, B. P., Gleeson, J. T., … Saijo, K. (1999). Polystyrene-block-poly(2-cinnamoylethyl methacrylate) Nanofibers—Preparation, Characterization, and Liquid Crystalline Properties. *Chemistry - A European Journal*, *5*(9), 2740–2749. https://doi.org/10.1002/(SICI)1521-3765(19990903)5:9<2740::AID-CHEM2740>3.0.CO;2-V

Liu, J., Zhou, P., Zhang, L., Ma, Z., Liang, J., & Fong, H. (2009). Thermo-chemical reactions occurring during the oxidative stabilization of electrospun polyacrylonitrile precursor nanofibers and the resulting structural conversions. *Carbon*, *47*(4), 1087–1095. https://doi.org/10.1016/j.carbon.2008.12.033

López-Manchado, M. A., & Arroyo, M. (2000). Thermal and dynamic mechanical properties of polypropylene and short organic fiber composites. *Polymer*, *41*(21), 7761–7767. https://doi.org/10.1016/S0032-3861(00)00152-X

Low, K., Horner, C. B., Li, C., Ico, G., Bosze, W., Myung, N. V., & Nam, J. (2015). Composition-dependent sensing mechanism of electrospun conductive polymer composite nanofibers. *Sensors and Actuators, B: Chemical*, *207*(Part A), 235–242. https://doi.org/10.1016/j.snb.2014.09.121

Ma, P. X., & Zhang, R. (1999). Synthetic nano-scale fibrous extracellular matrix. *Journal of Biomedical Materials Research*, *46*(1), 60–72. https://doi.org/10.1002/(SICI)1097-4636(199907)46:1<60::AID-JBM7>3.0.CO;2-H

Ma, Sai, Liu, J., Liu, Q., Liang, J., Zhao, Y., & Fong, H. (2016). Investigation of structural conversion and size effect from stretched bundle of electrospun polyacrylonitrile copolymer nanofibers during oxidative stabilization. *Materials and Design*, *95*, 387–397. https://doi.org/10.1016/j.matdes.2016.01.134

Maarouf, E. B., Billaud, D., & Hannecart, E. (1994). Electrochemical cycling and electrochromic properties of polyindole. *Materials Research Bulletin*, *29*(6), 637–643. https://doi.org/10.1016/0025-5408(94)90119-8

Mahmoud, W. H. (2001). Iron ion-selective electrodes for direct potentiometry and potentiotitrimetry in pharmaceuticals. *Analytica Chimica Acta*, *436*(2), 199–206. https://doi.org/10.1016/S0003-2670(01)00892-3

Marcano, D. C., Kosynkin, D. V, Berlin, J. M., Sinitskii, A., Sun, Z., Slesarev, A. S., … Tour, J. M. (2018, February 27). Correction to: Improved Synthesis of Graphene Oxide (ACS Nano (2010) 4: 8 (4806-4814) DOI: 10.1021/nn1006368). *ACS Nano*, Vol. 12, p. 2078. https://doi.org/10.1021/acsnano.8b00128

Masson, J. (1995). *Acrylic fiber technology and applications*. Retrieved from https://content.taylorfrancis.com/books/download?dac=C2006-0-01777-X&isbn=9781482260359&format=googlePreviewPdf

Mičušík, M., Nedelčev, T., Omastová, M., Krupa, I., Olejníková, K., Fedorko, P., & Chehimi, M. M. (2007). Conductive polymer-coated textiles: The role of fabric treatment by pyrrole-functionalized triethoxysilane. *Synthetic Metals*, *157*(22–23), 914–923. https://doi.org/10.1016/j.synthmet.2007.09.001

Mittal, J., Bahl, O. P., Mathur, R. B., & Sandle, N. K. (1994). IR studies of PAN fibres thermally stabilized at elevated temperatures. *Carbon*, *32*(6), 1133–1136. https://doi.org/10.1016/0008-6223(94)90222-4

Mittal, J., Konno, H., Inagaki, M., & Bahl, O. P. (1998). Denitrogenation behavior and tensile strength increase during carbonization of stabilized pan fibers. *Carbon*, *36*(9), 1327–1330. https://doi.org/10.1016/S0008-6223(98)00113-4

Mochida, I., Yoon, S. H., Takano, N., Fortin, F., Korai, Y., & Yokogawa, K. (1996). Microstructure of mesophase pitch-based carbon fiber and its control. *Carbon*, *34*(8), 941–956. https://doi.org/10.1016/0008-6223(95)00172-7

Molina, J., del Río, A. I., Bonastre, J., & Cases, F. (2008). Chemical and electrochemical polymerisation of pyrrole on polyester textiles in presence of phosphotungstic acid. *European Polymer Journal*, *44*(7), 2087–2098. https://doi.org/10.1016/j.eurpolymj.2008.04.007

Morgan, P. (2005). *Carbon fibers and their composites*. Retrieved from https://content.taylorfrancis.com/books/download?dac=C2010-0-47960-8&isbn=9781420028744&format=googlePreviewPdf

Murray, E. P., Tsai, T., & Barnett, S. A. (1998). Oxygen transfer processes in (La,Sr)MnO3/Y2O3-stabilized ZrO2 cathodes: an impedance spectroscopy study. *Solid State Ionics*, *110*(3–4), 235–243. https://doi.org/10.1016/S0167-2738(98)00142-8

Musser, R.D., O'Neil, J. J. (1969). *Pharmacology and Therapeutics*. The Macmillan Company.

Naraghi, M., Arshad, S. N., & Chasiotis, I. (2011). Molecular orientation and mechanical property size effects in electrospun polyacrylonitrile nanofibers. *Polymer*, *52*(7), 1612–1618. https://doi.org/10.1016/j.polymer.2011.02.013

Nataraj, S. K., Yang, K. S., & Aminabhavi, T. M. (2012, March). Polyacrylonitrile-based nanofibers - A state-of-the-art review. *Progress in Polymer Science (Oxford)*, Vol. 37, pp. 487–513. https://doi.org/10.1016/j.progpolymsci.2011.07.001

Nitti, P., Gallo, N., Natta, L., Scalera, F., Palazzo, B., Sannino, A., & Gervaso, F. (2018). Influence of nanofiber orientation on morphological and mechanical properties of electrospun chitosan mats. *Journal of Healthcare Engineering*, *2018*. https://doi.org/10.1155/2018/3651480

Novoselov, K. S., Geim, A. K., Morozov, S. V., Jiang, D., Zhang, Y., Dubonos, S. V., … Firsov, A. A. (2004). Electric field in atomically thin carbon films. *Science*, *306*(5696), 666–669. https://doi.org/10.1126/science.1102896

Ogawa, H., & Saito, K. (1995). Oxidation behavior of polyacrylonitrile fibers evaluated by new stabilization index. *Carbon*, *33*(6), 783–788. https://doi.org/10.1016/0008-6223(95)00007-Z

Oh, G. Y., Ju, Y. W., Jung, H. R., & Lee, W. J. (2008). Preparation of the novel manganese-embedded PAN-based activated carbon nanofibers by electrospinning and their toluene adsorption. *Journal of Analytical and Applied Pyrolysis*, *81*(2), 211–217. https://doi.org/10.1016/j.jaap.2007.11.006

Ondarçuhu, T., & Joachim, C. (1998). Drawing a single nanofibre over hundreds of microns. *Europhysics Letters*, *42*(2), 215–220. https://doi.org/10.1209/epl/i1998-00233-9

Ouyang, Q., Cheng, L., Wang, H., & Li, K. (2008). Mechanism and kinetics of the stabilization reactions of itaconic acid-modified polyacrylonitrile. *Polymer Degradation and Stability*, *93*(8), 1415–1421. https://doi.org/10.1016/j.polymdegradstab.2008.05.021

Palumbo, A., d'Ischia, M., Misuraca, G., Prota, G., & Schultz, T. M. (1988). Structural modifications in biosynthetic melanins induced by metal ions. *Biochimica et Biophysica Acta (BBA) - General Subjects*, *964*(2), 193–199. https://doi.org/10.1016/0304-4165(88)90166-3

Pandey, P. C., & Prakash, R. (1998). Polyindole modified potassium ion-sensor using dibenzo-18-crown-6 mediated PVC matrix membrane. *Sensors and Actuators, B: Chemical*, *46*(1), 61–65. https://doi.org/10.1016/S0925-4005(97)00332-8

Park, O. K., Lee, S., Joh, H. I., Kim, J. K., Kang, P. H., Lee, J. H., & Ku, B. C. (2012). Effect of functional groups of carbon nanotubes on the cyclization mechanism of polyacrylonitrile (PAN). *Polymer*, *53*(11), 2168–2174. https://doi.org/10.1016/j.polymer.2012.03.031

Park, S., An, J., Potts, J. R., Velamakanni, A., Murali, S., & Ruoff, R. S. (2011). Hydrazine-reduction of graphite- and graphene oxide. *Carbon*, *49*(9), 3019–3023. https://doi.org/10.1016/j.carbon.2011.02.071

Park, S. J., & Im, S. H. (2008). Electrochemical behaviors of PAN/Ag-based carbon nanofibers by electrospinning. *Bulletin of the Korean Chemical Society*, *29*(4), 777–781. https://doi.org/10.5012/bkcs.2008.29.4.777

Prilutsky, S., Zussman, E., & Cohen, Y. (2008). The effect of embedded carbon nanotubes on the morphological evolution during the carbonization of poly(acrylonitrile) nanofibers. *Nanotechnology*, *19*(16). https://doi.org/10.1088/0957-4484/19/16/165603

Qu, D., & Shi, H. (1998). Studies of activated carbons used in double-layer capacitors. *Journal of Power Sources*, *74*(1), 99–107. https://doi.org/10.1016/S0378-7753(98)00038-X

Rahaman, M. S. A., Ismail, A. F., & Mustafa, A. (2007, August). A review of heat treatment on polyacrylonitrile fiber. *Polymer Degradation and Stability*, Vol. 92, pp. 1421–1432. https://doi.org/10.1016/j.polymdegradstab.2007.03.023

Rajasudha, G., Nancy, A. P., Paramasivam, T., Boukos, N., Narayanan, V., & Stephen, A. (2011). Synthesis and Characterization of Polyindole–NiO-Based Composite Polymer Electrolyte with $LiClO_4$. *International Journal of Polymeric Materials*, *60*(11), 877–892. https://doi.org/10.1080/00914037.2010.551367

Raymundo-Piñero, E., Kierzek, K., Machnikowski, J., & Béguin, F. (2006). Relationship between the nanoporous texture of activated carbons and their capacitance properties in different electrolytes. *Carbon*, *44*(12), 2498–2507. https://doi.org/10.1016/j.carbon.2006.05.022

Rodriguez, A. J., Guzman, M. E., Lim, C. S., & Minaie, B. (2011). Mechanical properties of carbon nanofiber/fiber-reinforced hierarchical polymer composites manufactured with multiscale-reinforcement fabrics. *Carbon*, *49*(3), 937–948. https://doi.org/10.1016/j.carbon.2010.10.057

Rodriguez, N. M. (1993). A review of catalytically grown carbon nanofibers. *Journal of Materials Research*, *8*(12), 3233–3250. https://doi.org/10.1557/JMR.1993.3233

Rubinson, J. F., & Kayinamura, Y. P. (2009). Charge transport in conducting polymers: Insights from impedance spectroscopy. *Chemical Society Reviews*, Vol. 38, pp. 3339–3347. https://doi.org/10.1039/b904083h

Ruoff, R. (2008). Graphene: Calling all chemists. *Nature Nanotechnology*, Vol. 3, pp. 10–11. https://doi.org/10.1038/nnano.2007.432

Rutledge, G. C., & Fridrikh, S. V. (2007). Formation of fibers by electrospinning. *Advanced Drug Delivery Reviews*, Vol. 59, pp. 1384–1391. https://doi.org/10.1016/j.addr.2007.04.020

Ryu, K. S., Park, N. G., Kim, K. M., Lee, Y. G., Park, Y. J., Lee, S. J., … Chang, S. H. (2003). The physicochemical properties of polyindole / thiol composites. *Synthetic Metals*, *135–136*, 397–398. https://doi.org/10.1016/S0379-6779(02)00648-3

Sadeghian, R., Gangireddy, S., Minaie, B., & Hsiao, K. T. (2006). Manufacturing carbon nanofibers toughened polyester/glass fiber composites using vacuum assisted resin transfer molding for enhancing the mode-I delamination resistance. *Composites Part A: Applied Science and Manufacturing*, *37*(10), 1787–1795. https://doi.org/10.1016/j.compositesa.2005.09.010

Saleh, M., Chandra, V., Christian Kemp, K., & Kim, K. S. (2013). Synthesis of N-doped microporous carbon via chemical activation of polyindole-modified graphene oxide sheets for selective carbon dioxide adsorption. *Nanotechnology*, *24*(25). https://doi.org/10.1088/0957-4484/24/25/255702

Sanchez, C., Julián, B., Belleville, P., & Popall, M. (2005). Applications of hybrid organic–inorganic nanocomposites. *Journal of Materials Chemistry*, *15*(35–36), 3559. https://doi.org/10.1039/b509097k

Sarac, A. S. (2016). Nanofibers of conjugated polymers. In *Nanofibers of Conjugated Polymers*. https://doi.org/10.1201/b19844

Saraji, M., & Bagheri, A. (1998). Electropolymerization of indole and study of electrochemical behavior of the polymer in aqueous solutions. *Synthetic Metals*, *98*(1), 57–63. https://doi.org/10.1016/S0379-6779(98)00151-9

Sayyar, S., Moskowitz, J., Fox, B., Wiggins, J., & Wallace, G. (2019). Wet-spinning and carbonization of graphene/PAN-based fibers: Toward improving the properties of carbon fibers. *Journal of Applied Polymer Science*, *136*(36). https://doi.org/10.1002/app.47932

Sazou, D. (2002). The dynamical behavior of the electrochemical polymerization of indole on Fe in acetonitrile–water mixtures. *Synthetic Metals*, *130*(1), 45–54. https://doi.org/10.1016/S0379-6779(02)00110-8

Shahriary, L., & Athawale, A. A. (2014). Graphene Oxide Synthesized by using Modified Hummers Approach. In *International Journal of Renewable Energy and Environmental Engineering* (Vol. 02). Retrieved from https://www.researchgate.net/file.PostFileLoader.html?id=543e9ea6d11b8b7a6d8b46cc&assetKey=AS%3A272120699916290%401441890038575

Shao, D., Wei, Q., Zhang, L., Cai, Y., & Jiang, S. (2008). Surface functionalization of carbon nanofibers by sol-gel coating of zinc oxide. *Applied Surface Science*, *254*(20), 6543–6546. https://doi.org/10.1016/j.apsusc.2008.04.055

Sharma, C. S., Katepalli, H., Sharma, A., & Madou, M. (2011). Fabrication and electrical conductivity of suspended carbon nanofiber arrays. *Carbon*, *49*(5), 1727–1732. https://doi.org/10.1016/j.carbon.2010.12.058

Shokuhfar, A., Sedghi, A., & Farsani, R. E. (2006). Effect of thermal characteristics of commercial and special polyacrylonitrile fibres on the fabrication of carbon fibres. *Materials Science and Technology*, *22*(10), 1235–1239. https://doi.org/10.1179/174328406X129887

Sil, A., Ijeri, V. S., & Srivastava, A. K. (2005). Coated-wire iron(III) ion-selective electrode based on iron complex of 1,4,8,11-tetraazacyclotetradecane. *Sensors and Actuators B*, *106*, 648–653. https://doi.org/10.1016/j.snb.2004.09.013

Singh, K., Ohlan, A., Kotnala, R. K., Bakhshi, A. K., & Dhawan, S. K. (2008). Dielectric and magnetic properties of conducting ferromagnetic composite of polyaniline with γ-Fe2O3 nanoparticles. *Materials Chemistry and Physics*, *112*(2), 651–658. https://doi.org/10.1016/J.MATCHEMPHYS.2008.06.026

Standage, A. E., & Matkowsky, R. D. (1971). Thermal oxidation of polyacrylonitrile. *European Polymer Journal*, *7*(7), 775–783. https://doi.org/10.1016/0014-3057(71)90043-7

Sutasinpromprae, J., Jitjaicham, S., Nithitanakul, M., Meechaisue, C., & Supaphol, P. (2006). Preparation and characterization of ultrafine electrospun polyacrylonitrile fibers and their subsequent pyrolysis to carbon fibers. *Polymer International*, *55*(8), 825–833. https://doi.org/10.1002/pi.2040

Syed Abthagir, P., Dhanalakshmi, K., & Saraswathi, R. (1998). Thermal studies on polyindole and polycarbazole. *Synthetic Metals*, *93*(1), 1–7. https://doi.org/10.1016/S0379-6779(98)80125-2

Tai, Z., Yan, X., Lang, J., & Xue, Q. (2012). Enhancement of capacitance performance of flexible carbon nanofiber paper by adding graphene nanosheets. *Journal of Power Sources*, *199*, 373–378. https://doi.org/10.1016/j.jpowsour.2011.10.009

Takahagi, T., Shimada, I., Fukuhara, M., Morita, K., & Ishitani, A. (1986). XPS studies on the chemical structure of the stabilized polyacrylonitrile fiber in the carbon fiber production process. *Journal of Polymer Science Part A: Polymer Chemistry*, *24*(11), 3101–3107. https://doi.org/10.1002/pola.1986.080241134

Tamura, T., & Kawakami, H. (2010). Aligned electrospun nanofiber composite membranes for fuel cell electrolytes. *Nano Letters*, *10*(4), 1324–1328. https://doi.org/10.1021/nl1007079

Taylan, N. B., Sari, B., & Unal, H. I. (2010). Preparation of conducting poly(vinyl chloride)/polyindole composites and freestanding films via chemical polymerization. *Journal of Polymer Science, Part B: Polymer Physics*, *48*(12), 1290–1298. https://doi.org/10.1002/polb.22023

Teixeira, M. F. D. S., Aniceto, C., & Fatibello-Filho, O. (1998). Ion-selective electrode for the determination of iron(III) in vitamin formulations. *Journal of the Brazilian Chemical Society*, *9*(5), 506–510. https://doi.org/10.1590/S0103-50531998000500017

Tesfaldet, Z. O., Van Staden, J. F., & Stefan, R. I. (2004). Sequential injection spectrophotometric determination of iron as Fe(II) in multi-vitamin preparations using 1,10-phenanthroline as complexing agent. *Talanta*, *64*(5 SPEC. ISS.), 1189–1195. https://doi.org/10.1016/j.talanta.2004.02.044

Thadathil, A., Pradeep, H., Joshy, D., Ismail, Y. A., & Periyat, P. (2022). Polyindole and polypyrrole as a sustainable platform for environmental remediation and sensor applications. *Materials Advances*, *3*, 2990–3022. https://doi.org/10.1039/d2ma00022a

Tibbetts, G. G., Lake, M. L., Strong, K. L., & Rice, B. P. (2007). A review of the fabrication and properties of vapor-grown carbon nanofiber/polymer composites. *Composites Science and Technology*, *67*(7–8), 1709–1718. https://doi.org/10.1016/j.compscitech.2006.06.015

Toh, S. Y., Loh, K. S., Kartom Kamarudin, S., Ramli, W., & Daud, W. (2014). *Graphene production via electrochemical reduction of graphene oxide: Synthesis and characterisation*. https://doi.org/10.1016/j.cej.2014.04.004

Unal, H. I., Sahan, B., & Erol, O. (2012). Investigation of electrokinetic and electrorheological properties of polyindole prepared in the presence of a surfactant. *Materials Chemistry and Physics*, *134*(1), 382–391. https://doi.org/10.1016/j.matchemphys.2012.03.006

Vieira, R., Pham-Huu, C., Keller, N., & Ledoux, M. J. (2002). New carbon nanofiber/graphite felt composite for use as a catalyst support for hydrazine catalytic decomposition. *Chemical Communications*, *2*(9), 954–955. https://doi.org/10.1039/b202032g

Waite, T. D., & Morel, F. M. M. (1984). Coulometric Study of the Redox Dynamics of Iron in Seawater. *Analytical Chemistry*, *56*(4), 787–792. https://doi.org/10.1021/ac00268a045

Wan, F., Li, L., Wan, X., & Xue, G. (2002). Modification of polyindole by the incorporation of pyrrole unit. *Journal of Applied Polymer Science*, *85*(4), 814–820. https://doi.org/10.1002/app.10672

Wang, G., Yang, J., Park, J., Gou, X., Wang, B., Liu, H., & Yao, J. (2008). Facile Synthesis and Characterization of Graphene Nanosheets. *The Journal of Physical Chemistry C*, *112*(22), 8192–8195. https://doi.org/10.1021/jp710931h

Wang, Y., Serrano, S., & Santiago-Aviles, J. J. (2002). Conductivity measurement of electrospun PAN-based carbon nanofiber. *Journal of Materials Science Letters*, *21*(13), 1055–1057. https://doi.org/10.1023/A:1016081212346

Wu, Q., Xu, Y., Yao, Z., Liu, A., & Shi, G. (2010). Supercapacitors based on flexible graphene/polyaniline nanofiber composite films. *ACS Nano*, *4*(4), 1963–1970. https://doi.org/10.1021/nn1000035

Xu, L. Q., Liu, Y. L., Neoh, K. G., Kang, E. T., & Fu, G. D. (2011). Reduction of graphene oxide by aniline with its concomitant oxidative polymerization. *Macromolecular Rapid Communications*, *32*(8), 684–688. https://doi.org/10.1002/marc.201000765

Xu, W., Wu, Y., Yi, H., Bai, L., Chai, Y., & Yuan, R. (2014). Porous platinum nanotubes modified with dendrimers as nanocarriers and electrocatalysts for sensitive electrochemical aptasensors based on enzymatic signal amplification. *Chemical Communications*, *50*(12), 1451–1453. https://doi.org/10.1039/c3cc46725b

Xue, T. J., McKinney, M. A., & Wilkie, C. A. (1997). The thermal degradation of polyacrylonitrile. *Polymer Degradation and Stability*, *58*(1–2), 193–202. https://doi.org/10.1016/s0141-3910(97)00048-7

Xue, Y., Liu, J., & Liang, J. (2013). Correlative study of critical reactions in polyacrylonitrile based carbon fiber precursors during thermal-oxidative stabilization. *Polymer Degradation and Stability*, *98*(1), 219–229. https://doi.org/10.1016/j.polymdegradstab.2012.10.018

Yördem, O. S., Papila, M., & Menceloğlu, Y. Z. (2008). Effects of electrospinning parameters on polyacrylonitrile nanofiber diameter: An investigation by response surface methodology. *Materials and Design*, *29*(1), 34–44. https://doi.org/10.1016/j.matdes.2006.12.013

Yusof, N., & Ismail, A. F. (2012). Post spinning and pyrolysis processes of polyacrylonitrile (PAN)-based carbon fiber and activated carbon fiber: A review. *Journal of Analytical and Applied Pyrolysis*, *93*, 1–13. https://doi.org/10.1016/j.jaap.2011.10.001

Zhang, L., Aboagye, A., Kelkar, A., Lai, C., & Fong, H. (2014). A review: Carbon nanofibers from electrospun polyacrylonitrile and their applications. *Journal of Materials Science*, *49*(2), 463–480. https://doi.org/10.1007/s10853-013-7705-y

Zhang, W. X., Wang, Y. Z., & Sun, C. F. (2007). Characterization on oxidative stabilization of polyacrylonitrile nanofibers prepared by electrospinning. *Journal of Polymer Research*, *14*(6), 467–474. https://doi.org/10.1007/s10965-007-9130-x

Zhang, Y., Zhu, B., Cai, X., Yuan, X., Zhao, S., Yu, J., … Qin, R. (2021). Rapid In Situ Polymerization of Polyacrylonitrile/Graphene Oxide Nanocomposites as Precursors for High-Strength Carbon Nanofibers. *ACS Applied Materials & Interfaces*, acsami.1c02643. https://doi.org/10.1021/acsami.1c02643

Zhijiang, C., Xingjuan, S., & Ruihan, Z. (2013). A comparative study of polyindole nanofibers membrane and polyindole film. *Materials Letters*, *92*, 271–273. https://doi.org/10.1016/j.matlet.2012.10.092

Zhijiang, C., Xingjuan, S., & Yanan, F. (2013). Electrochemical properties of electrospun polyindole nanofibers as a polymer electrode for lithium ion secondary battery. *Journal of Power Sources*, *227*, 53–59. https://doi.org/10.1016/j.jpowsour.2012.10.081

Zhou, Z., Lai, C., Zhang, L., Qian, Y., Hou, H., Reneker, D. H., & Fong, H. (2009). Development of carbon nanofibers from aligned electrospun polyacrylonitrile nanofiber bundles and characterization of their microstructural, electrical, and mechanical properties. *Polymer*, *50*(13), 2999–3006. https://doi.org/10.1016/j.polymer.2009.04.058

Zhu, G., Zhu, Z., & Qiu, L. (2002). A fluorometric method for the determination of iron(II) with fluorescein isothiocyanate and iodine. *Analytical Sciences : The International Journal of the Japan Society for Analytical Chemistry*, *18*(9), 1059–1061. https://doi.org/10.2116/ANALSCI.18.1059

Zhu, Yanwu, Murali, S., Cai, W., Li, X., Suk, J. W., Potts, J. R., & Ruoff, R. S. (2010). Graphene and graphene oxide: Synthesis, properties, and applications. *Advanced Materials*, *22*(35), 3906–3924. https://doi.org/10.1002/adma.201001068

Zhu, Ying, Feng, L., Xia, F., Zhai, J., Wan, M., & Jiang, L. (2007). Chemical dual-responsive wettability of superhydrophobic PANI-PAN coaxial nanofibers. *Macromolecular Rapid Communications*, *28*(10), 1135–1141. https://doi.org/10.1002/marc.200600902

Zussman, E., Chen, X., Ding, W., Calabri, L., Dikin, D. A., Quintana, J. P., & Ruoff, R. S. (2005). Mechanical and structural characterization of electrospun PAN-derived carbon nanofibers. *Carbon*, *43*(10), 2175–2185. https://doi.org/10.1016/j.carbon.2005.03.031

CURRICULUM VITAE

Name Surname : İlknur BOZKAYA GERGİN

EDUCATION :

- **B.Sc.** : 2001, Istanbul University, Faculty of Science and Letters, Physics.
- **M.Sc. (non-thesis)** : 2002, Istanbul University, Institute of Science, Secondary School Teacher Training in Physics.
- **M.Sc.** : 2009, Gebze Institue of Technology, Institute of Engineering and Sciences, Physics.
- **Ph.D.** : 2023, Istanbul Technical University, Graduate School, Polymer Science and Technology.

PROFESSIONAL EXPERIENCE AND REWARDS:

- 2002-2003 Physics Teacher, Erol Altaca Dershanesi.
- 2003-2005 Pysics Teacher, Çağdaş Dershanesi.
- 2005-2006 Pysics Teacher, Özel Tek Yörünge Dershanesi.
- 2006-2008 Pysics Teacher, Pi Analitik Dershanesi.
- 2010-2016 Research Assistant, Polymer Science and Technology, Istanbul Technical University.

PUBLICATIONS, PRESENTATIONS AND PATENTS ON THE THESIS:

- **Gergin, İ.,** Gökçeören, A. T., and Sarac, A. S. 2013: Morphological and Electrical Characterization of Polyindole (PIN) Containing Electrospun Fibers, *European Polymer Congress*-(EPF 2013), June 16-21, 2013 Pisa, Italy (Poster Presentation).

- **Gergin, İ.,** Gökçeören, A. T., and Sarac, A. S. 2014. Poliakrilonitril/Poliindol Nanofiberlerinin Elektrokimyasal Karakterizasyonu, *III. Ulusal Uygulamalı Elektrokimya Lisansüstü Yaz Okulu ve Çalıştayı,* June 3-7, 2014, Balıkesir, Turkey (Poster Presentation) (Best Poster Award).
- **Gergin, İ.,** Gökçeören, A. T., and Sarac, A. S. 2015. Morphological and Electrochemical Characterization of Graphene Containing Electrospun Nanofibers of Polyacrylonitrile, *I. Ulusal Karbon Konferansı*, March 12-13, 2015, ITU, Turkey (Poster Presentation)
- **Gergin, İ.,** Sarac, A. S. 2016. Electrochemical and Morphological Proporties of Graphene Oxide Containing Polyacrylonitrile-based Carbon Nanofibers, *12th International Nanoscience and Nanotechnology (Nano TR-12)*, June 3-5, 2016 Kocaeli (Poster Presentation).
- Sarac, A.S., **Gergin, İ.,** Ismar, E. 2017. Graphene Oxide Containing Stabilized Nanofibers: Morphologic, Spectroscopic & Electrochemical Study, *Baltic Polymer Symposium*, September 20-22, 2017, Tallinn, Estonia (Extended Abstract & Presentation).
- **Gergin, İ.,** Gökçeören, A. T., and Sarac, A. S. 2015. Synthesis and electrochemical investigation of polyindole based fiber as sensor electrode by EIS method. *Fibers and Polymers, 16*(7), 1468-1477.
- **Gergin,** İ., Ismar, E., and Sarac, A. S. 2017. Oxidative stabilization of polyacrylonitrile nanofibers and carbon nanofibers containing graphene oxide (GO): a spectroscopic and electrochemical study. *Beilstein Journal of Nanotechnology, 8*(1), 1616-1628.
- **Gergin,** I., Micusik, M., Ismar, E., Omastova, M., and Sarac, A. S. 2020. Thermally Treated Graphene Oxide/Polyacrylonitrile Based Electrospun Carbon Nanofiber Precursor. *Journal of Nanoscience and Nanotechnology, 20*(6), 3448-3459.

OTHER PUBLICATIONS, PRESENTATIONS AND PATENTS:

- **Gergin, İ.,** Gökçeören, A. T., and Sarac, A. S. 2013. Morphological and Electrical Characterization of Electrospun Fibers of PNVCz/PAN Blends, *10th International Electrochemistry Meeting in Turkey,* September 4-8 2013 Konya, Turkey (Poster Presentation).
- **Gergin, İ.,** Gökçeören, A. T., and Sarac, A. S. 2015. Synthesis and Characterization of Polyindole Containing Poly(Acrylonitrile-co-Styrene) Nanofibers, *5th International Istanbul Textile Congress*, September 11-12, 2015 ITU, Turkey (Poster Presentation).
- **Gergin, İ.,** Gümrükçü, S., and Sarac 2017. Güç Tutuşur/Yanmaz Özellikteki Bor Katkılı Poliakrilonitril Nanoliflerinin Üretimi, *UTİB Türkiye Tekstil ve Konfeksiyon Sektöründe IX. Uluslararası AR-GE Proje Pazarı Zirvesi*, April 27-28, 2017 Bursa, Turkey (Poster Presentation).

- Gülercan, D., **Gergin, İ.,** and Sarac, A. S. 2018. Preparation and Electrochemical Performances of Graphene Oxide/PEDOT and Reduced Graphene Oxide/PEDOT Nanofibers and Nanocomposites. *Fibers and Polymers*, *19* (10), 2178-2187.Ismar, E., Micusik, M., Gergin, I., Omastova, M., Sarac, A.S. 2020. Thermal stabilization of poly (acrylonitrile-co-itaconic acid) nanofibers as carbon nanofiber precursor. *Polymer Degradation and Stability*, *175*, 109142.
- Ismar, E., Micusik, **M., Gergin, I.,** Omastova, M., Sarac, A.S. 2020. Thermal stabilization of poly (acrylonitrile-co-itaconic acid) nanofibers as carbon nanofiber precursor. *Polymer Degradation and Stability*, *175*, 109142.